Defence Research and Development Canada
Recherche et développement pour la défense Canada

DEFENCE R&D DÉFENSE

Radar systems for monitoring objects in geosynchronous orbit

Chuck Livingstone

Defence R&D Canada – Ottawa

Technical Report
DRDC Ottawa TR 2013-009
June 2013

Canada

Radar systems for monitoring objects in geosynchronous orbit

Chuck Livingstone
DRDC Ottawa

Defence R&D Canada – Ottawa

Technical Report
DRDC Ottawa TR 2013-009
June 2013

-Principal Author

Original signed by Chuck Livingstone

Chuck Livingstone

Defence Scientist

Approved by

Original signed by Anthony Damini

Anthony Damini

A/H Radar Exploitation section

Approved for release by

Original signed by Chris McMillan

Chris McMillan

Head DRP, DRDC Ottawa

Abstract

Current deep-space surveillance systems are incapable of detecting small (~30cm) debris objects in the geosynchronous orbit belt that contains active geostationary satellites. Because of battery and residual fuel explosions in derelict spacecraft and rocket bodies in this orbit regime, small debris objects are expected to exist and to pose a hazard to the increasing population of geostationary satellites. Possible ground and space based radar sensors have been examined as part of a larger exploration of alternatives for systems to perform deep-space object detection and orbit determination for small, geosynchronous debris objects in the context of Canadian contributions to the Space Surveillance Network following the demise of the Sapphire space surveillance satellite circa 2019.

A first-order investigation of possible ground-based radars, designed under the small target detection and tracking constraint, shows that cost roughly tracks capability as the complexity of possible solutions ranges from: a deep-space radar upgrade to a large radio telescope (ROM cost $5M to$10M), to a purpose-designed dish-antenna deep-space radar (ROM cost $100 M to $150 M), to an electronically-steered-array radar (ROM cost $1.5 B to $2.0 B). The cost figures are guesses that are based on the costs for systems with related complexity.

First-order investigations of possible space-based deep-space surveillance systems examine the concepts of using a secondary sensor payload on a geostationary satellite platform for local area debris monitoring; and developing a dedicated debris surveillance radar that would fly in a sub-geosynchronous orbit.

All investigations in this study were constrained to consider technologies that are available and are considered to be robust in 2012.

Résumé

Les systèmes actuels de surveillance de l'espace lointain sont incapables de détecter de petits débris (~30 cm) dans la ceinture des orbites géosynchrones où se trouvent les satellites géostationnaires. Suite à des explosions de batteries et de restes d'ergols dans des engins spatiaux et des étages de fusées à la dérive dans des orbites de ce genre, on croit qu'il existe de petits débris capables de menacer la population croissante des satellites géostationnaires. On a examiné des capteurs radar terrestres et spatiaux possibles dans le cadre d'un examen plus approfondi de solutions de rechange visant à créer des systèmes de détection d'objets spatiaux lointains et de détermination d'orbites pour déceler les petits débris géosynchrones. Cette démarche s'inscrit dans le contexte des contributions canadiennes au Space Surveillance Network après la fin de la vie utile du satellite de surveillance spatiale Sapphire vers 2019.

Une étude de premier ordre des radars terrestres, conçue en fonction des contraintes de détection et de poursuite de petites cibles, montre qu'il existe une certaine corrélation entre le coût et les capacités, à mesure que croît la complexité des solutions envisagées : mise à niveau d'un grand radiotélescope grâce à l'ajout d'un radar pour l'espace lointain (OGA des coûts de 5 M$ à

10 M$), radar à antenne parabolique spécialement conçu pour l'espace lointain (OGA des coûts de 100 M$ à 150 M$), radar à réseau plan et à faisceau orienté électroniquement (OGA des coûts de 1,5 G$ à 2 G$). Les coûts indiqués sont des estimations basées sur les coûts de systèmes à complexité comparable.

Des études de premier ordre de systèmes spatiaux possibles pour surveiller l'espace lointain portent sur les concepts d'utilisation de capteurs secondaires dans un satellite géostationnaire pour la surveillance des débris locaux et le développement d'un radar dédié de surveillance des débris qui serait placé sur une orbite inférieure à celle des satellites géostationnaires.

Toutes les études menées dans le cadre de cette enquête devaient porter exclusivement sur des technologies disponibles et considérées comme robustes en 2012.

Executive summary

Radar systems for monitoring objects in geosynchronous orbit

Chuck Livingstone; DRDC Ottawa TR 2013-009; Defence R&D Canada – Ottawa; June 2013.

Introduction:
The radar system study reported here examines system concepts at a high level and forms part of a much broader options analysis activity conducted by the DND Surveillance-of-Space-2 project office. The outcomes of the broad study will be a small set of implementable deep-space surveillance options that may be further examined as Canadian contributions to the Space Surveillance Network (SSN).

Current deep-space surveillance systems are incapable of detecting small (~30cm) debris objects in the geosynchronous orbit belt that contains active geostationary satellites. Because of battery and residual fuel explosions in derelict spacecraft and rocket bodies in this orbit regime, small debris objects are expected to exist and to pose a hazard to the increasing population of geostationary satellites. A study was conducted to examine the possible use of ground-based and space-based radar systems that could detect and track small debris objects in the protected geosynchronous orbit belt that extends ±200 km in radius about geostationary orbit radius 42164 km and extends ±15^{o} of earth center angle along a north-south arc that is centered on the equatorial plane of the earth. The probable deployment date for the systems considered is the expected demise of the Sapphire deep-space monitoring satellite circa 2019. Technologies that were considered by the study were constrained to those known to be available and robust in 2012.

Four ground based radar concepts were considered for systems that could detect and monitor small, geosynchronous debris objects:

1. Employ an existing radio telescope facility as a component of a bistatic radar that uses a US transmitter.
2. Build a deep-space radar mode for the Algonquin radio telescope and operate it for space surveillance as a secondary mission of the telescope facility.
3. Build a dish-antenna based deep-space radar and operate it as dedicated space surveillance radar with deep-space capabilities.
4. Build an electronically steered beam planar array radar that would be dedicated to space surveillance activities for all satellite altitudes.

Two space-based radar concepts were considered for systems that could detect and monitor small geosynchronous debris objects:

1. Build secondary sensors that can be mounted on geostationary satellites to monitor and track debris items in the local area that surrounds the satellite.
2. Build a radar space surveillance satellite that operates in a sub-geosynchronous orbit to detect and measure the orbit parameters of debris objects in the geosynchronous orbit belt.

Low-earth-orbit radar systems for monitoring geosynchronous debris objects are subject to the same size and power constraints as ground-based systems and are totally impractical.

This report examines each concept at a high level to determine its critical properties for geosynchronous belt debris surveillance. In most cases order of magnitude costs have been estimated from historical, grossly similar systems.

Results: All of the concepts that were examined are capable of detecting and monitoring small (30 cm) debris objects in geosynchronous orbit and are judged to be feasible to build using existing technology. For ground-based systems the order of magnitude costs are roughly proportional to their capabilities as space-surveillance systems.

1. Test results show that the bistatic geometries attainable for radars in the same hemisphere provide little added capability.
2. Adapting an existing radio telescope facility to add a space surveillance radar capability provides the lowest cost (between $5M and $10M) but has limited space-surveillance usage time due to the secondary mission role of the space surveillance radar function.
3. Building a space surveillance radar based on a large dish antenna is the next most economical option (between $ 100M and $150M) and provides a dedicated capability but suffers from the beam pointing time and dwell limitations that are common to all radars of this type.
4. Building an electronically steered beam, planar array radar is the most expensive option (approximately $1.5B) but is the most flexible system and can easily perform debris detection and tracking operations out to and including the geosynchronous orbit belt.

For space-based radars, the dedicated, sub geosynchronous belt, dedicated space surveillance radar option is capable of accumulating debris orbit data for the geosynchronous belt over approximately one year of operation and can maintain orbit data at an on-orbit cost greater than $800M.

The secondary-sensor geostationary radar approach can easily provide very good monitoring of debris in a sphere with 250 km radius centered on its platform. Many such systems would be required to accumulate good data on the debris environment of the entire geosynchronous belt. Much more detailed engineering analysis is required to estimate the cost of systems of this type.

Each of the cases examined has engineering or operational challenges but these are within the scope of existing practice.

Significance: Space surveillance radar systems that are capable of detecting and tracking small space debris objects in the geosynchronous orbit belt are technically feasible using current technology and some capability can be created at modest cost as a Canadian contribution to SSN operations.

All space surveillance radar developments are within the scope and capability of 2012 engineering practice.

Future plans: Further work in this area will be engineering studies and development activities that will depend on whether radar or optical systems are selected by the Surveillance-of-Space-2 analysis of alternatives for deep space surveillance systems.

Sommaire

Radar systems for monitoring objects in geosynchronous orbit

Chuck Livingstone ; DRDC Ottawa TR 2013-009 ; R & D pour la défense Canada – Ottawa; juin 2013.

Introduction ou contexte : L'étude sur les systèmes radar qui fait l'objet du présent rapport concerne des concepts de systèmes de haut niveau et fait partie d'une étude beaucoup plus vaste des options que mène le bureau du projet Surveillance de l'espace 2 du MDN. Cette vaste étude débouchera sur un petit ensemble d'options réalisables de surveillance de l'espace lointain qui pourraient être étudiées davantage comme contributions canadiennes au Space Surveillance Network (SSN).

Les systèmes actuels de surveillance de l'espace lointain sont incapables de détecter de petits débris (~30 cm) dans la ceinture d'orbites géosynchrones où se trouvent les satellites géostationnaires. Suite à des explosions de batteries et de restes d'ergols dans des engins spatiaux et des étages de fusées à la dérive dans des orbites de ce genre, on croit qu'il existe de petits débris capables de menacer la population croissante des satellites géostationnaires. Une étude a été menée sur l'utilisation possible de capteurs radar terrestres et spatiaux pouvant détecter et poursuivre les petits débris qui se trouvent dans la ceinture protégée des orbites géosynchrones qui s'étend à ±200 km du rayon orbital géostationnaire de 42 164 km, et à un angle de $\pm 15^0$ par rapport au centre de la Terre le long d'un arc orienté nord-sud et centré sur le plan équatorial de la Terre. La date de déploiement probable des systèmes envisagés est la fin prévue de la vie utile du satellite de surveillance de l'espace lointain Sapphire vers 2019. Les technologies examinées dans cette étude étaient limitées à celles que l'on savait disponibles et robustes en 2012.

On a évalué quatre concepts de radars terrestres pouvant détecter et surveiller de petits débris géosynchrones.

1. Utiliser un radiotélescope existant comme composant d'un radar bistatique faisant appel à un émetteur américain.

2. Construire un mode radar espace lointain pour le radiotélescope Algonquin et donner à cet observatoire une mission secondaire de surveillance de l'espace.

3. Construire un radar à antenne parabolique et l'utiliser comme système dédié pour surveiller l'espace lointain.

4. Construire un radar à réseau plan et à faisceau orienté électroniquement dédié à la surveillance spatiale à toutes les altitudes où l'on trouve des satellites.

On a également évalué deux concepts de radars spatiaux pouvant détecter et surveiller de petits débris géosynchrones.

1. Construire des capteurs secondaires pouvant être installés dans des satellites géostationnaires pour surveiller et poursuivre localement les débris dans la zone où se trouvent ces satellites.

2. Construire un satellite radar de surveillance spatiale exploité à une altitude inférieure à celle des satellites géosynchrones pour détecter les débris dans la ceinture d'orbites géosynchrones et en mesurer les paramètres orbitaux.

Les systèmes radar en orbite basse terrestre servant à surveiller les débris géosynchrones sont soumis aux mêmes contraintes de taille et de consommation d'énergie que les systèmes terrestres et ils sont totalement irréalistes.

Ce rapport contient un examen de haut niveau de chacun des concepts pour en déterminer les propriétés critiques en matière de surveillance des débris dans la ceinture d'orbites géosynchrones. Dans la plupart des cas, un ordre de grandeur des coûts a été estimé à partir de systèmes antérieurs assez similaires.

Résultats : Tous les concepts examinés sont capables de détecter et de surveiller de petits débris (30 cm) en orbite géostationnaire et on estime qu'ils sont réalisables à l'aide de technologies existantes. Pour les systèmes terrestres, les ordres de grandeur des coûts sont assez proportionnels à leurs capacités comme systèmes de surveillance spatiale.

1. Les résultats des tests ont démontré que les géométries bistatiques atteignables par des radars dans un même hémisphère n'accroissent pas beaucoup la capacité.

2. L'adaptation d'un radiotélescope existant en y ajoutant un radar de surveillance spatiale est la solution la moins coûteuse (de 5 M$ à 10 M$), mais son temps d'utilisation pour la surveillance spatiale est limité, car la surveillance spatiale n'est qu'une mission secondaire pour une telle installation.

3. La construction d'un radar de surveillance spatiale sur une grande antenne parabolique est la deuxième solution la plus économique (de 100 M$ à 150 M$) et elle offre une capacité dédiée, mais elle présente les mêmes désavantages que les autres radars de ce type, soit le temps de pointage du faisceau et le temps de maintien limité.

4. La construction d'un radar à réseau plan et à faisceau orienté électroniquement est l'option la plus coûteuse (environ 1,5 G$), mais il s'agit de la solution la plus flexible qui peut facilement faire la détection et la poursuite des débris, et ce, jusqu'à la ceinture d'orbites géosynchrones.

Pour ce qui est des radars spatiaux, le système de surveillance spatiale dédié, fonctionnant à une altitude inférieure à celle des satellites géostationnaires, est capable d'accumuler des données orbitales sur les débris dans la ceinture d'orbites géostationnaires pendant environ un an et de tenir des données orbitales à un coût en orbite de plus de 800 M$.

L'approche d'un capteur secondaire installé dans un satellite radar géostationnaire permettrait facilement de très bien surveiller les débris dans une sphère d'un rayon de 250 km centrée sur la plateforme. Il faudrait un grand nombre de systèmes de ce genre pour accumuler de bonnes données sur l'environnement de débris dans toute la ceinture d'orbites géosynchrones. Il faut mener une analyse d'ingénierie beaucoup plus poussée pour estimer le coût des systèmes de ce genre.

Chacun des cas examinés présente des défis techniques ou opérationnels, mais ils sont réalisables avec les pratiques actuelles.

Importance : Les systèmes radar de surveillance capables de faire la détection et la poursuite des petits débris spatiaux dans la ceinture d'orbites géosynchrones sont techniquement réalisables avec les technologies actuelles et une certaine capacité peut être créée à coût modeste comme contribution canadienne aux opérations du SSN.

Tous les développements des radars de surveillance spatiale sont réalisables avec les pratiques techniques de 2012

Perspectives : Les travaux à venir dans ce domaine seront des études techniques et des activités de développement qui dépendront du choix des systèmes, radar ou optiques, dans le cadre de l'analyse des solutions de rechange du projet Surveillance de l'espace 2 pour les systèmes de surveillance de l'espace lointain.

Table of contents

List of figures

List of tables

Acknowledgements

The author thanks Dr. Brad Wallace for providing the documents that describe the Algonquin Radio Observatory and Dominion Radio Astronomical Observatory bistatic studies, the Algonquin Radio Observatory upgrade study and the CSA study on a space-debris monitoring system.

This page intentionally left blank.

1 Introduction

As the geosynchronous orbit belt becomes more populated with global observation and communications satellites, the problem of debris interaction with active satellites becomes increasingly serious. In 1997, the Inter-Agency Space Debris Coordination Committee (IADC) endorsed a re-orbiting strategy to remove geostationary / geosynchronous belt active satellites to orbits outside of a ± 200 km reserved belt centered at the geostationary orbit radius of 42164 km to larger radius disposal orbits [1] at the end of the satellite lifetime. Following further IADC supported studies, it was decided that objects in disposal orbits must have orbit perigees greater than

$$R_P = R_G + 235 + 1000 C_R \frac{A}{M} \text{ km}, \tag{1}$$

where C_R is a radiation pressure coefficient ($1 \leq C_R \leq 2$); A/M is the spacecraft area to mass ratio; and R_G is the geostationary orbit radius, to account for orbit eccentricity modulation by solar radiation pressure [1].

Discussions in [1] define the maximum disposal orbit injection eccentricities for the minimum perigee radius to be 0.005 if the debris argument of perigee is unconstrained and 0.3 if the debris argument of perigee was selected to be in the sun-pointing direction when the lunar orbit right ascension angle is 0°. The argument of perigee constraint conditions occur in June and December and often do not correspond to required satellite disposal dates. IADC space debris mitigation guidelines were issued in 2007 [12].

Although the IADC disposal orbit recommendations have been accepted by the international community, there remain historical, uncontrolled, satellites and rocket motors in the geosynchronous belt as debris objects. Over time, the number of geosynchronous belt debris objects has been increased by satellites whose control systems have failed before end-of-life re-orbiting [2] and by debris object fragments that have been generated by mechanical failures and explosions of debris objects within the protected geosynchronous orbit belt.

Satellite and rocket body debris objects are large enough to be tracked by currently active space surveillance sensors and their orbits are monitored to allow active satellites to avoid them by orbit maneuver. Structural failures of dead satellites and rocket bodies by battery explosions and by explosions caused by residual fuel generate clouds of debris whose components magnify the debris collision hazard and are too small to track using existing space surveillance systems. Collisions between uncontrolled satellites pose the risk of generating additional, multiple pieces of small debris.

Current space surveillance systems are capable of detecting debris items as small as 1 m^2 in the geosynchronous orbit belt but as the debris size approaches the optical and / or radar detection limit, the ability to determine and maintain accurate debris orbit information decreases. The difficulty of debris orbit monitoring is compounded by the lack of attitude stability of debris objects. They tumble as they progress around their orbits, have variable optical and radar reflectivity and have variable solar radiation pressures due to the object shape [35] and attitude variation.

The work reported here was performed to provide inputs to an analysis of alternatives for the development of Canadian deep space surveillance-systems following the demise of the Sapphire deep-space surveillance satellite. This report looks at the gross properties of possible space surveillance radar systems that can detect and track debris items as small as 0.07 m^2 (cross sectional area of a 30 cm sphere) in geosynchronous orbit. As required for the analysis of alternatives work, the technologies examined are limited to those that are readily available for use in 2012.

The report is organized as follows:

- Section 2 discusses properties of geosynchronous debris orbits.
- Section 3 discusses ground-based deep-space radar systems.
- Section 4 discusses ground-based and space based radar alternatives for geosynchronous debris monitoring that could form Canadian SSN (Space Surveillance Network) contributions.
- Section 5 summarizes the discussions in the report.
- Annex A details model calculations for radar observations of debris targets from a geostationary satellite platform.

2 The geosynchronous orbit belt

Following the IADC recommendations between 1997 and 2000 [1], the protected geosynchronous satellite orbit belt was defined as an annular ring with mean radius 42164 km, radial thickness ±200 km and an inclination angle extent of ±15° centered on the earth's equatorial plane. By 2007 it was accepted practice for all geostationary satellite owners to remove satellites from this protected belt at the satellite end of life. In 2004, there were 1124 known active and debris objects in the protected geosynchronous belt [3]. This number had grown to 1344 objects by 2009 [5].

Although most end-of-life geostationary satellites and orbit insertion motors have been actively removed from the protected geosynchronous belt since 2007, satellite control failures [2] and failed satellite components (telescope sun shields, etc [5]) have slowly grown the population of debris objects in this region.

2.1 Natural forcing functions

Satellites in the geosynchronous orbit belt are subject to a number of natural forces that perturb their orbits [1]. The dominant perturbation forces are:

1. solar radiation pressure effects,
2. asymmetry of the earth's gravitational field,
3. the lunar gravitational field, and
4. the solar gravitational field.

Although these forces are small, they act on satellites for long periods of time and can have substantial cumulative effects on the satellite orbits. As a result, active geostationary satellites require station-keeping maneuvers to maintain their assigned positions.

Other perturbation forces exist but have smaller effects.

2.1.1 Solar radiation pressure effects

Solar radiation pressure primarily affects the orbit eccentricity and its impact is strongly dependent on the area to mass ratio of the affected object [1], [5]. Objects with large area to mass ratios (5 to 15 m^2/kg) originating in the geostationary orbit disposal zone can cross the geostationary ring because of solar radiation pressure effects on orbit eccentricity. Modeling and analysis of observational data [6] indicates that objects with area to mass ratios less than 1 m^2/kg are weakly affected by solar radiation pressure and objects with area to mass ratios greater than 5 m^2/kg are strongly affected. The modulation of the object orbit eccentricity appears to be nearly periodic with an annual period.

In addition to its influence on debris orbit eccentricity, solar radiation pressure can act to increase debris orbit inclination angles beyond the range that is driven by solar and lunar gravity perturbations.

Model calculations in [1] show that solar radiation pressure effects on orbit eccentricity have an annual periodicity. The peak-to-peak eccentricity amplitude shows longer period (~ 30 years) modulation. The model presented in [1] shows a maximum peak to peak variation in the orbit eccentricity of 0.0006 over a 20 year interval for a complete satellite. For objects that have large area to mass ratios, eccentricities can become as large as 0.03 [4].

Objects with area to mass ratios greater than 1 m^2/kg can exceed the maximum gravitational orbit inclination modulation limit of 15^o due to solar radiation effects and objects with area to mass ratios in the vicinity of 20 m^2/kg show evidence of a periodic modulation of orbit inclination corresponding to the second harmonic of the gravitational inclination modulation and show maximum orbit inclinations in the vicinity of 20^o. Observations indicate that object tumbling can modulate the modeled effects and these modulations will depend on the shape of the object [35].

Assuming that the orbit energy remains constant, the effect of varying the orbit eccentricity, *e*, for debris in a geostationary orbit plane results in a debris true anomaly (debris orbit central angle from perigee) of $\nu = \mathrm{acos}(-e)$ at the points where the debris orbit intersects a circular geostationary orbit. The debris trajectory intersects the circular geostationary orbit trajectory at an angle, $\phi = atan2((e * \sin(\nu)), (1 + e * \cos(\nu)))$ and with a relative velocity of ~ $3.07\frac{e^2}{1-e^2}$ km/s. For e=0.1, the relative velocity is approximately 30 m/s. Larger relative velocities come from large eccentricity debris originating in the geosynchronous disposal orbit.

2.1.2 Earth gravity field asymmetry

The gravity field of the earth is not symmetrical as is illustrated in Figure 1.

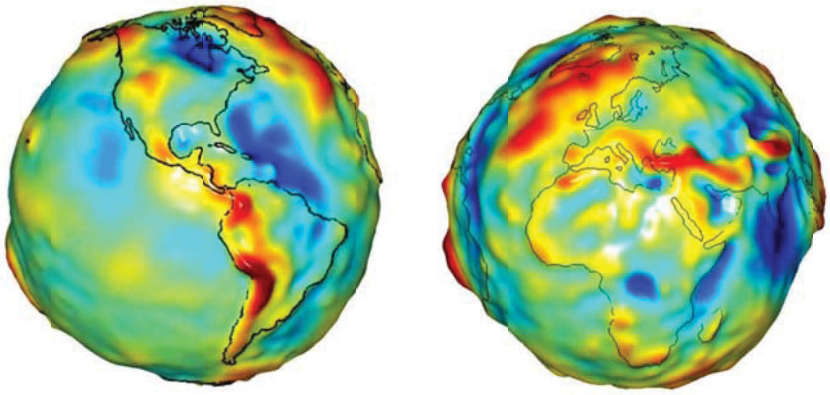

Figure 1: Earth gravity field schematic representation from GRACE. The radial scale in this image is highly distorted to emphasize the gravity field variability. Red codes areas with the strongest gravity field and blue codes areas with the weakest gravity field. [7]

For medium precision satellite orbit determination, adequate for the determination of the major geosynchronous orbit perturbations caused by gravity field asymmetry, the gravity field can be modeled as an oblate spheroid (for example, the WGS 84 (World Geodetic System 1984) earth ellipsoid model) which is modified to have an ellipsoidal profile in the equatorial plane. The

semi-major axis of the equatorial plane ellipse links the gravity field maxima at longitudes E 75° and W 105°.

Using the ellipsoidal equatorial asymmetry approximation, the gravity gradient causes debris orbit arguments of perigee to drift towards and oscillate about the gravitational maxima (there is a gravity gradient torque applied to the orbit angular moment vector). Debris orbit drift rates, modeled in [1] result in a periodic variation in satellite longitude with a primary period of approximately 8 years that has a second harmonic (4 year period) component superimposed on it. Drifting objects tend to oscillate about the two equatorial gravity maxima that are also known as orbit libration points. Longitude drift velocities can be estimated from the catalogued two-line orbit ephemeris mean motion parameter, n, as $\omega_A = (1.00274 - n)360$ in degrees/day [8]. A sampling of drifting satellites [4], [8] shows longitude drift rates from -3.9 to 12.8 degrees/day.

The effect of the equatorial asymmetry on the orbital velocity causes the orbit semi-major axis to vary periodically with a primary period of approximately 8 years which is summed with a third harmonic component. The case modeled in [1] shows a peak to peak variation in orbit semi-major axis of ±35 km.

2.1.3 Solar and lunar gravitational effects

The moon orbits the earth about the gravitational barycentre of the two bodies (approximately 4600 km from the gravitational center of the earth) in an orbit plane that is inclined 5.1° to the ecliptic plane. The semi-major axis of the moon's orbit is 384748 km, its mean orbit eccentricity is 0.0549, and its orbital period is approximately 27.3 days (one sidereal month). The argument of perigee of the moon's orbit progresses by one earth revolution every 8.85 years.

Since the earth equatorial plane is inclined at 23.5° to the ecliptic plane, the moon's inclination to the earth equatorial plane varies between 18.29° and 28.58° over an annual cycle. The gravitational field of the moon exerts an out-of-plane force on objects that are in geosynchronous orbits that has both a monthly and an annual periodicity.

The earth's orbit about the sun has a semi-major axis of 149598261 km, an eccentricity of 0.0167 and a perigee on January 3. The gravity field of the sun on geosynchronous objects generates an out-of-plane force that has a period of one sidereal year.

The combined lunar and solar out-of-plane force effects on the orbits of geosynchronous debris can be represented in terms of periodic torques on the orbit angular momentum vector. These torques generate an orbit inclination oscillation with a peak inclination angle of ± 15° and a half period of 53 years [3], [9]. The torques that generate orbit inclination oscillation have little effect on the debris-orbit radius and result in relative latitude-direction debris velocities across the geostationary orbit plane of 3.07sin(θ) km/s for orbit inclination angle θ. Typical values are shown in Table 1.

Table 1: Debris crossing speeds at the equatorial plane due to debris orbit inclination.

Orbit plane inclination	Crossing velocity normal to the equatorial plane
15°	795 m/s
10°	533 m/s
5°	268 m/s
2°	107 m/s
0°	0 m/s

In most cases uncontrolled satellite orbit planes and debris orbit planes intersect at angles within the ±15° inclination angle perturbation range. There is some observational evidence [6] that a small number of objects with area-to-mass ratio of two or more have maximum orbit plane intersection angles between ±15° and ±20°.

The primary collision hazards between debris objects and between debris objects and geostationary satellites occur at the intersection points for relatively inclined orbits.

The total relative velocity between an uncontrolled object (debris) and a geostationary satellite will include the relative drift velocities of the debris orbit plane and the satellite with respect to a libration point. For satellites that retain longitude control, the satellite drift velocity is small and is periodically adjusted.

2.2 Station keeping for geostationary satellites

A geostationary satellite acquires its geographic position stability by executing planned orbit control maneuvers to keep it within an assigned control box with a nominal width of either ±0.05° longitude or ±0.1° longitude. Station keeping is performed by controlling the eccentricity, semi-major axis and inclination of the satellite orbit and by controlling the longitudinal drift of the satellite in its orbit by means of impulsive thrusts from small chemical rocket motors mounted on the satellite or by longer period thrust from ion rocket motors [10]. Typically satellite orbits are constrained in inclination to a ±0.1° range due to control restrictions on their associated ground systems.

Orbit inclination control requires more energy than longitude station-keeping and for some satellites, nearing their end of life, the allowed range of orbit inclination variation is relaxed.

For satellite control, a local, Cartesian coordinate system is defined by:

1. a unit vector, X, that is parallel to the outward radial position vector of the satellite,
2. a unit vector, Z, normal to the position vector, that lies in the plane defined by the satellite position vector and the earth rotation axis and is positive north,
3. and the mutually orthogonal unit vector, Y, that is positive in the direction of satellite motion.

From the viewpoint of an individual satellite control box, longitude drift control alters positions along the Y axis, inclination angle drift control alters positions along the Z axis (local latitude) and semi-major axis variation control alters positions along the X axis. Satellite control consists of longitude adjustment by thrust applied along the Y axis and latitude (inclination angle) adjustment by thrust applied along the Z axis. The timing of the longitude control thrust is also used to adjust the orbit eccentricity (X axis adjustment). Thrust applied along the positive or negative X axis changes the orbit radius and is used for moving the satellite from one longitude box to another one.

The process of keeping a spacecraft in its assigned geostationary longitude box is relatively fuel efficient as is the process of controlling the orbit eccentricity but the process of controlling the orbit inclination over the satellite lifetime requires much more fuel.

For satellites whose longitude and inclination angles are controlled, the orbit plane inclinations are controlled to lie within the range between 0.0001^{o} and 0.29^{o} with most satellites constrained to have orbit inclinations much less than 0.08^{o} [4]. Meteorological observation satellites have the loosest constraints.

For satellites with longitude control only (this condition is often used near the end of the satellite's useful life to conserve fuel), the orbit inclination angles are allowed to drift and can reach 11.5^{o} (TDRS West) for active satellites [4].

2.3 Geostationary satellite clusters

Increasing demand for geostationary orbit positions has resulted in the operation of geostationary satellite clusters where several satellites occupy the same 0.05^{o} or 0.1^{o} longitude box for some period of time. Satellite avoidance within a cluster is typically controlled by managing the relative orbit inclinations and eccentricities of the individual satellites so that they move systematically with respect to each other in a type of cartwheel orbit [11] in (or near) an X, Z plane.

2.4 Geosynchronous debris

The term geosynchronous debris refers to all uncontrolled objects in the geosynchronous orbit belt. The debris objects fall into three classes:

1. defunct satellites in the geosynchronous belt,
2. rocket motors in and near the geosynchronous belt and
3. debris clouds of satellite and rocket motor components that were:
    a. dispersed by battery and fuel tank explosions,
    b. dispersed by collisions between debris objects and defunct satellites, or
    c. individual satellite components (e.g. telescope cover lids) that became detached from their satellites due to mechanical failures.

Defunct satellites include:

- Satellites that were placed in geosynchronous orbit prior to 2000 (when the US started to use disposal re-orbiting) or prior to 2007 when disposal re-orbiting became universally accepted; and
- satellites that have failed prior to re-orbiting disposal attempts [2].

Rocket motors that were used for geostationary orbit insertion prior to broad acceptance of the geosynchronous disposal orbit protocols and motors that failed to achieve disposal orbit remain in the geosynchronous belt. A few of these motor orbits have relatively large eccentricities (up to 0.015) [4].

Debris clouds and small debris items consist of satellite or rocket motor fragments. Transtage 5 debris (semi-major axis 41989 km and orbit eccentricity 0.0146), LES 6 operational debris (semi-major axis 41953 km and orbit eccentricity 0.012) and Ekran2 fragmentation debris (semi-major axis42142 km and orbit eccentricity 0.0007) are among the known and tracked examples [4]. Present radar and optical deep space surveillance technology can only detect and track the debris articles whose cross-range sizes are 1 m^2 and larger. The existence of at least 67 untracked debris objects and debris clusters was known in 2009 [4]. The location of these with respect to the protected geosynchronous orbit belt is unknown.

3 Geosynchronous object observations by ground-based radars

There are two options for radar observations of active satellites and debris in geosynchronous orbits: use large, ground-based radar systems or use modest space-based radars located in or near the geosynchronous belt. Space based radars in low earth orbit are subject to the same range, size and power constraints as large ground-based systems and are impractical to implement.

3.1 The observation geometry

Debris in the geosynchronous/geostationary belt is either in drifting orbits that remain in the ± 200 km belt thickness or is in elliptical orbits that pass through the belt. Debris orbits are uncontrolled and will usually have inclinations that lie within ± 15° but debris objects with high area to mass ratios can have larger orbit inclinations due to solar radiation pressure effects.

Although all geosynchronous belt orbits are elliptical, their eccentricities are small. To estimate the major properties of ground-based radars designed to monitor geosynchronous debris, the debris orbits can be simply modeled using inclined circular orbits whose radius is the geostationary orbit radius, a_T = 42164 km. The position vector of a geosynchronous debris target can be expressed in Earth Centered Earth Fixed (ECEF) coordinates as:

$$\vec{R}_T = \begin{bmatrix} X_T \\ Y_T \\ Z_T \end{bmatrix} = a_T \begin{bmatrix} cos(\varphi_T)\cos(I) \\ sin(\varphi_T)\cos(I) \\ \sin(I) \end{bmatrix}, \tag{2}$$

where: φ_T is the target longitude at the observation time and I is the target inclination angle from the equatorial plane at the observation time. The basis of the ECEF reference frame are the unit vectors $\hat{X}, \hat{Y}, \hat{Z}$ which point from the earth's center to: the Greenwich Meridian equator crossing, the equatorial point at 90° east longitude and the north pole respectively.

For objects that are under geostationary orbit control, φ_T is dynamically constrained in longitude to a ±0.1° or a ±0.05° orbit control box. These constraints correspond to along-orbit distances of 147.2 km and 73.6 km respectively. For objects that are in drifting orbits $\varphi_T = \varphi_0 + \gamma t$ where φ_0 is the longitude of the debris object at the start of the observation period, γ is the debris object's orbit drift rate in degrees / day and t is the fractional time of day.

The apparent inclination of the debris object at the observation time can be expressed as

$$I = I_O \sin(\omega t_1) \tag{3}$$

where: I_O is the inclination of the debris object's orbit, $\omega = 2\pi/T$ (T=86164.2 seconds or one sidereal day) and t_1 is time referenced to the ascending node time of the debris object.

Assume that ground-based radar that observes the geosynchronous orbit debris is located at latitude λ_R , longitude φ_R and height h above the reference ellipsoid earth model used. Its position vector measured from the center of the earth is

$$\vec{R}_{Rad} = \begin{bmatrix} (N_\lambda + h)cos(\lambda_R)cos(\varphi_R) \\ (N_\lambda + h)cos(\lambda_R)sin(\varphi_R) \\ \big((1-e^2)N_\lambda + h\big)sin(\lambda_R) \end{bmatrix} \tag{4}$$

where, e = 0.0818191908426 is the earth ellipsoid eccentricity and N_λ is the ellipsoidal radius of curvature along a meridian of longitude,

$$N_\lambda = \frac{R_{Eq}}{\sqrt{1-e^2 sin(\lambda_R)^2}}, \tag{5}$$

R_{Eq} = 6378.1370 km is the equatorial earth radius and λ_R is the geodetic latitude of the radar.

The ellipsoid earth-normal unit vector at the radar position is

$$\widehat{U}_N = \begin{bmatrix} \cos(\lambda_R)\cos(\varphi_R) \\ \cos(\lambda_R)\sin(\varphi_R) \\ \sin(\lambda_R) \end{bmatrix}. \tag{6}$$

Defining the longitude to be positive east: the east pointing unit vector along the latitude parallel is

$$\hat{E} = \begin{bmatrix} -\sin(\varphi_R) \\ \cos(\varphi_R) \\ 0 \end{bmatrix} \text{ and} \tag{7}$$

the north pointing unit vector along a longitude meridian is

$$\widehat{N} = \hat{E} \times \widehat{U}_N. \tag{8}$$

The radar range vector to the target is

$$\vec{R}_{Targ} = \vec{R}_T - \vec{R}_{Rad} \text{ and} \tag{9}$$

the radar range of the target is

$$R = \sqrt{\vec{R}_{Targ} \cdot \vec{R}_{Targ}{}'}. \tag{10}$$

The symbols, · and ′ in equation 10 are, respectively, the vector scalar-product operator and the vector transposition operators.

Defining a unit vector generator by the function $Unit\big(\vec{A}\big) = \left[\frac{\vec{A}}{\sqrt{\vec{A}\cdot\vec{A}'}}\right]$, the radar range unit vector seen at the radar is

$$\widehat{U}_{Targ} = Unit(\vec{R}_{Targ}). \tag{11}$$

The radar elevation angle of the target is

$$\theta = 90 - \text{acos}(\widehat{U}_N \cdot \widehat{U}_{Targ}), \tag{12}$$

the radar azimuth angle of the target is

$$\xi = atan2(\widehat{N} \cdot \widehat{U}_{Targ}, \hat{E} \cdot \widehat{U}_{Targ}), \tag{13}$$

and the angle between the radar range vector and the target position vector is

$$\beta = \text{acos}(\widehat{U}_{Targ} \cdot Unit\big(\hat{R}_T\big)). \tag{14}$$

The debris target's velocity vector in the ECEF observation frame is given by the time derivative of $\vec{R}_{Targ}$ taking the debris orbit drift rate, γ, into account. The longitude φ_T is the debris longitude at $t = 0$.

(15)

$$\vec{V}_{Targ} = \frac{d\vec{R}_{Targ}}{dt} = \frac{d\vec{R}_T}{dt} =$$
$$a_T \begin{bmatrix} -\omega I_O \cos(\varphi_T + \gamma t)\sin(I)\cos(\omega t) - \gamma \sin(\varphi_T + \gamma t)\cos(I) \\ -\omega I_O \sin(\varphi_T + \gamma t)\sin(I)\cos(\omega t) + \gamma \cos(\varphi_T + \gamma t)\cos(I) \\ \omega \mathrm{I_O} \cos(I)\cos(\omega t) \end{bmatrix}.$$

The radar range rate is the projection of V_{Targ} onto the radar range vector

(16)
$$v_{Targ} = \vec{V}_{Targ} \cdot \hat{U}_{Targ}.$$

Both equations 15 and 16 ignore the effects of debris orbit eccentricity, which are small but not completely insignificant.

3.2 Deep-space radars capable of geosynchronous belt measurements

A number of international ground-based radar systems are used to support the detection, cataloguing and monitoring of geosynchronous belt objects. Some of these are dedicated to the space object monitoring and tracking and some are used part of the time to augment other measurements. These deep-space observation radars fall into two classes, steered dish-antenna radars and fixed planar-array antenna, steered beam radars. Representative, active systems are outlined in Table 2 with their parameters used for geosynchronous belt observations. In Table 2, the abbreviations PRF and LFM mean Pulse Repetition Frequency and Linear Frequency Modulation respectively.

All of these systems use incoherent integration over 256 to 1000 pulses to allow the detection of debris items with radar cross sections down to 1 m^2 in the geosynchronous belt and measurement of radial velocities down to less than 1 m/s.

The first four entries in Table 2 are radar systems that are part of the Space Surveillance Network. The Eglin Air Force Base (AFB) AN-FPS-85, ALTAIR and Millstone Hill radars are deep-space detection and tracking instruments, the GLOBUS II radar has deep space imaging capability [16] and was used to construct an inverse SAR image of a Molniya orbit spacecraft near geosynchronous range. In Table 2, the abbreviations:

- USAF is United States Air Force and
- MIT is Massachusetts Institute of Technology

Two different strategies are used for radar monitoring of geosynchronous belt targets:

1. A radar staring strategy is used to identify and establish initial orbit parameters for un-catalogued objects.
2. A periodic revisit strategy is used to refine orbit estimates.

Table 2: Radar systems that have geosynchronous belt observation capability

Radar	Owner	Location	Primary mission	Antenna	Beam width	Beam steering	Frequency	Pulse length	Transmit power	PRF	Bandwidth	Waveform	Reference
AN-FPS-85 Eglin AFB	USAF	N 30.6°, W 68.22°	Space surveillance	Tx 27 m x 27 m array Rx 58 M octagon array	Tx 1.4°, Rx 0.67°	±60° azimuth 3° to 105° elevation	422 MHz	250 µs	32 MW peak	20 Hz	10 MHz	LFM	[13]
ALTAIR	USAF	N 8.72° W 167.73°	Space surveillance	45.7 m dish	1.1°	360° azimuth 0° to 90° elevation	414 to 440 MHz	1 ms	6.4 MW peak	20 Hz to 120 Hz	250 kHz to 1 MHz	LFM	[14 and 15]
Millstone Hill	MIT	N 43.62° W 71.49°	Space surveillance	25.6 m dish	0.6°	360° azimuth 5° to 90° elevation	1.295 GHz	1 ms	3 MW	40 Hz	10 MHz	LFM	[16]
Globus II	Norway	N 70.367° WE 31.127°	Space surveillance	27 m dish	0.08°	360° azimuth 0° to 90° elevation	9.5 to 10.5 GHz	Not available	200 kW	Not available	Not available	LFM	[17]
Tira	Fraunhoffer FHR	N 50.617° E 7.130°	Radar research	34 m dish	0.45°	360° azimuth 0° to 90° elevation	1.333 GHz	1 ms	1.5 MW	37 Hz	250 kHz	LFM	[18]

3.2.1 Search for un-catalogued targets

Deep-space radar observations of un-catalogued geosynchronous objects typically use a beam-stare antenna steering strategy [20 and 21] to accumulate observations needed to estimate the orbits of observed pieces of debris. Used in this mode, a steered-dish radar observes the contents of a cone whose -3 dB cross-range diameter is $D(R) = R\Phi$ where Φ is the -3 dB beam width of the radar. For a radar range of 37751 km and a -3 dB beam width of 0.62^{o} (Millstone Hill example) each radar range gate has a -3 dB cross-range diameter of 408 km. The complex signal data from all targets within this disk are summed for any given radar pulse but may be separated by range migration and range rate over a sequence of many pulses. Observation periods of one or two days will allow initial orbit and tumble-rate estimation for un-catalogued debris targets.

Typical measurement strategies sum the radar returns from bursts of 256 to 1000 pulses for each measurement, use Doppler measurements over many bursts to estimate range rates and use two-dimensional mono-pulse antenna beams to estimate the cross-range position of the target object. Target orbits and target tumble rates are determined by accumulating measurements of target strength, position and range rate over time.

Using this approach to search the portion of the geosynchronous belt that is visible to a radar system is time-consuming because of the long dwell time required for each observed region.

3.2.2 Debris and satellite orbit knowledge maintenance

Once an orbit has been established the orbit can be maintained by periodic observations as evidenced by the ALTAIR radar operating procedures [15]. Orbit maintenance observation times quoted in [15] are described to be six to ten minutes per object (tracked satellite). A similar strategy could be applied to small debris objects, down to the detection limit, but the observation period needs to be longer due to orbit instability, tumble rate and low radar cross section.

4 Investigation of Canadian options for SSN radar system augmentation

At the time of writing, an options analysis is in progress to identify surveillance of space sensor options that can be used to provide a Canadian contribution to the space surveillance network after the demise of the Sapphire deep-space observation satellite. A driving parameter for the options analysis studies is the ability to detect and determine orbits for geosynchronous debris articles with nominal diameters of 0.3 m (radar cross sections of -11.5 dBm^2). There are currently no space surveillance systems that have this capability.

There are two basic approaches that can be reasonably employed to use radar systems to detect and measure geosynchronous satellites and debris:

1. Build and operate large, ground-based radars that have been designed for geosynchronous belt observations, and
2. Build and operate space-based radar systems that are located within or near the geosynchronous belt.

4.1 Ground-based systems for the observation of geosynchronous belt targets

When defining the position and motion of geosynchronous belt objects from the gravitational center of the earth, the earth's equatorial plane and the longitude of the equatorial plane crossing form position references. Geosynchronous plane objects occupy a shell whose instantaneous radius is determined by the orbit semi-major axis, the orbit eccentricity, and the time of sidereal day. The orbits have periods close to one sidereal day and the orbit semi-major axes are very close to 42164 km for objects that have their origin as geostationary satellites or satellite components.

Noting that uncontrolled (debris) objects have orbit inclinations that vary under the influence of the solar and lunar gravity fields, the instantaneous angle between the position vector of a debris object and the equatorial plane varies as equation 3 where the time parameter, t_1 is determined by the true anomaly of the object position (the angle between the object position and its orbit perigee) at the observation time. This instantaneous inclination angle has a period of one sidereal day.

Debris object orbits drift in longitude under the influence of asymmetries in the earth's gravitation field.

From the viewpoint of a ground-based radar at the equator, the observational position of a geosynchronous object takes the form of a lemniscate, Figure 2, where the angular height of the pattern (apparent inclination angle) is determined by the inclination of the debris orbit and the angular width of the pattern is determined by the eccentricity of the debris orbit. When the debris orbit plane does not drift, the pattern repeats daily.

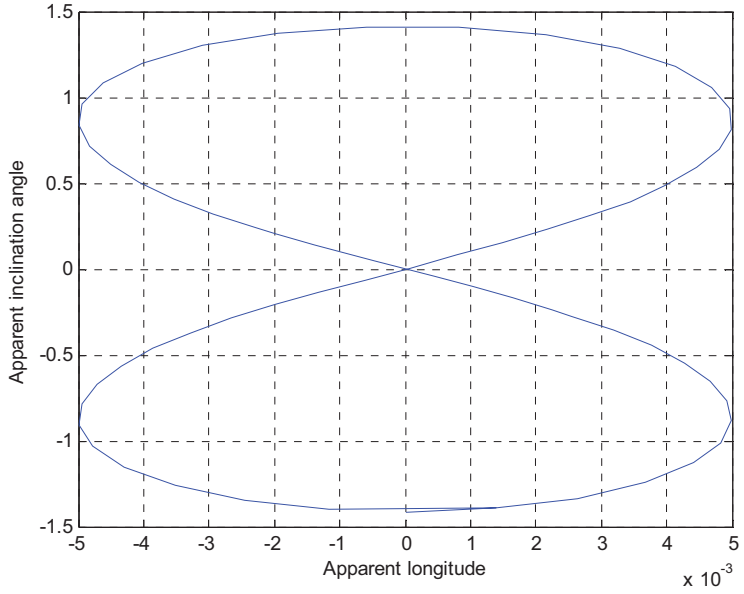

Figure 2: The apparent position in degrees of a piece of geosynchronous debris that has 1.4° orbit inclination, as observed from the equator.

Figure 2 is an illustration that would correspond to a debris orbit inclination of 1.4° and an orbit eccentricity of 0.0002 as observed from the equator when the debris orbit does not drift.

Figure 3 illustrates the effect of debris orbit drift for the debris orbit illustrated in Figure 2.

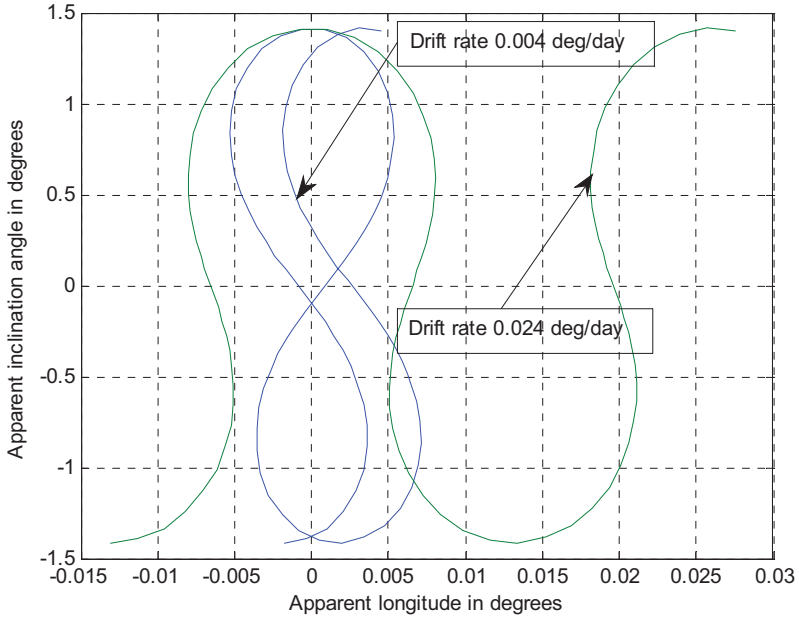

Figure 3: Debris orbit position motion in figure 1 with two orbit drift rates.

From Figure 3, it is seen that radar observations over several days may be required to quantify debris orbit drift rates when the rates are low enough that their daily displacement is not easily distinguishable at a fixed radar beam pointing angle.

Geosynchronous debris observations from a ground-based radar vary with the latitude of the radar and with the relative longitude of the radar and the debris. The simplest radar observation case occurs when the debris and the radar are at the same longitude. In this case the radar range of the debris varies with both radar latitude and debris position vector inclination angle measured from the equatorial plane. Using equations 2 to 5 and 10, Figure 4 shows the relationship between debris range and radar latitude for radars at north latitudes up to 75°.

Under this condition, the apparent motion of the satellite illustrated in Figure 2 is centered on a north-south arc and the vertical symmetry of the motion pattern in Figure 2 is changed by the latitude-dependent observation geometry.

The debris range rate that is observed by the radar is computed by evaluating equations 9, 11, 15 and 16. The effect of the relative longitudes of the radar and the debris on range rate measurements enters range rate estimates through the directions of the radar range vector and the target velocity vector as expressed in equation 16.

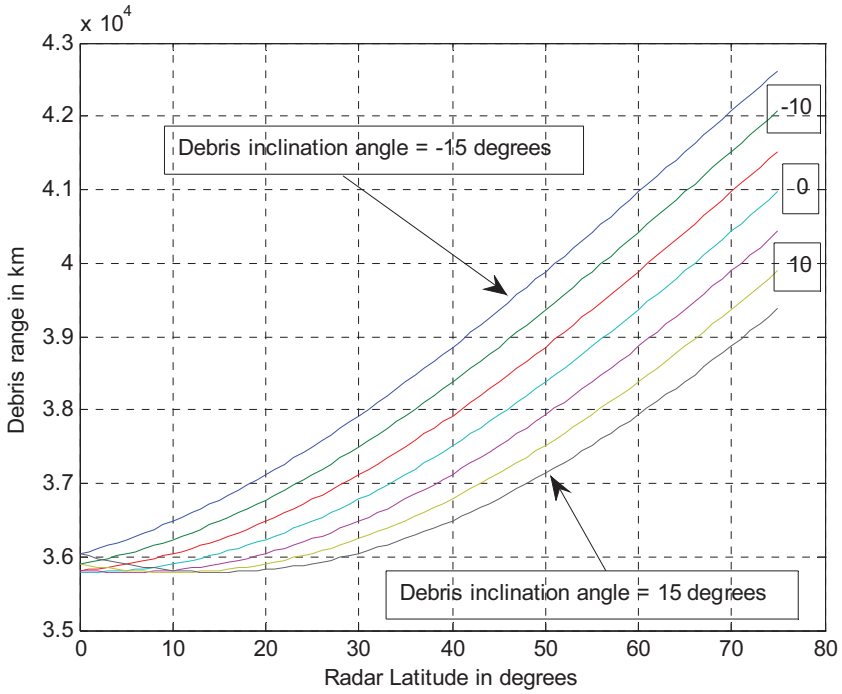

Figure 4: Geosynchronous debris range as a function of radar latitude and debris inclination angle when the debris is at the radar longitude.

To examine the properties of the radar observation geometry, we:

1. Choose a radar latitude of N 45° and a radar longitude of W 75°.
2. Choose initial debris longitudes spaced by 5° from W 75° to W 40°.

3. Allow the debris orbits to drift westward at 2º per day.
4. Choose circular debris orbits with inclination 15º.
5. Define the debris orbit radius to be 42164 km.
6. Define the term inclination to mean the angle between the debris position vector (measured from the center of the earth) and the earth equatorial plane as given by equation 3.
7. Compute the geometric radar properties for debris observation over one sidereal day using equations 2 to 16.

The results shown in Figures 5 through 10 display some of the geosynchronous debris observation implications of this list of assumptions for debris articles whose orbit plane is inclined at 15°. The displayed parameters are specific to a radar system that is sited an N 45°, W 75°. Similar results can be easily generated for other radar sites.

The time history radar range-rate observations, shown in Figure 5, is nearly independent of the longitude difference between the radar and debris positions over the observation period. The range rates are largest when the debris is in the opposite hemisphere from the radar. The two minima in Figure 5 occur when the debris crosses the earth's equatorial plane. The magnitude of the range rate measurements is dependent on the inclination angle of the debris orbit plane.

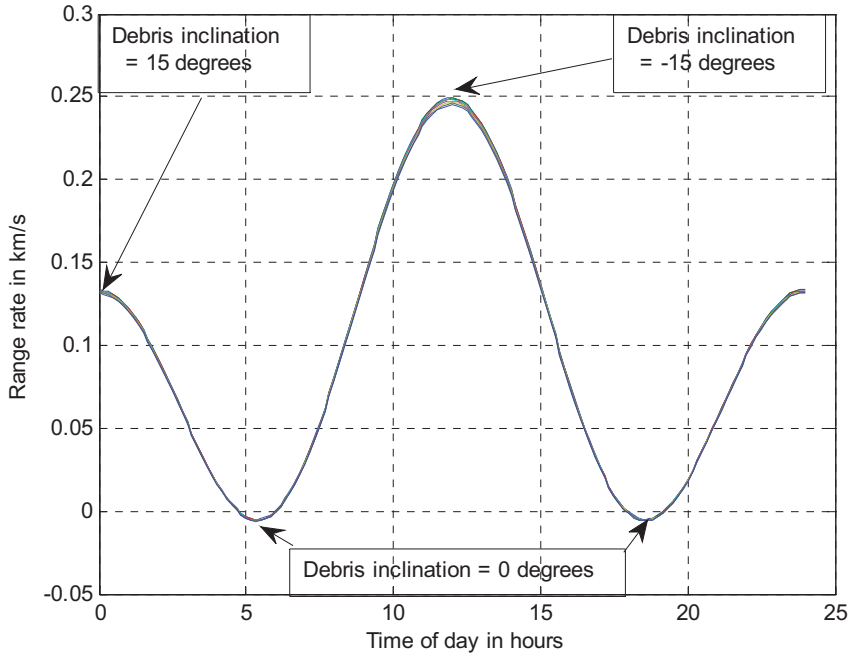

Figure 5: Radar measurements of debris range rate over one day

The relationship between radar range and range rate is shown in Figure 6 for a debris orbit plane drift rate of 2°/day west. The eight curves illustrate the observed range, range-rate behavior for debris whose initial longitudes are W 40°, W 45°, W 50°, W55°, W 60°, W65°, 70° and W 75°. In Figure 6, the curves corresponding to initial longitudes W 70° and W 75° are close enough that they are not readily distinguishable at this scale. The instantaneous debris inclination given by equation 3 is used in computation. Looking at the W 40° longitude curve, the graph starts a time t=0 and inclination 15° and continues for one sidereal day. The longitudinal drift of the debris orbit plane affects the measured range over time to yield the two traces whose common point is seen at inclination -15°.

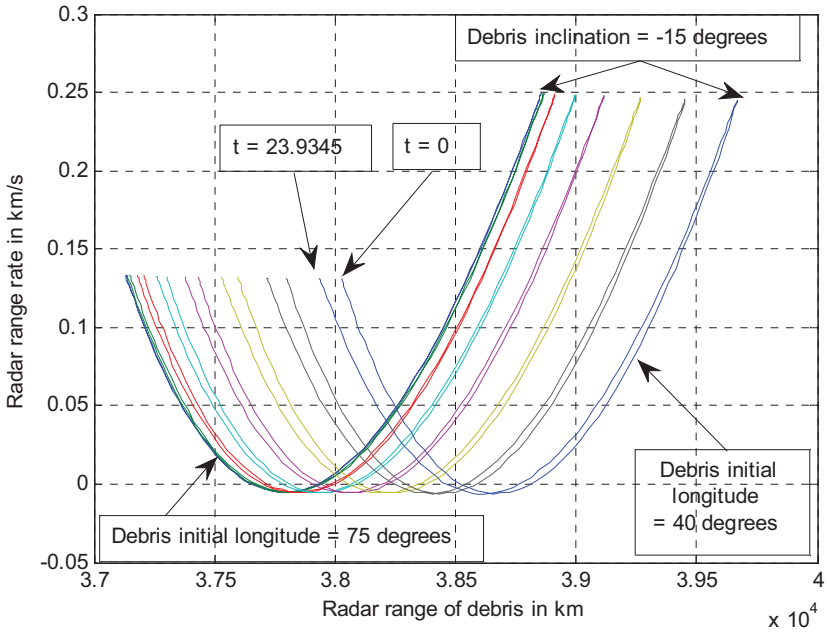

Figure 6: The relationship between radar range and range rate for initial debris longitudes between W 75° and W 40°

The longitude dependence of the debris range / range-rate relationship comes from the dependence of the radar range on the relative longitude of the debris. Measurements taken at the northern limit of the debris inclination one day apart provide a measurement of debris-orbit drift rate and drift rate. Measurements are best made when the longitude difference between the radar and the debris is large.

The time history of the radar range of the debris, shown in Figure 7, shows the sensitivity of radar range to both the debris inclination angle and the initial debris longitude. The same eight initial debris longitudes used in Figure 6 result in the vertically displaced curves in this view. The graph displays one sidereal day of debris range variation, starting and ending at debris inclination 15°.The maximum range occurs at debris inclination -15°. The drift if the debris orbit plane brings the debris closer to the radar at the end of the day when the debris starts more than 2° east of the radar longitude.

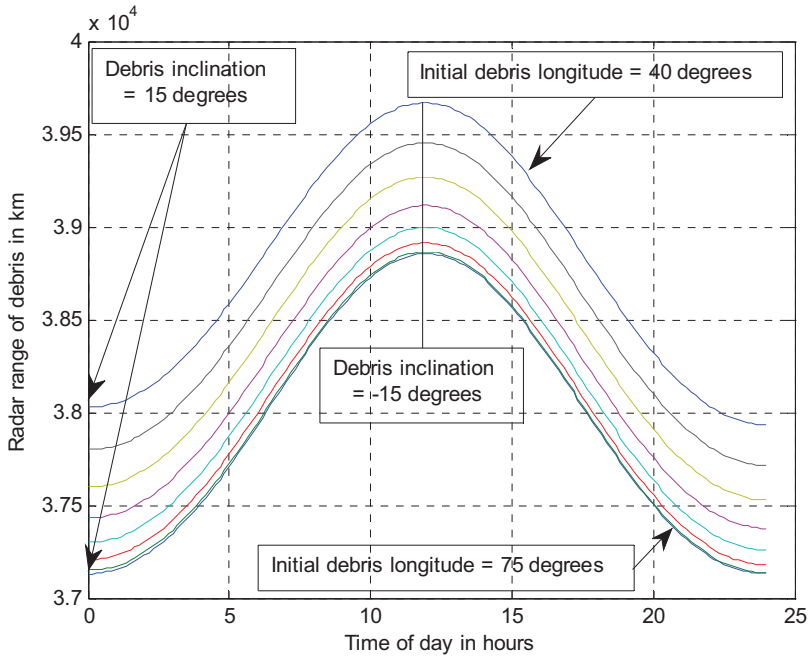

Figure 7: Time history of radar measurements of geosynchronous debris for debris initial longitudes between W 75º and W 40º when the radar is at N 45º and W 75º

Figures 8 and 9 show the radar elevation and azimuth angles needed to measure the modeled debris.

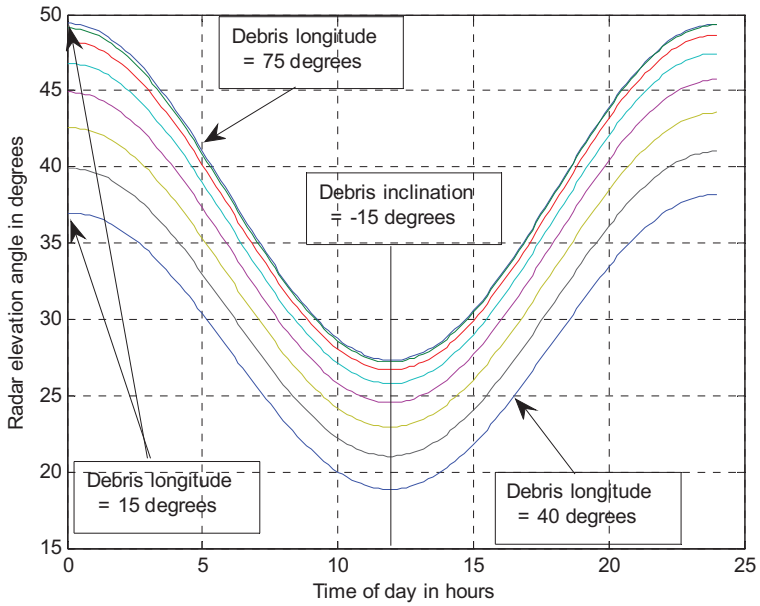

Figure 8: Radar antenna elevation angle required for debris measurements

Both graphs again use the same set of initial debris longitudes that were used for the previous figures. The radar elevation angle has maximum values when the debris is at the northern limit of its orbit at inclination angle 15°. The minimum radar elevation angle occurs when the debris is at the southern limit of its orbit. The largest elevation steering angle excursion, 24°, occurs when the initial debris longitude is

the radar longitude. The effect of orbit drift is most visible when the initial and final elevation angles for the W 40° curve are compared.

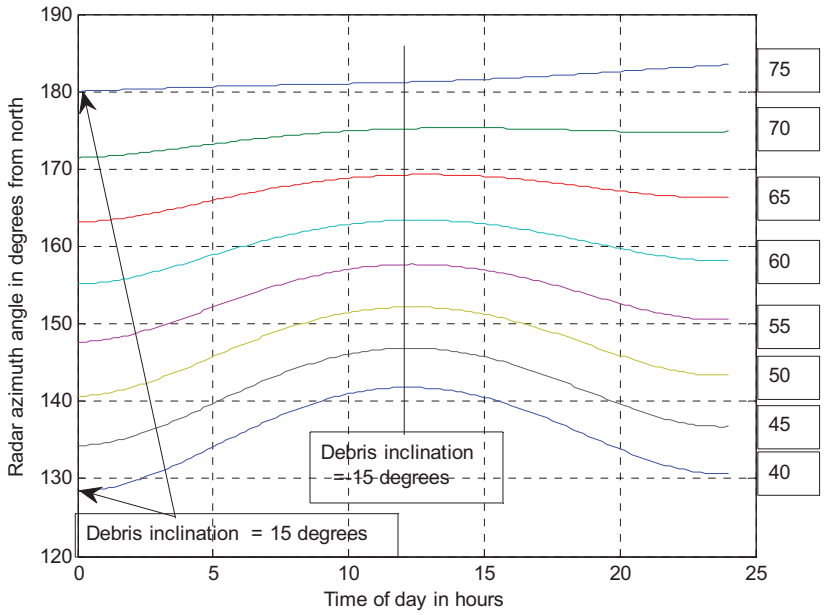

Figure 9: Radar azimuth angle (measured from north) required for debris measurements.

As expected, the radar azimuth angle is sensitive to the drift rate of the debris orbit plane and can be used to make debris orbit drift rate estimates over periods of several hours. The elevation angle is most sensitive to debris orbit drift rate when the initial debris longitude is close to the radar longitude. The numbers in the boxes at the right side of Figure 9 are the initial debris longitudes corresponding to each trace. The curves in Figure 9 span one sidereal day of debris motion and start and end at the northern limit of the debris orbit.

Figure 10 shows the time history of the debris zenith angle between the radar range vector and the debris position vector. The figure covers one sidereal day of debris motion for the same eight initial debris longitudes used in the previous figures. The zenith angle of the debris as seen by the radar is not very sensitive to either the initial debris longitude or to the orbital position of the debris. The maximum variation in debris zenith angle is approximately 2.1° for debris near the radar longitude.

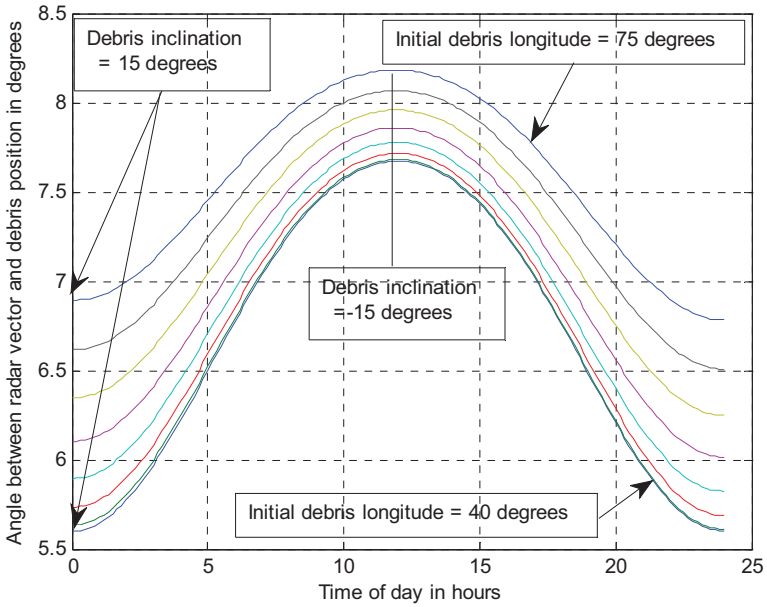

Figure 10: Time history of the debris zenith angle.

4.1.1 Bistatic observation geometry and experiments

Some work has been done to combine space surveillance radars with radio telescopes to form bistatic space observation radars. In 1993, the FGAN TIRA (34 M dish) radar was used with the Effelsberg radio telescope (100 m dish) to form a bistatic radar system [20], [22]. In this experiment, the two sensors were set up to observe a region centered at 850 km altitude. Theoretical predictions based on the experimental results of the 1996 Tira-Effelsberg COBEAM experiment [20], [22] suggest that the bistatic radar could observe targets with cross sections as small as -5 dBm^2 (0.6 m diameter sphere) at the minimum geosynchronous range. The radar and radio telescope are only separated by 20 km and enhancements to geosynchronous range performance is due to the gain and sensitivity of the radio telescope receiving system.

In a proof-of-concept experiment in 2002, the Algonquin Radio Observatory 64 m dish was used in conjunction with the Millstone Hill space surveillance radar (25.6 m dish) to form a small-angle bistatic radar system [23]. The satellite target for this experiment was MSAT which was stationed at W 106.4^o and was under full longitude and gravity perturbation control. The target range from the Millstone radar was 37751 km and the target range from the Algonquin observatory was 37581 km. The bistatic angle between the radar observation beams was 1.2486^o. The observation geometry is captured in Table 3 which was not included in [23] but is derived from report data.

A second, follow-on, proof of concept experiment [24] was run in 2003. In this case, the MIT Millstone Hill space surveillance radar was used as the transmitter and the Algonquin Radio Observatory (ARO) and the Dominion Radio Astrophysical Observatory (DRAO) (Near Penticton B.C.) radio telescopes were used as bi-static receivers. The selected targets were MSAT 1 and Intelsat-3. Table 4 lists the observation geometry parameters that were derived from data presented in [24].

Table 3: Experiment 1: Millstone Hill / Algonquin Radio Observatory bistatic radar

	Millstone Hill	Algonquin	MSAT 1 S23846
Latitude (deg)	N 42.46	N 45.9555	0
Longitude (deg)	W 71.49	W 80.9269444	W 106.4
Height (ASL) m	123.1	264.1060	
Earth center distance (km)	6268.5	6367.4	41264
Target range (km)	37751	37581	
Target azimuth (deg)	225.9779	213.5556	
Target elevation (deg)	29.5204	31.3133	
Target bistatic angle (deg)			1.2486
Zenith angle at target (deg)	7.7171	7.5624	
Beam width (3 dB) deg	0.62	0.40	
First beam intersection range (km)	26803	26682	
Last beam intersection range (km)	63871	63992	

Table 4: Experiment 2 Millstone Hill – Algonquin Radio Observatory and Millstone Hill – DRAO bistatic radars

	Millstone Hill	Algonquin	DRAO	MSAT 1 S23486	Intelsat 903 S27438
Latitude (deg)	N 42.46	N 45.9555	N 49.321	0	0
Longitude (deg)	W 71.49	W 80.9269444	W 119.624	W 106.4	W 34.5
Height (ASL) (m)	123.1	260.4	545		
Earth center distance (km)	6368.5	6367.4	6366.4	41264	41264
Target range (km) MSAT 1	37751	37581	37531		
Target range (km) Intelsat 903	37860	38608	41401		
Target azimuth (deg) MSAT 1	225.9779	213.5556	162.7726		
Target azimuth (deg) Intelsat 903	132.7757	125.9828	N/A		
Target elevation (deg) MSAT 1	29.5204	31.3133	31.8718		
Target elevation (deg) Intelsat 903	28.8357	20.8626	-5.079		
Target bistatic angle (deg) Algonquin				1.2486	0.5681

Target bistatic angle (deg) DRAO				5.6017	N/A
Zenith angle at MSAT 1 target (deg)	7.7171	7.5624	7.5138		
Zenith angle at Intelsat 903 target (deg)	7.8087	8.3145	N/A		
Beam width (-3dB) deg	0.62	0.40	0.51		

The MSAT geostationary communications satellite was visible to the radio telescope receivers in both experiments. As can be seen in Table 4, Intelsat-3 was below the radio horizon for the DRAO receiver.

An examination of the data in Tables 3 and 4 and Figure 10 provides the following information on the viability of bistatic observation geometries for monitoring geosynchronous space debris.

1. The bistatic angles observed at the target position are too small to provide much help in localizing the target in a plane normal to the radar range vector.
2. Bistatic observation geometry that uses sufficiently large receiver separation can be used to eliminate range-ambiguous targets that lie outside of the beam overlap region.
3. Geosynchronous object motion primarily lies on and near an annular sphere surface segment (± 15^{o} from the equatorial plane) and daily motion of objects in inclined orbits have primary components along the orbit inclination sphere shell on paths that are approximately normal to the local geostationary orbit axis.
    a. The radar zenith angle will vary with the temporal position of the target object in its orbit plane in a manner illustrated in Figure 10.
    b. Range rate measurements will depend on the inclined orbit phase and will be time of day dependent.
    c. The bistatic observation angles, while small, will allow the separation of some targets that are at the same range for one bistatic radar element.
    d. Bistatic observation zenith angle dependence does not significantly augment information that can be obtained from a monostatic radar.
4. The primary observational advantage to using a radio telescope to augment a monostatic radar is the receiver gain of the telescope if it is larger than the receiver gain of the radar.

Bistatic observation of geosynchronous objects using ground based systems offers few observational and measurement advantages.

4.1.2 A monostatic radar based on the Algonquin Radio Observatory

One approach to developing a deep-space radar at reduced cost is to adapt an existing radio telescope to include a radar mode and accept the observation time limitations inherent in it's primary use schedule. The most suitable Canadian site is the Algonquin Radio Observatory [25].

Since the Algonquin site longitude 80.9^{o} is relatively close to the Millstone Hill radar longitude, 71.5^{o}, the two radars would have a large spatial overlap in the geosynchronous belt. The burden sharing role of a part-time (shared use) Algonquin radar would be targeting small debris that is invisible to the Millstone

Hill radar and sharing geosynchronous belt observation tasks for other objects. Both radars would easily observe the geosynchronous belt libration point at W 105º which contains a number of Canadian communications satellites.

To minimize mutual jamming possibilities, the Algonquin radar should operate at a frequency not used by either the Millstone Hill radar or the Haystack and HAX radars that share the Millstone Hill site. The selection of 5.5 GHz would satisfy interference issues. A DRDC funded study performed by Cannon, [26] looked at an X-band option for the radio telescope upgrade.

If we choose a nominal radar frequency of 5.5 GHz and a nominal bandwidth of 10 MHz (15 m two-way resolution) and use the full surface of the Algonquin radio telescope reflector, the antenna aperture efficiency[1] would be 0.49, its beam efficiency[2] would be 0.73 [26] and its transmitter antenna gain, G_{Tx} would be 66.9 dB.

For ECEF coordinates we have the parameters in Table 5 for the cases:

1. The target is at the radar longitude.
2. The target is 45º east of the radar longitude.
3. The target is 45º west of the radar longitude.

Table 5: Target range and angle estimates

Case	**Parameter**	**Elevation Angle**	**Range**	**Zenith Angle**
Target longitude = W 80.9º (E 279.1º)	Geostationary orbit	37.17º	37104 km	7.0630º
	+ 15º geosynchronous orbit	53.6651º	37327 km	5.0780º
	- 15º geosynchronous orbit	21.7457º	39852 km	7.9758º
Target longitude = W 35.9º (E 324,1º)	Geostationary orbit	21.2882º	38524 km	8.2666º
	+ 15º geosynchronous orbit	33.9579º	38738 km	7.1177º
	- 15º geosynchronous orbit	8.8485º	41177 km	8.4884º
Target longitude = W 125.9º (E 234.1º)	Geostationary orbit	21.2882º	38524 km	8.2666º
	+ 15º geosynchronous orbit limit	33.9579º	38738 km	7.1177º
	- 15º geosynchronous orbit limit	8.8485º	41177 km	8.4884º

In Table 5, the Elevation Angle parameter is the radar antenna elevation above the local horizontal plane (equation 12) and the Zenith Angle parameter is the angle between the radar range vector and the target position vector at the target (equation 14). All elevation angles are within the antenna control range.

The analysis in Table 5 covers a 90º azimuth sector.

[1] The transmit aperture efficiency for a dish antenna captures the fraction of the antenna feed signal energy that intercepts the dish surface and includes electrical conduction losses on the dish surface.

[2] The beam efficiency of a dish antenna captures the fraction of the received signal energy illuminating the dish that is coupled to the antenna feed. For dish antennas, the transmit aperture efficiency and the beam efficiency values are different.

Noting that at least 16 dB SNR (Signal-to-Noise Ratio) after received-pulse integration is required to reliably estimate range rates [8, 20,and 28] assume:

1. The radar pulse length is 1 ms [20] and [28].
2. The radar PRF is 30 Hz [20] to 40Hz [27] selected for range.
3. The standard coherent integration length is (at least) 25 pulses to accommodate tumbling targets. The corresponding integration gain is 14 dB.
4. The radar can detect and measure range rates for a 30 cm sphere (-11.51 dBm^2) at the maximum range in Table 5.
5. The diameter of the instantaneous observation plane at 37000 km range is 31.8 km.
6. The antenna feed is a two-plane monopulse antenna. (There are four parallel receivers.)

Table 6 illustrates the link loss budget for the maximum and minimum range cases in Table 5.

Table 6: Algonquin radar link budget

Parameter	Target range 37104 km	Target range 41777km
Range spreading loss dB	-324.8	-326.8
Atmospheric loss dB	-0.18	-0.4
Target cross section dB	-11.5	-11.5
Transmitter feed loss dB	-2.5	-2.5
Transmit antenna gain dB	66.9	66.9
Receive antenna effective area ($A_{rec}\eta_{Beam}$) dBm^2	33.7	33.7
Receiver feed loss dB	-2.5	-2.5
(Noise power dBW @ Noise figure 3 dB)$^{-1}$	130.8	130.8
Received signal SNR / peak transmitted Watt in dB	**-110.88**	**-112.30**
Range compression gain dB	40	40 dB
Pulse integration gain for 25 pulses in dB	14	14
Peak transmitted power for 0 dB output SNR in dBW	**56.88**	**58.3**
Minimum acceptable output SNR	16	16
Minimum peak transmitted power in dBW	**72.88**	**74.3**

The proposed radar model requires a peak transmitter power of 27 MW due to the small number of integrated pulses and is marginally feasible. By relaxing the coherent integration requirement to allow a 256 pulse integration (6.4 second integration time at 40 Hz PRF) that has been used by some systems [15] and [16], the peak power requirement can be reduced to 2.7 MW. The design and construction of a 2.7 MW 5.5GHz transmitter that has a 3% duty cycle is feasible with available coherent transmitter technology and with current engineering practice.

Much of the analysis presented in [26] can be applied to a more detailed study of this option.

The cost of modifying the Algonquin Radio Observatory to create a deep-space radar has not been estimated in detail but should be in the vicinity of $10 M (somewhere between $5 M and $10 M is a reasonable guess). There is an on-going operating cost that cannot be estimated until an operating plan is proposed because of the shared use of the facility as a radio observatory. Since the deep-space radar function would be a secondary mission for the ARO, the available operating time per year would be limited.

4.1.3 A monostatic, purpose-designed dish radar

Given the usage constraints of the Algonquin Radio Observatory, it may be advantageous to consider the construction of a dish-antenna radar that is specifically designed for geosynchronous belt satellite and debris observations. Depending on external interest and the planned primary mission observation schedule it may be feasible to engage others to share the construction and operating costs by allowing some dedicated radio astronomy observation time as a secondary mission.

If a purpose-built system is considered, both the antenna design and the location of the instrument become system design choices.

If the Effelsberg radio telescope antenna (100 m diameter) is used as a model, the transmitting antenna gain and effective receiver aperture (Table 6) scale to, 70.8 dB and 37.6 dBm^2 respectively to yield a reduction in peak power from 2.7 MW to 432 kW for a 256 pulse averaging process. At this power level, the transmitter development is reasonably straight-forward using current technology, however, the dish construction cost is expected to be significant.

The geostationary belt observation strategy required for a deep-space radar of this type is similar to those used for the Mill Stone Hill and the ALTAIR instruments. The diameter of a staring mode observation plane at 37000km range would be approximately 20.4 km which provides a reasonable spatial resolution for debris localization and debris orbit parameter estimation with repeated observations but can pose some challenges for initial detection of debris items.

A CSA (Canadian Space Agency) study for an S-band LEO (Low Earth Orbit) debris monitoring array [27] selected a CFB (Canadian Forces Base) Suffield site at N50.2966^o, W 111.0660^o for its relative security and low RF background noise. The W 105^o geosynchronous orbit libration point, that is used by many Canadian geostationary satellites, is readily visible from the Suffield site. The Suffield site field of view bridges the geostationary belt segments that are observable from both the Mill Stone Hill and the ALTAIR radars and could provide a useful addition to the geostationary belt observation coverage.

The fully instrumented Effelsberg radio telescope cost 34M DM to build in 1972 [28]. A similar instrument, the Robert C Byrd Green Bank radio telescope, cost $88M to build in 2001[29]. Since the Green Bank radio costs include specialized radio astronomy receiving facilities that are not needed for the primary deep-space radar mission, the total cost of a dedicated deep-space radar should be comparable to the Green Bank facility. When costs are adjusted for inflation and constraints imposed by Canadian regulations the deep-space radar construction costs would be between $100 M and $150 M in 2020.

A rough guess at the operating and maintenance costs of an instrument of this type is between 5% and 10% of the development cost per year for an instrument that has a 20 year design life.

4.1.4 A monostatic electronically-steered array radar

A viable alternative to ground based dish radars for geosynchronous orbit debris observation is a planar-array radar that is conceptually similar to the AN/FPS-108 (Cobra Dane) instrument [36]. Given the current availability of C-band TR (Transmit-Receive) modules it is suggested that a C-band instrument would be a viable option and could be readily adapted for LEO, MEO (Medium Earth Orbit) and geosynchronous orbit debris monitoring applications. The major design driver will be the deep-space operating modes.

Applying the calculations used to generate Tables 3 and 5 we have the observation geometry results shown in Table 7. From the data in Table 7, if geosynchronous belt debris is the primary task of the radar, the antenna array needs to be able to steer the radar beam over 43° in elevation and 90° in azimuth. To minimize the control range, the planar array would be south facing (centered at 180° north angle) and would have the planar face inclined at 27.25° from the local vertical. The beam steering range would be ±21.5° in elevation and ±45° in azimuth.

Noting that observation of the -15° limit of gravitationally controlled geosynchronous orbit inclinations at azimuth angles approaching ±45° require radar beam grazing angles approaching 5.7°, multi-path control measures will be required. These can take the form of beam elevation pattern side-lobe control through element phasing and multi-path fences on the south side of the array.

Table 7: CFB Suffield electronically steered array geosynchronous belt observation geometry

	Radar	Targ. 1	Targ. 2	Targ. 3	Targ. 4	Targ. 5	Targ. 6
Latitude	50.2966						
East longitude	248.934	248.934	248.934	248.934	293.934	293.934	293.934
Height above geoid (m)	770						
Earth centre distance (km)	6366.3	41264	41264	41264	41264	41264	41264
Orbit inclination angle (deg)		15	0	-15	15	0	-15
Radar range		37630	37500	40307	38919	38794	41514
Radar elevation angle		48.7520	32.408	17.1778	31.8563	18.5585	5.7414
Radar beam azimuth angle		180	180	180	118.1387	127.5474	135.0705
Target zenith angle		5.6514	7.4842	8.2040	7.2883	8.4102	8.5465

For a planar-array radar, the antenna element spacing controls the generation of grating lobes as the radar beam is steered. The azimuth steering range of ±45° requires a maximum element spacing, d, of

(17) $$d = \frac{\lambda}{1+\sin(45)} = 0.585\lambda$$

for radar wavelength, λ. At 5.5 GHz, λ=0.0545 m and the maximum azimuth element spacing is 0.0319 m. For elevation beam steering over ±21.5°, d=0.732λ and the maximum allowable spacing is 0.04 m. Given the need to approach low grazing angles (and possibly use electronic side-lobe control), the analysis will be based on a 0.0319 m radiating-element spacing for both azimuth and elevation.

Scaling the results in Table 6 (as modified for 256 pulse integration) in terms of the power-aperture product, $PA = P_T\sqrt{A_{Te}\,A_{Re}}$ where P_T is the peak transmitted power, A_{Te} is the effective transmitting antenna area and A_{Re} is the effective receiving antenna area, the Algonquin radar option has a minimum power-aperture product of 3.1069×10^9 Wm^2 (when the antenna transmit and beam efficiencies are taken into account) to measure a 0.3 m diameter sphere at 45° longitude displacement from the radar. Using the same figure for a 30 m x 30 m planar array with the required geosynchronous belt beam steering range, the broadside power aperture needs to be increased by $(\cos(21.5)\cos(45))^{-1}$ to compensate for the angular dependence of the antenna array surface projection. The minimum power-aperture product for the array is 4.7224×10^9 Wm^2.

Using a nominal 30 m x 30 m antenna surface, the generated transmitted power needs to be 7.00 MW when the planar array radiation efficiency of 0.75 is included. With a radiating element spacing of 0.032 m there are 8.84425 x 10^5 radiating elements over the array surface. To meet the power requirement, each element needs to use a single transmit-receive (TR) module that generates 8.44 W of RF power. 10 W TR modules have been developed for space applications and are readily adapted for surface radar use. Phase control on transmit and amplitude and phase control on receive in each TR module will provide beam forming and steering control.

The beam steering operation requires true-time-delay between blocks of TR modules where the block size depends on the steering angle range and the bandwidth of the RF pulse. The block dimension, D is determined by the relationship $D \leq 0.1\frac{c}{2W}\cot(\theta)$ where c is the speed of light, W is the radar pulse bandwidth and θ is the maximum steering angle. A radar bandwidth of 10 MHz and a maximum steering angle of 45^{o} results in a block dimension, D, of 1.5 m for azimuth steering. Similarly, for elevation steering, the block dimension is D=3.8 m.

If the radar bandwidth is constrained to 10 MHz and the steering requirements are constrained to $\pm 45^{o}$ in azimuth and $\pm 21.5^{o}$ in elevation, the antenna surface must be partitioned into 600 1.5 m x 3.75 m tiles and each tile must have a true-time-delay control. A possible implementation of this architecture is to design the system so that each tile contains a separate exciter and receiver both of which have coherent local oscillators and distance-compensated timing controls and have digital signal feeds and outputs. Time delay is then implemented by digital signal processing.

If an extended radar bandwidth is required for other applications such as LEO debris tracking there is a trade-off between the tile size (and number) and the radar scan angles allowed.

Current deep-space dish radars use right-hand circular (RCP) antenna feed polarizations. The polarization is preserved over the radar observation angles by the fact that the feed, the dish surface and the radar beam are fixed with respect to each other. In a planar array, the radiating surface is fixed and the beam is steered. In this case a circular polarization along the antenna bore-sight becomes an elliptical polarization at all other beam angles. For a planar array, each element requires two, well isolated linearly polarization feeds that can either be used to generate linearly polarized signals or can be combined electronically to create circularly polarized signals in the radar beam direction. For simplicity, a linearly polarized transmit signal is proposed and dual, linear (H and V) polarized signal receivers are proposed. This is a standard configuration for the current generation of TR modules.

By implication, each radiator requires two linear polarization feeds that can be selected for signal transmission and are in simultaneous use for signal reception. Each TR module requires two receive channels and each tile-based receiver requires two full receive channels.

For full array performance, the radiated signal phase fronts need to be flat to within 10% of the radar wavelength when projected back to the antenna surface. This can be achieved by mechanically controlling the planarity of the radiating array to within 0.1λ or by electronically adjusting the phases of the radiating elements and the antenna tile delays using external planarity measurements. A trade-off study is required to determine the best implementation.

The discussions in the previous section can be flowed down to a set of high level requirements shown in Table 8 to form a starting point for system design considerations.

The radar requirements outlined in Table 8 can be met using currently existing technology. Noting the large antenna size, the need for large numbers (884000) TR modules and radiating elements and the precision mounting requirements for these, this radar system could be expected to cost somewhere in the vicinity of $1.5 B.
As with the steered dish-antenna option, a best guess of nominal operating cost (including all operating, maintenance and evolutionary upgrades) would be between 5% and 10% of the development cost per year.

Table 8: Nominal, high-level radar implementation requirements

Parameter	**Nominal value**	**Comments**
Primary mission	Geosynchronous belt debris	Secondary missions could include MEO and LEO debris detection and tracking
Radar Frequency (GHz)	5.5	
Radar bandwidth (MHz)	10	The could be higher bandwidth beams for other applications
Transmitted signal waveform	Linear FM	
Pulse repetition frequency	40 Hz	
Radar pulse length (s)	.001	
Transmitter duty cycle %	4	Maximum value
Azimuth steering angle (deg)	±45°	
Elevation steering angle (deg)	±21.5°	
Transmitter power-aperture product (Wm^2)	4.7224×10^9	
Antenna bore-sight elevation (deg)	27.5	
Antenna bore-sight azimuth (deg)	180	
Minimum beam grazing angle (deg)	5.7414	
Array type	Rectangular, planar	
Array width (m)	30 m	
Array length (m)	30 m	
Maximum planarity deviation (m)	0.0054	Combined mechanical and electronic control
Radiating element spacing (m)	0.0319	
Number of radiating elements	8.84425×10^5	
Radiating element polarization	H and V linear	Subject to trade-off studies
Number of TR modules	8.84425×10^5	
Number or TR receiver channels	2	
RF power generated power TR module (W)	10	Standard available component
Total RF power generated (MW)	8.845	
Radiated power (MW)	6.633	
Number of antenna tiles	600	Subject to low earth orbit application decisions
Tile dimensions (m x m)	1.5 x 3.75	Subject to low earth orbit application decisions
Number of receivers	600	Subject to low earth orbit application decisions
Number of receiver channels per tile	2	
Thermal dissipation (kW) estimated from TR module, receiver, exciter and digital component efficiencies with 100% margin	500	Does not include control and processing or environmental power requirements

4.2 Geosynchronous object observations by space-based radars

The radar power-aperture constraints for the observation of small (30 cm sphere with a radar cross section of -11.7 dBm^2) space debris items in the geosynchronous orbit belt require that the radar be located in or near the geosynchronous belt. Low earth orbit radars designed for this purpose are subject to the same power-aperture constraints, and thus similar antenna size and transmitted power constraints as ground-based radars due to the comparable radar ranges of the debris for the two cases. Two high earth orbit possibilities are considered:

1. A radar system is mounted on a geostationary satellite as a secondary payload and observe debris in the immediate vicinity of the radar platform, or
2. A dedicated radar satellite is flown near the geosynchronous orbit belt at sub-geostationary orbit radius and scans a geosynchronous belt band near the earth's equatorial plane with repeat scans occurring every 14 to 24 days.

4.2.1 Auxiliary radar sensors on geostationary satellites

If the debris-monitoring radar system is carried on a geostationary satellite as an auxiliary sensor, the relative motions of debris items with respect to the satellite platform need to be modeled to estimate the radar properties and parameters. Some simple debris motion model calculations are presented in Annex A. The models examine the observation geometry for a debris field that may exist in the vicinity of the geostationary radar platform from the vantage point of the radar platform and extract range, range rate and observation angle requirements based on simple descriptions of the satellite and the debris orbits. The results obtained are applicable to a large range of real cases.

4.2.1.1 Debris motion summary

The model calculations in Annex A are based on a local coordinate system that is attached to the satellite radar platform where the X axis is defined to be parallel to the outward projection of the satellite position vector, the Y axis is defined to be in the direction of the satellite velocity vector for a circular orbit and the Z axis is defined to be parallel to the satellite orbital angular momentum vector.

The orbit of the satellite that carries the radar is assumed to be perfectly circular and to be at the geostationary radius of 42164 km. Perfect station keeping is assumed but is not required for the results to be valid. The inclined debris orbit results will be valid for geostationary satellite orbit eccentricities up to 0.005, subject to the relationship between the arguments of perigee of the satellite and debris orbits. The general case of inclined, elliptical satellite orbits and inclined, elliptical debris orbits have not been studied here.

The modeled conditions in this document consider the cases where the debris passes within 10 km of the satellite. Two major conditions are examined:

1. The debris orbit eccentricity matches the satellite orbit eccentricity and the debris orbit is inclined with respect to the satellite orbit. This case is modeled in terms of the intersections of two, relatively inclined, circular orbits.
2. The debris orbit eccentricity differs from the satellite orbit eccentricity and the relative inclinations of the two orbits are smaller than 0.05^{o}. This is the coplanar orbit case.

Model calculations for both cases include the effects of the drift rate of the debris orbit plane. Emphasis is placed on observations made by a radar that has a 250 km effective range for the smallest debris objects that can be reliably measured.

Results for the inclined orbit modeling show that:

1. Radar observations can be constrained to a spatial volume that is within 3° of the X,Z plane for radar ranges that are greater than 50 km.
2. The angle between the radar range vector and the Y axis is only significant as the debris passes the satellite and depends on both the separation of the orbit crossing point and the radar and on the debris orbit drift rates.
3. Measurements of the radar range and range-rate (debris radial velocity) during the periods that the debris approaches and recedes from the radar can be used to estimate:
    a. the debris orbit inclination angle,
    b. the debris orbit drift rate, and
    c. the distance between the satellite and the point where the debris crosses the satellite orbit.

    The debris orbit drift rate estimate errors using this measurement approach are largest for small drift rates for all inclination angles.
4. Measurements of the radar range and the angle between the radar range vector and the Z axis can be used to estimate debris orbit drift rates at debris orbit inclination angles less than 4° and can be used to measure the distance between the satellite and the debris orbit crossing point.
5. Available observation times for debris approaching from 250 km range vary from approximately 5 minutes for a debris orbit inclination of 15° to approximately 83 minutes for a debris orbit inclination of 1° when the debris orbit drift rate is 10°/day. There will be two observation opportunities per day.

Results for the modeling of variable eccentricity, debris orbits that have small inclination angles (<0.5°) with respect to the satellite orbit show that:

1. Radar range and range-rate observations provide a sensitive measure of the relative eccentricity of the debris orbits.
2. Range/range-rate measurements for ranges less than 50 km allow the distance between the satellite and the debris orbit crossing point to be measured.
3. Measurements of the radar range and the angle between the radar range vector and the X axis are not sensitive to the debris orbit eccentricity but allow estimates of the closest approach of the debris to the satellite (the debris orbit crossing point distance).
4. Measurements of debris radial velocity and the angle between the debris range vector and the Y axis while the debris passes the satellite allow direct measurement of the debris orbit drift rate.
5. Available observation times for approaching or receding debris vary from approximately 15 minutes for an orbit eccentricity of 0.03 to approximately 5.5 hours at an orbit eccentricity of 0.007. Depending on the radar's maximum range along the Y axis, debris orbit drift rates smaller than 0.3°/day will permit two observations of the debris orbit during one day. Debris orbits that have eccentricities less than 0.006 will be observable by the radar all day, every day.

For all cases modeled, debris tracking during the measurement process is important and measurements made on both approaching and receding debris allow the debris orbits to be estimated with reasonable accuracy.

4.2.1.2 Geostationary satellite clusters

In recent years it has become a common practice to expand the number of active geostationary satellites by placing several satellites into one 0.1^{o} or 0.05^{o} of longitude station-keeping box [30]. This is accomplished by controlling the satellite orbit eccentricities and arguments of perigee so that they circulate about the nominal geostationary orbit center point [30 and 31] in the X, Z plane defined in the previous section and in Annex A. If one of the satellites in a local cluster of this type carries a debris monitoring radar, the radar control needs to know the relative positions of the other satellites to schedule its debris search and tracking operations. Alternatively a low-power radar mode can be used to monitor the relative positions of the local satellites and the measurements made by this radar mode can be used to aid station keeping management.

4.2.1.3 Radar design considerations

The geostationary satellite radar system needs to:

1. confirm and predict the positions of the satellites in its local cluster so that it can schedule its debris search and tracking observations (Coordination of satellite station keeping operations between members of a local cluster can be used to optimize the debris search problem.);
2. estimate the debris orbit with sufficient accuracy that avoidance maneuvers can be scheduled when required; and
3. generate debris orbits and debris radar cross section estimates for transmission to the ground systems that compile and maintain debris catalogues.

Monitoring debris in the presence of a local satellite cluster suggests that there is a low-power, directional observation radar function that must be active for one or more short periods each day and a higher power limited angle radar function that must be active for many time intervals each day.

The radar controller must maintain a regularly updated model of the relative positions of all satellites in its cluster to schedule high-power operations.

Since know debris (and suspected unknown debris) is spatially sparse in the geosynchronous orbit belt, the radar system can regularly search for previously un-observed debris and activate a debris tracking or orbit modeling operation only if something of interest is found. Most of the operating time will be spent in search mode.

A crude definition of the radar properties follows. This is a very preliminary look at the radar design problem and it is expected that significant simplification is possible.

4.2.1.3.1 Radar frequency considerations

The radar frequency must be selected so that the debris search radar does not interfere with the primary functions of the satellite platform or with any other satellite in the field of view of the radar. Radar operating frequencies in the X or Ku bands are probably the most suitable from a cost point of view. Higher frequencies may be required from an interference point of view. Detailed trade-off studies are required to examine useful spectral windows and to examine inter-modulation interference issues for surrounding satellites.

4.2.1.3.2 Radar antenna system requirements

To monitor satellites in the local cluster, the radar requires one or more dual monopulse antennas (to allow angle measurements in two orthogonal directions) mounted on the X and/or Z faces of the satellite bus. The number that is chosen depends on the observation scheduling to be used. Nominal beam widths 22.5^{o} on transmit and 45^{o} on receive are suggested. This yields a two-way monopulse gain of approximately 50 dB when losses are considered.

To monitor debris, the radar requires:

1. one monopulse antenna on each of the +Z and –Z faces of the satellite bus to monitor debris position and orbit inclination angle (by range and range rate measurements) and signal angle of arrival (to estimate orbit crossing proximity),
2. one monopulse antenna on each of the +X and –X faces of the satellite bus to monitor debris position, debris orbit eccentricity, debris orbit drift rate (range and range rate measurements) and signal angle of arrival (orbit crossing proximity), and
3. one monopulse antenna on each of the +Y and –Y faces of the satellite bus to monitor debris orbit drift rate.

In total, six antennas are required for debris monitoring and each antenna has two receive output channels. Since the relative approach speeds of debris objects are less than 900 m/s, the receive antenna outputs can be multiplexed into either two or four physical receiver channels.

The antennas mounted on the X and Z faces of the bus are nominally identical array antennas that have a beam width of approximately 3^{o} in the narrow beam direction and two contiguous apertures with approximately 30^{o} beam width in the wide beam direction (the two-way antenna gains are approximately 60 dB for each receive aperture). The two antennas that are mounted on the ±Z faces of the satellite bus have their long dimension parallel to the Y axis of the bus and the two antennas that are mounted on the ±X faces of the bus have their long dimension parallel to the Z axis. The antennas that are mounted on the ±Y faces of the bus are two-aperture array antennas that consist of two single element wide columns whose long-axis beam widths are approximately 10^{o} and whose two-way gains are approximately 40 dB. These antennas are mounted with their long direction parallel to the Z axis.

4.2.1.3.3 Transmitter power requirements

The radar mode that monitors the positions of satellites in the local cluster is looking for objects with approximate radar cross sections that are greater than 10 dBm^2 at ranges that do not exceed 20 km. It is assumed that a processed signal to noise ratio of 20 dB provides sufficient accuracy for signal angle-of arrival estimation. Assuming: 10 MHz bandwidth, 40μs, LFM coded transmitted pulses, 1000 Hz pulse repetition frequency, and integration over bursts of 100 pulses, the radar equation calculation in Table 9 yields a required peak transmitter power of 35.5 W and an average transmitted power of 1.42 W.

Assuming that a set of 100 pulse bursts provides sufficient measurement accuracy, this radar modes needs to operate for durations of ten seconds up to six times per day.

Table 9: Peak transmitter power requirements for satellite cluster monitoring

Signal to noise ratio dB	20
Receiver noise figure dB	5
Thermal noise power dBW	-133.8
$(\text{range})^4$ dBm^4	172
$(4\pi)^3$ dB	33
$(\text{two-way antenna gain})^{-1}$ dB	-50
$(\text{target cross section})^{-1}$ dBm^2	-10
$(\text{radar wavelength})^{-2}$ dBm^2	25.3
$(\text{range compression gain})^{-1}$ dB	-26
$(\text{coherent burst processing gain})^{-1}$ dB	-20
Peak transmitter power (dBW)	**15.5**

The debris detection and measurement radar modes have two functions:

1. Detect the presence of debris at maximum range and
2. Measure the orbital parameters of the debris with respect to the radar platform.

The debris search problem is influenced by the possible presence of range-ambiguous targets within the radar beam. A radar pulse repetition frequency of 100 Hz places the ambiguous range at 1500 km. If the radar is designed for 250 km range with a target cross section of -11.5 dBm^2 ambiguous targets must have radar cross sections greater than 19.6 dBm^2 to be confused with a real target at 250 km range whose cross section is -11.5 dBm^2. Such ambiguities will be seen but will have very different range/range-rate histories and these histories can be used to identify them.

For detection, choose a peak pulse power of 2 kW, a pulse length of 40μs, a LFM pulse bandwidth of 10 MHz, and a pulse repetition frequency of 100 Hz. After pulse compression, incoherently integrate 1000 pulses (10 seconds of data) in overlapping blocks of 54 range samples and test the results against a 10 dB detection threshold. If this process is repeated four times and the detection pattern moves as expected, a new target is declared and the radar switches to a pulse tracking mode. Larger targets at the detection range will return stronger signals and can be recognized by their detected signal magnitudes. The initial search process is the same for the antennas mounted on the Z faces of the bus and for those mounted on the X faces of the bus.

For debris object tracking and orbit parameter estimation, time histories of radar range, range rate and angle of arrival need to be accumulated and compared to an internally generated debris orbit model. The process needs to be adaptive and may use several observation time blocks to create a stable orbit model. Further work is required to create the computational models.

4.2.1.3.4 Radar scheduling considerations for debris monitoring

From the discussions in Annex A, the debris observation windows are sufficiently long that the radar can sequence through its set of antennas in a cyclic manner that takes into account known debris objects in its field of view. Debris searches along the ± Z axis have the fastest debris search cycle rates (every two minutes) and debris searches along the ± X axis have the lowest search cycle rates (every 10 to 12 minutes). When no debris has been detected, the repeated search operations are the only radar activity.

When a debris object is in the satellite field of view, the radar controller executes a debris tracking mode which adapts the radar measurement activities to the estimated location and motion parameters of the detected debris. The debris tracking operation makes the measurements required to establish (or refresh) debris orbit parameters. Upon completion of orbit parameter estimation, the controller returns the radar to the debris search (detection) mode.

4.2.1.3.5 On-board computing

Since the radar is a secondary sensor in the satellite payload, its use of communications bandwidth must be tightly constrained to minimize conflict with the primary payload. In addition, the long propagation time from the satellite to the earth and the need for local interactive control favors minimum lags between radar observations and radar mode adjustment. On-board computing is favored for radar management and data reduction.

Although the radar has multiple operating modes, it is a relatively simple device. The most complex system component is the on-board computing system which must be capable of autonomous operation in detecting debris targets, tracking the targets, computing and adapting orbit models and managing the target property estimation process. Although the average computational load is low there will be intense bursts of activity to interactively manage the radar functions on the basis of debris models developed from observations.

The on-board computer develops and retains orbit models for the observed debris items and packages debris orbit information for transmission to the ground.

The radar operations and the data processing and analysis functions need to be closely linked and must make autonomous decisions based on the observed target environment. The control software design could be challenging.

4.2.1.3.6 Radar property summary

A geostationary satellite-based debris-surveillance radar detects and monitors debris objects that approach within 250 km of the radar's platform satellite and needs to perform three groups of operations:

1. measure and maintain a model of the positions of the satellites in the local satellite cluster that it resides in and track satellites that transit through its assigned, geostationary, longitude block,
2. detect debris objects as they approach the radar platform satellite, and
3. track the detected objects to issue satellite position adjustment warnings and to establish debris orbit parameters.

A first look at the debris detection and tracking radar suggests that it requires six debris tracking antennas of two different designs that need to be time multiplexed into a single radar equipment block. The radar has multiple modes that are managed by a control and data analysis computer, which must operate autonomously.

Most of the radiofrequency and radar instrumentation equipment can be built using current technology. The transmit antenna switching design will require some innovative work to manage losses and to have a sufficiently long design life. The computing equipment can be based on currently available technology but the measurement and control algorithms and their optimization will require extensive engineering design study.

No estimates of the probable cost, mass and power requirements have been attempted. It is noted that the geostationary satellite platform will be in the earth's shadow approximately 35 minutes per day and the satellite requires sufficient battery capacity to support debris search radar operation during this period.

4.2.2 Geosynchronous belt observation radars at sub-geosynchronous altitudes

4.2.2.1 Orbit radius considerations

A debris search and tracking radar that is mounted on a geostationary satellite can provide good debris coverage for debris that is within a few hundred kilometers of the radar platform but provides no information on the whole geosynchronous belt debris field. An alternative space-based radar design approach is to employ a purpose-built, free flying radar satellite that orbits just inside the geostationary orbit ring. Noting that the orbital period for any elliptical orbit with semi-major axis length A is

(18) $$p = \sqrt{\frac{4\pi^2 A^3}{GM}}$$

where GM=3.986005 x 10^{14} m^3/s^2 is the earth's gravitational constant. Using the geostationary orbital radius, A = 42164 km, and defining p = one sidereal day or 23.9345 hours, the time required for a satellite in circular orbit with radius R_S = A-Δ to scan the geostationary belt is

(19) $$T_{scan} = p\left(\frac{1}{1-\sqrt{\left(1-\frac{\Delta}{A}\right)^3}}\right)$$

as shown in Table 10.

Table 10: Geostationary belt scan time in days

Δ in km	**T_{scan} in days**
500	56.4
1000	28.3
2000	14.2
3000	9.6

Choosing 14.2 days as a reasonable scan repetition rate, the radar satellite orbits 2000 km inside of the geostationary ring and makes radar observations over a 25.35º segment of the ring each day. This scan rate corresponds to a geostationary ring scan rate of 1.056º or 777 km per hour.

Choose the earth's equatorial plane as the radar satellite orbit plane. In this plane, the minimum and maximum radar ranges to the geosynchronous protection belt are 1800 km and 2200 km respectively.

4.2.2.2 Radar design considerations

4.2.2.2.1 Antenna concept

Design the satellite antenna so that it has a ± 20º electronic scan capability along one axis and a 5º electronic scan capability along the orthogonal axis and orient the antenna so that the large scan axis is orthogonal to the equatorial plane. Design the antenna to have four equal receive apertures arranged as orthogonal pairs to provide angle of arrival measurements for the returned signals. An active phased array radar design is probably the best choice for the antenna design and current technologies limit these to X-band frequencies and below for high-power radars.

The proposed antenna concept will allow the radar to continuously monitor debris whose orbit inclination angle is 1º or smaller. Debris whose orbit inclinations are greater than 1º will only be observed when it is within approximately 730 km of the geostationary orbit plane and within the radar beam.

4.2.2.2.2 Working swath and pulse repetition frequency

Since the radar is designed to detect and determine orbital parameters for debris items, select a radar bandwidth of 10 MHz (15 m resolution). The maximum and minimum target ranges are 2340 km and 1800 km respectively and the working swath width is 450 km for measurements through the geostationary protected belt. If a single waveform is used for radar transmissions, the maximum pulse repetition frequency is 300 Hz to prevent range ambiguities from occurring in the measurement swath. If two, orthogonal (e. g. different center frequencies) waveforms are used on alternate pulses either the pulse repetition frequency or the range ambiguity distance can be doubled.

From the analysis in Annex A, debris whose orbit plane inclination is near 15º crosses the equatorial plane at 800 m/s. The radar sampling rate needed for swath coverage is too small for use in direct Doppler measurement of fast moving debris but the choice of ±5º steering along the geostationary belt direction does allow adaptive dwell times of up to 26 minutes to acquire range and angle of arrival histories needed to create an orbit track.

4.2.2.2.3 Transmitted power and antenna aperture

To constrain the range of choices and to keep design considerations near current technology levels, fix the antenna radiated power density at 392 W(peak)/m^2 which is nearly double the power density of the RADARSAT-2 and RCM systems. Because of the four aperture receiving antenna constraint, the receiving antenna gain is 25% of the transmitting antenna gain. Noting that the mean duty cycle for RADARSAT-2 is approximately 2.8% when cooling time is included, and that the geosynchronous belt observation radar needs to operate continuously (this is the worst case), and noting that the debris surveillance radar duty cycle will need to approach 10% (300 μs for 300 Hz PRF) to accommodate the required range interval, antenna cooling will be a significant issue to address.

Choose a nominal C-band operating frequency of 6.0 GHz. Choose a signal to noise ratio after signal processing of 16 dB for a debris target with radar cross section -11.5 dBm^2 to allow reasonable estimates of target parameters.

Using the radar equation to estimate the required post range-compression processing gain required we have the results shown in Table 11.

Table 11: Processing gain requirements for radars with 40 m^2 and 50 m^2 antennas that are divided into four sub-apertures on receive.

Antenna area (m^2)	**40**	**50**
Signal to noise ratio (dB)	16	16
Receiver noise figure (dB)	5	5
Thermal noise power (dBW)	-133.8	-133.8
$(\text{range})^4$ (dBm^4)	253.7	253.7
$(4\pi)^3$ (dB)	33	33
$(\text{radar wavelength})^{-2}$ dBm^2	26.0	26.0
$(\text{two-way antenna gain})^{-1}$ (dB)	-100.1.	-102.0
$(\text{target cross section})^{-1}$ (dBm^2)	11.5	11.5
$(\text{range compression gain})^{-1}$ (dB)	-34.8	-34.8
$(\text{Peak transmitter power})^{-1}$ (dBW)	-42.0	-42.9
burst processing gain required (dB)	34.5	31.7

The large burst processing gain needed to provide sufficient signal-to-noise for small target detection and measurement suggests a need for a moving-target coherent integration strategy that can accommodate sampling ambiguities. The antenna beam steering range can be used to mitigate the sampling ambiguity problem. This is a development area. The results in Table 11 show that a 50 m^2 antenna is preferred and that a coherent burst length of at least 1479 pulses (4.93 seconds of observation time at 300 Hz PRF) will be needed to detect a 30 cm diameter debris target at maximum range.

Alternatively, the satellite can be moved closer to the protected geosynchronous belt to decrease the coherent integration time required. An orbit with radius 41164 km (1000 km offset from the geostationary ring) would decrease the range spreading loss by 12 dB at the cost of a longer geosynchronous orbit scan time (28.3 days instead of 14.2 days) and would reduce the coherent integration to 256 pulses or 0.85 seconds of observation time per burst.

The antenna has a nominally square form factor and would have dimensions 7.1 m x 7.1 m and for any beam pointing position will illuminate a segment of a cone whose near cross section has a minimum near-range diameter of 12.7 km and a minimum far-range diameter of 15.5 km.

The required antenna is larger than any active array that has been launched to date but is deemed to be within present day engineering capabilities. The other radar parameters used are somewhat conservative and some design margin is expected. Given current mass densities for large arrays, it is expected that the

resulting satellite mass will be in the vicinity of 3500 kg when the power system is scaled to allow operation during the expected 35 minute eclipse periods.

4.2.2.2.4 Radar operations scheduling and on-board computing

The proposed radar is a scan and dwell instrument that has been specified for the detection and orbit determination of small debris objects in the geosynchronous belt. The beam steering flexibility allows considerable debris search and measurement capability but will need to be optimized by a scheduling algorithm that could combine the allocations of radar beam pointing and signal processing resources to accommodate debris search and detect activities with debris tracking and orbit determination activities.

The processor algorithms will need to contain coherent moving-target detection and measurement algorithms which may need to be coupled to pulse-length and PRF control and to radar beam steering. The processor functions will need to adapt to the observed debris content of a scene.

Since geosynchronous belt radar targets are assumed to be sparse, the radar will spend much of its time performing search and detect functions and a limited amount of its time performing tracking and orbit determination functions. The system will need to perform autonomously and link its debris orbit outputs to the ground after target decisions have been made. The system should have a regularly updated, on-board data base of known and tracked targets.

The processing and scheduling algorithms are not considered in this report. Algorithm design research will be required.

4.2.2.3 Radar and satellite property summary

A sub-geosynchronous orbit, free-flying radar satellite could be built to detect, monitor and provide orbit parameters for small debris articles in the geosynchronous belt. Preliminary calculations indicate that the radar would require a 50 m^2, nominally square antenna that has two orthogonal pairs of receiving antenna apertures. The modeled operating parameters suggest that the satellite mass would be in the vicinity of 3500 kg. The satellite would use a circular orbit with radius 40164 km and would scan the central region of the geosynchronous belt (limited to the $\pm 1^{o}$ debris orbit inclination band). It would capture debris articles in higher inclination orbits as they pass through the scanned band during radar observations on successive orbits.

The radar would scan the entire geostationary orbit band every 14.2 days and would complete 25.7 scans per year. There is a trade-off between geostationary orbit scan time and pulse integration strategy that needs to be examined.

An initial analysis suggests that the radar would execute debris search and detection operations using a scan and dwell beam control mode and would enter a tracking mode when debris orbit determinations are in progress.

The proposed design uses a 10 MHz bandwidth linear frequency modulated signal to perform the search and tracking operations. The instrument could have higher resolution modes to perform SAR imaging functions.

The proposed instrument operates autonomously to perform its debris detection and tracking functions.

Given the high cost of placing a satellite of this size in a geostationary or near geostationary orbit (up to $100M) it is suggested that the satellite and instrument be designed for up to 15 years of operating life. The cost of building a satellite of this type has not been estimated but based on the RADARSAT-2 and RCM experiences is expected to be in the vicinity of, or greater than $800M.

The satellite and its radar system could be built with tested technologies that are available in 2012. The major engineering challenges identified are:

1. Antenna electronics cooling design will be a challenge. The radiating face of the antenna receives direct solar heating for approximately one half of the orbit and the back surface is exposed to the sun for most of the other half orbit.
2. Thermal distortion due to variable solar heating will be a challenge. The solar illumination geometry is similar to that experienced by a geostationary satellite in that the solar illumination angle varies over 360^{o} over the course of each day.
3. The array antenna would be larger than any space based radar antenna that has been built to date.
4. The antenna size and form factor could result in deployment mechanism challenges and deployed antenna stiffening challenges.
5. Autonomous control, on-board, adaptive data processing and target decision software are required.

5 Summary of deep-space surveillance radar options

The work reported in this document describes possible ground and space-based radar systems that could be used to monitor small debris in the geosynchronous orbit belt whose radar cross sections are as small as -11.5 dBm^2 (a 30 cm diameter sphere). The work was driven by a need to define possible Canadian contributions to the North American Space Surveillance Network following the demise of the Sapphire satellite.

Three ground-based deep-space radars that are capable of detecting and monitoring 30 cm debris on the geosynchronous orbit belt have been described. The expected cost of these systems grows proportionately with their capability and utility.

The least expensive and least capable option upgrades the Algonquin radio telescope to a deep space radar by adding a 2.7 MW C-band transmitter, receiver modifications and processing equipment at a rough cost between $ 5 M and $10 M. The operating constraints for the radar mode of this system are expected to parallel those of the MIT Haystack radar [32 and 33] where the instrument's primary function is a radio observatory and its secondary function is a space surveillance radar. The time allocated to the space surveillance function will be limited and will depend on negotiated use agreements.

The next least expensive approach is to build a deep-space surveillance radar based on the Effelsberg [34] or Green Bank [29] radio telescope dish design. Depending on where this radar is sited, C or X-band operating frequencies are suitable to avoid interference with active space assets that will be observed. Rough calculations for a C-band version suggest that a 432 kW C-band transmitter would be required. The probable cost for this radar (based on the Green Bank radio telescope development cost) would be $100M and a possible site would be CFB Suffield. This instrument would have space surveillance as its primary role and would be capable of detecting and determining orbit parameters for debris down to 30 cm size in the geosynchronous belt. It suffers from the limitations of all dish radars in that long dwell times are required to detect previously unknown debris items and to establish their orbital elements.

The most expensive and most capable deep-space radar is modeled on the AN/FPS-108 active array radar concept using a single antenna for signal transmission and reception (Cobra Dane [36] concept). Instruments of this class use electronic beam forming and beam steering and are capable of performing debris detection and tracking functions much more quickly than dish based radars. They are also easily used for both deep-space and near-space surveillance. A rough examination of the radar design requirements suggests that a C-band version of this radar class that is capable of detecting and tracking 30 cm debris in the geosynchronous belt would cost approximately $1.5B. CFB Suffield would be a suitable site for this instrument.

Two space based radar systems were investigated for monitoring geosynchronous orbit belt debris.

One approach would use a radar mounted on a geostationary satellite platform as a secondary payload to monitor active satellites and debris objects within 250 km of the radar platform. A design concept for this type of radar was investigated and was judged to be feasible. No power, mass or cost budgets were estimated. Many satellites around the geostationary orbit belt would need to be equipped with surveillance radars of this type to provide a reasonable picture of small debris within the geosynchronous belt.

The second approach that was examined was to use a dedicated radar satellite in a sub-geosynchronous orbit to survey the geosynchronous belt for debris objects. A radar design concept was investigated and

was judged to be feasible. Radars of this type could survey the central region of the belt every 14 days and could build a fairly complete picture of the population and orbits of small debris articles over periods of the order of a year. A rough on-orbit cost of this type of space surveillance radar was estimated to be $800M (and is probably larger).

6 References

1. Anselmo, L. and Pardini, C., Space debris mitigation in geosynchronous orbit, Advances in Space Research, V 41, P1091-1099, 2008.
2. Weeden, B., Zombiesats and on-orbit servicing, MilsatMagazine, September 2010.
3. Gao, L., Behavior and relative velocity of debris near geostationary orbit, MSc thesis, Cranfield University School of Engineering, May 2010.
4. Choc, R. and Jehn, R., Classification of geosynchronous objects Issue 11, European space operations center, Ground Engineering Department, February 2009.
5. Anselmo, L. and Paradini, C., Orbital evolution of geosynchronous objects with high area to mass ratios, ESA SP-587, P 279-284, 2005.
6. Kelecy, T., Payne, T., Thurston, R. and Stansbery, G., Solar radiation pressure estimation and analysis of a geo class of high area to mass ration debris objects, Air Force Space Command report, AAS 07-391.
7. Romans, D.R. Geoid surfaces and theory, NOAA presentation, 2007.http://www.ngs.noaa.gov/GEOID?PRESENTATIONS/2007_02_04_DDPS, reference http://www.csr.utexas.edu/grace/gravity. (Accessed October 17, 2012).
8. Mehrholz, D., Radar observations of geosynchronous orbits, Proc. 2nd European Conference on space debris, ESA-SP 393, P 51-58, Darmstadt, March 1997.
9. Shi, H-L, Han, Yp-B, Ma, L-H, Pei, J, Yin, Z-Q and Ji, H-F, Beyond life-cycle utilization of geostationary communication satellites in end-of-life., Satellite Communications, Chapter 16, National Astronomical Observatories, Chinese Academy of Sciences, 2009.
10. Abbot, R.I. and Wallace, T.P., Decision support in space situational awareness, Lincoln Laboratory Journal, V 16. No. 2, 2007.
11. Massonet, D., The interferometric cartwheel: a constellation of passive satellites to produce radar images to be coherently combined, International Journal of Remote Sensing, V 22, Issue 12, 2001.
12. IADC Space debris mitigation guidelines, IADC 02-01, July 2007.
13. Space surveillance sensors, The FPS-85 radar (April 12, 2012), http://mostlymissiledefence.com (accessed July 23, 2012).
14. Space surveillance sensors: ALTAIR radar (May 11, 2012), http://mostlymissiledefense.com (Accessed June 25, 2012).
15. Knepp, D.L., Preliminary results of the peak experiment: ALTAIR deep space measurements, Defense Nuclear Agency, DNA-TR-89-76, March 1990.
16. Space surveillance sensors: The Millstone Hill radar (May 5, 2012). http://mostlymissiledefense.com (Accessed June 25, 2012).
17. Globus II / HAVE STARE sourcebook, V 2008-08-25.
18. A sourcebook for the use of the FGAN tracking and imaging radar for satellite imaging, V 2012-04-22, http://fhr.fgan.de (Accessed July 23, 2012).
19. Rosenberg, F.D., The launch of Gorizont 45 on the first Proton K/Breeze M, MIT Lincoln Laboratory Space Control Conference, 2001, http://dtic.mil (Accessed June 27, 2012).
20. Mehrholz, D., Leushacke, L., Flury, Jenn, R.,W., Klinkrad, H. and Landgraf, M., Detecting, tracking and imaging space debris, ESA bulletin 109, February 2012.

21. Mehrholz, D., Radar observations of geosynchronous orbits, Proc. 2nd European Conference on space debris, ESA-SP 393, P 51-58, Darmstadt, March 1997.
22. Leushacke, L., Mehrholz, D. and Jehn, R., Cooperative debris campaign experiment outline and first results, P 45-50, Proc. 2nd European conference on space debris, Darmstadt, March 1997.
23. Cannon, W.H., Novikov, A.Y., Berube, M., Brazeau, S. and Sparkes, D., Bistatic radar L-band feasibility experiment, Final report, contract W7714-9-028, March 25, 2003.
24. Cannon, W.H., Novikov, A.Y., Berube, M., Brazeau, S., Pertachenko, B. and Galt, J., Tri-static radar L-band feasibility experiment: A proof-of-concept demonstration of the Millstone Hill. Algonquin Radio Observatory and the Dominion Radio Astrophysical Observatory of observing geostationary targets, Final contract report for contract W7714-030745, March 2004.
25. Algonquin Radio Observatory: Technical specifications, www.arocanada.com, (Accessed July 26, 2012).
26. Cannon, W.H., Algonquin Radio Observatory: Deep space radar upgrade study, Contract W7714-4-0888, document TR794001, 2005
27. Study report on: Feasibility of a space debris monitoring system to support CSA satellite operations, CSA Doc. ID:14382209, August 2011.
28. Radio-Observatorium Effelsberg: Information about the 100 M telescope, Max-Plank-Instutut fur Radioastronomie, http://users8.jabry.com/steelpro/FAST/Effelsberg (Accessed November 7, 2012).
29. Decision announced in Green Bank Telescope arbitration Case, National Radio Astronomy observatory, February 12, 2001, http://www.nrao.edu/2001/arbitration (Accessed November 6, 2012).
30. Abbot, R.I. and Wallace, T.P., Decision support in space situational awareness, Lincoln Laboratory Journal, V 16, No. 7, P 297-335, 2007.
31. Eckstein, M.C., Rajasingh, C.K. and Blumer, P., Colocation strategy and collision avoidance for the geostationary satellites at 19 degrees west, CNES International Symposium on Space Dynamics, Toulouse, 6 – 10 November, 1989.
32. Stokely, C.L., Foster, J.L., Stanspery, E.G., Benbrook, J.R. and Juarez, Q., Haystack and HAX radar measurements of the orbital debris environment 2003, Lyndon B. Johnson Space Center report JSC-62815, November 2006.
33. MIT Haystack Observatory History, http://www.haystack.mit.edu/hay/history , (Accessed November9, 2012).
34. Hachenberg, O., Grahl, B.H. and Wiebinski, R., The 100 meter radio telescope at Effelsberg, Proc. IEEE, V61, No. 9, 1973.
35. Lyon, R.H., Geosynchronous orbit determination using space surveillance network observations for improved radiative force modeling, MSc Thesis, MIT, June 2004.
36. Space surveillance sensors: the Cobra Dane radar (April 12, 2012), http://mostlymissiledefense.com/2012/04/12/cobra-dane-radar-april-12-2012, (Accessed November13, 2012).

Annex A Model calculations of debris observation geometry for a radar mounted on a geostationary satellite

A.1 Introduction

This analysis and discussion addresses the problem of monitoring debris in geosynchronous orbits from a radar that is mounted on a geostationary satellite. It is assumed that the host satellite orbit is under active control and that the host satellite is not spinning and its attitude is actively controlled.

Debris in geosynchronous orbit includes:

1. defunct satellites and rocket bodies in the geosynchronous belt that have not been removed for historical or device failure reasons,
2. fragments of satellites or launch vehicles that have disintegrated for various reasons, and
3. satellite components, such as telescope lens covers, that have become detached from the parent satellite.

The hypothesis that is explored in this Annex is that the motion and orbits of such debris articles that are in the local vicinity of a geostationary satellite can be determined by observations that are made by a radar that resides on the satellite. The design of such a radar is based on the trajectories of debris articles that are in the vicinity of the satellite. Large articles such as defunct satellites and rocket bodies are observable by earth-based radars and optical telescopes. Small objects such as telescope lens covers and satellite fragments are unobservable from the earth using present technologies.

To determine the radar observation geometry required by a satellite-mounted radar, it can be assumed that the satellite station keeping is active and that the satellite orbit is circular and lies in the geostationary equatorial plane. The debris orbits can either be inclined to the satellite orbit (debris orbit inclination is different from the satellite orbit by more than $\pm 0.1^{o}$) or coplanar with the satellite orbit (debris orbit inclination is within $\pm 0.1^{o}$ of the satellite orbit inclination). A simple model that describes debris observations from an equatorial plane satellite can be applied to a longitudinally controlled satellite whose orbit plane inclination is allowed to drift provided that the debris orbit inclination is measured relative to the satellite orbit inclination.

For debris that is in an elliptical, inclined orbit, the minimum proximity of the debris to the satellite is limited by the difference in eccentricities of the two orbits. From discussions of satellite cluster control in [10], for controlled objects, any minimum radial proximity that is greater than two km is considered to be safe. For uncontrolled, but tracked, objects the minimum safe separation in longitude is taken to be six km. This corresponds to a debris eccentricity that is at least 5×10^{-5} greater than the satellite orbit eccentricity. Any debris that is in an inclined orbit and has an eccentricity that is greater than the minimum threshold will not intersect the satellite orbit if the debris originated in the geostationary ring (has the same semi-major axis as the satellite).

The debris that is monitored by the satellite radar is assumed to have the same semi-major axis as the satellite and is in an uncontrolled, geosynchronous orbit. The debris orbit inclination can vary over a $\pm 15^{o}$ range under the influence of lunar and solar gravity fields and the debris orbit plane can drift under the influence of the first order equatorial gravity field asymmetry of the earth with drift rates varying from 0^{o}/day to 12^{o}/day. Debris orbits that are in librational oscillation about the equatorial gravity field maxima can have either positive or negative drift rates with respect to a controlled, geostationary satellite.

Two cases are examined:

1. The debris orbit is circular and inclined to the satellite orbit plane.
2. The debris orbit is elliptical and lies in the satellite orbit plane.

Two coordinate systems are used.

1. An earth-centered, earth-fixed, Cartesian coordinate system, whose Z axis is aligned with the rotational axis of the earth, is used to describe the satellite and debris position vectors.
2. A satellite-based Cartesian coordinate system whose:
   a. Z axis is parallel to the earth rotation axis;
   b. X axis is parallel to the satellite position vector; and
   c. Y axis is parallel to the satellite (and earth) rotation direction,

   is used to describe the relative positions and motion of the satellite radar platform and debris objects.

The analysis presented here examines the relative motion of the debris with respect to the satellite to determine the required radar look directions and the radar properties needed to capture and measure the debris motion.

Satellite station keeping for satellite clusters currently use the convention that a longitudinal closest approach of an uncontrolled object to a satellite of 6 km or greater is safe and that a closest approach of 4 km or less is risky. In the radial direction, closest approaches greater than 2 km are considered safe. These tolerances are based on the orbits of known and tracked objects. Although the majority of debris objects moving near the satellite are large and have well known orbital properties, the radar will search for and attempt to track debris objects that are not observable from the earth including objects with dimensions of 30 cm or larger whose radar cross sections are as small as -11.5 dBm^2. For smaller objects observed at the same geometry, the power-aperture product of the radar must be scaled by the square of the object size ratio to the 30cm reference object.

A.2 Geostationary satellite parameters

The radar platform satellite is assumed to move in a circular, equatorial plane orbit (eccentricity = 0) and is under perfect longitudinal control (it has no longitudinal drift).

The orbit and local coordinate system of the satellite that serves as the radar platform can be described by:

- Longitude: $\varphi_S = \omega t$, where t is the time of sidereal day,
- Eccentricity: $e = 0$,
- Orbit radius: $r_S = 42164$ km,
- Orbit inclination: $I = 0$,
- Orbit angular speed: $\omega = 2\pi/T = 7.2921 \times 10^{-5}$ radians/second, where T is one sidereal day (86164.2 seconds). This is the earth rotational speed.

The satellite position vector in the geostationary plane is given by:

(A-1) $$\vec{R}_S = r_S \begin{bmatrix} \sin(\omega t) \\ \cos(\omega t) \\ 0 \end{bmatrix}$$ in earth centered coordinates .

The satellite velocity vector in earth centered coordinates is

(A-2) $$\vec{V}_S = v_S \begin{bmatrix} \cos(\omega t) \\ -\sin(\omega t) \\ 0 \end{bmatrix} = r_S \omega \begin{bmatrix} cos(\omega t) \\ -\sin(\omega t) \\ 0 \end{bmatrix},$$

and the satellite speed is

(A-3) $$v_S = \frac{631.348}{\sqrt{r_S}} = 3.108 \frac{km}{s}.$$

The satellite-based local coordinate system that is used to estimate the relative motion of the debris is given by the basis vectors:

- $\hat{X} = \begin{bmatrix} 1 \\ 0 \\ 0 \end{bmatrix}$ is a unit vector in the positive satellite position vector direction.
- $\hat{Y} = \begin{bmatrix} 0 \\ 1 \\ 0 \end{bmatrix}$ is a unit vector in the geostationary orbit velocity direction at the satellite.
- $\hat{Z} = \hat{X} \times \hat{Y} = \begin{bmatrix} 0 \\ 0 \\ 1 \end{bmatrix}$ is a north pointing unit vector on the constant-radius geosynchronous orbit shell.

$\hat{Z}$ is the geostationary plane normal vector.

A.3 Debris in inclined, circular orbits with orbit plane drift

A.3.1 Debris orbit parameters

Debris consists of geosynchronous orbit objects that do not have longitude station keeping, drift in longitude with respect to geostationary satellites, can oscillate about the east or west libration points and can have orbit plane inclinations between 15° and -15°. Debris orbit inclinations vary sinusoidally over the ±15° range with a period of 107 years.

Debris longitudinal drift rates are quite variable ranging from

- 0.001°/day (NATO IIB in oscillation about the western 105° libration point with orbit radius 41264 km, orbit inclination of 12.7° {in 2009}, and orbit eccentricity, 0.0005, [4]) to
- 12.8°/day (GSAT1 in drift mode at 41197 km semi-major axis, orbit eccentricity 0.022, and orbit plane inclination of 5.8° {in 2009}) or
- 11.4°/day (Proton K fourth stage in drift mode at 41300 km semi-major axis, orbit eccentricity of 0.0025 and orbit plane inclination of 11.57° [4]).

For model calculations assume that the debris is in a circular orbit with radius 42164 km. Assume that the debris orbit inclinations, I, lie in the range -15°≤I≤15° and that the debris orbit plane drifts in longitude at rates between 0°/day and 10°/day. The orbits of debris objects can be described by:

- Longitude: $\varphi_D = \omega_D t$,
- Eccentricity: 0,
- Orbit radius: $r_D = r_S = 41264$ km,
- Orbit inclination: I, -15°≤ I ≤ 15°,
- Orbit angular speed: $\omega = 7.2921 \times 10^{-5}$ radians/second,
- Debris speed: 3.108 km/s = $r_D\omega$,
- Debris longitude offset from the satellite at the geostationary plane crossing: δ,

- Debris orbit drift rate γ degrees/day = γ/T degrees / second,
- Debris position vector for $\omega_D = \omega+\gamma$ and debris orbit inclination I

(A-4) $$\vec{R}_{Deb} = r_S \begin{bmatrix} \cos(I)\sin((\omega+\gamma)t+\delta) \\ \cos((\omega+\gamma)t+\delta) \\ -\sin(I)\sin((\omega+\gamma)t+\delta) \end{bmatrix}$$, and the

- Debris velocity vector

(A-5) $$\vec{V}_{Deb} = \frac{d\vec{R}_{Deb}}{dt} = r_S(\omega+\gamma) \begin{bmatrix} \cos(I)\cos((\omega+\gamma)t+\delta) \\ -\sin((\omega+\gamma)t+\delta) \\ -\sin(I)\cos((\omega+\gamma)t+\delta) \end{bmatrix}.$$

A.3.2 Observation parameters for a satellite-mounted radar

For a radar mounted on a geostationary satellite, the debris observation parameters can be described in the local satellite coordinates by the radar range vector

(A-6) $$\vec{R} = \vec{R}_S - \vec{R}_{Deb} = r_S \begin{bmatrix} \sin(\omega t) - \cos(I)\sin\big((\omega+\gamma)t+\delta\big) \\ cos(\omega t) - \cos\big((\omega+\gamma)t+\delta\big) \\ \sin(I)\sin((\omega+\gamma)t+\delta) \end{bmatrix}$$ and,

the relative velocity vector of the debris with respect to the radar

(A-7) $$\vec{V}_{Rel} = \frac{d\vec{R}}{dt} = r_S\omega \begin{bmatrix} \cos(\omega t) \\ -\sin(\omega t) \\ 0 \end{bmatrix} + r_S(\omega+\gamma) \begin{bmatrix} -\cos(I)\cos((\omega+\gamma)t+\delta) \\ \sin((\omega+\gamma)t+\delta) \\ \sin(I)\cos((\omega+\gamma)t+\delta) \end{bmatrix}.$$

(A-8) The radar range is then $r = \sqrt{\vec{R}\cdot\vec{R}'}$,

(A-9) the radial speed of the debris with respect to the satellite is $v_{Radial} = \frac{\vec{V}_{Rel}\cdot\vec{R}}{\sqrt{\vec{R}\cdot\vec{R}'}}$,

(A-10) the angle between the debris and the Z axis is $\alpha = acos\left(\frac{\vec{R}\cdot\hat{Z}}{r_S}\right)$,

(A-11) the angle between the debris and the X axis is $\beta = \text{acos}\left(\frac{\vec{R}\cdot\hat{X}}{r_S}\right)$, and

(A-12) the angle between the debris and the Y axis is $\epsilon = acos\left(\frac{\vec{R}\cdot\hat{Y}}{r_S}\right)$.

A.3.3 Radar observations when the debris orbit drift rate is zero

To provide a baseline for radar system specifications, choose the point at which the debris crosses the satellite orbit to be 10 km ahead the satellite so that $\delta = 10/R_S$ radians, choose a time interval $dt = T/(2\pi R_S)$ in seconds per km displacement along the geostationary orbit and perform calculations over the time interval $-1000dt \le t \le 1000dt$ so that the results show the debris approaching and receding from the satellite. Choose debris orbit inclinations between -15° and 15° in 1° intervals and set the debris orbit plane longitudinal drift rate to zero.

With these conditions we see:

1. The angle between the debris and the Z axis is shown in Figure A1.

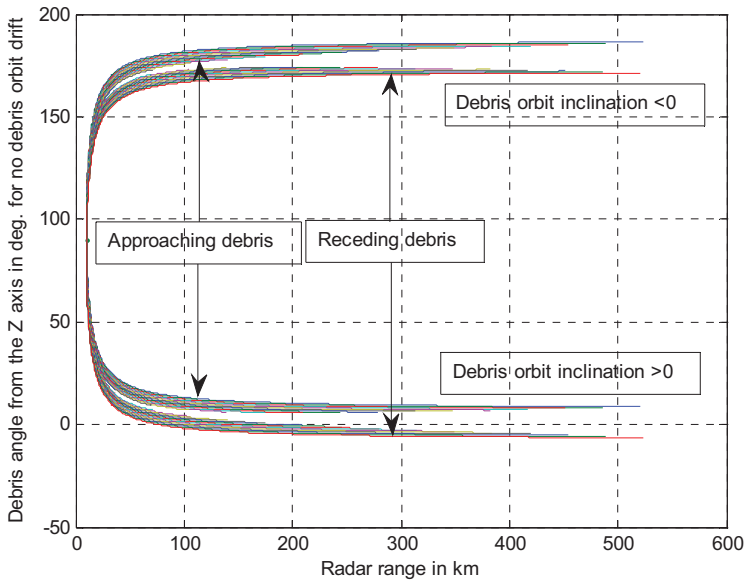

Figure A1: Debris nadir angle at the satellite as a function of radar range for debris orbit inclinations of -15º to 15º

For radar ranges greater than 50 km, the debris lies within 20º of the Z axis for both approaching and receding cases and for all debris orbit inclinations.

2. The angle between the debris and the X axis is shown in Figure A2.

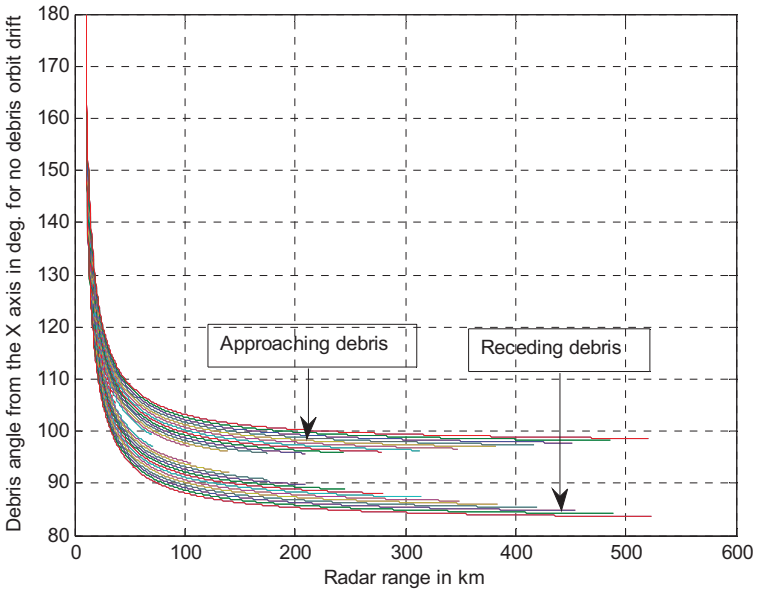

Figure A2: Debris azimuth angle seen by the satellite with respect to the satellite position vector for debris orbit inclinations -15 º to 15 º.

For radar ranges greater than 50 km, the debris lies within 12° of the X (satellite position vector) axis for all cases. For small radar ranges, the debris approaches and recedes towards the negative X axis (towards the earth center).

3. The angle between the debris and the Y axis is shown in Figure A3.

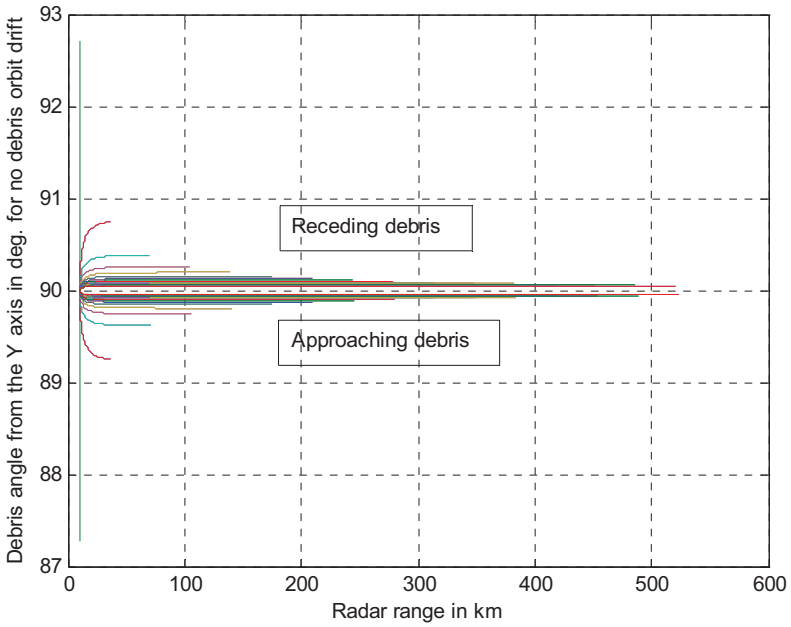

Figure A3: Debris range for debris orbit inclinations between -15° and 15° as seen from the satellite

For all radar ranges and all debris orbit inclinations, the debris lies within 1° of the plane that is normal to the satellite velocity vector. Debris whose orbit inclinations are in the interval $-2.8^{\circ} < I < 2.8^{\circ}$ are not seen at radar ranges greater than 50 km within the chosen observation time window.

4. The relationship between the radar range of the debris and the observation time is shown in Figure A4.

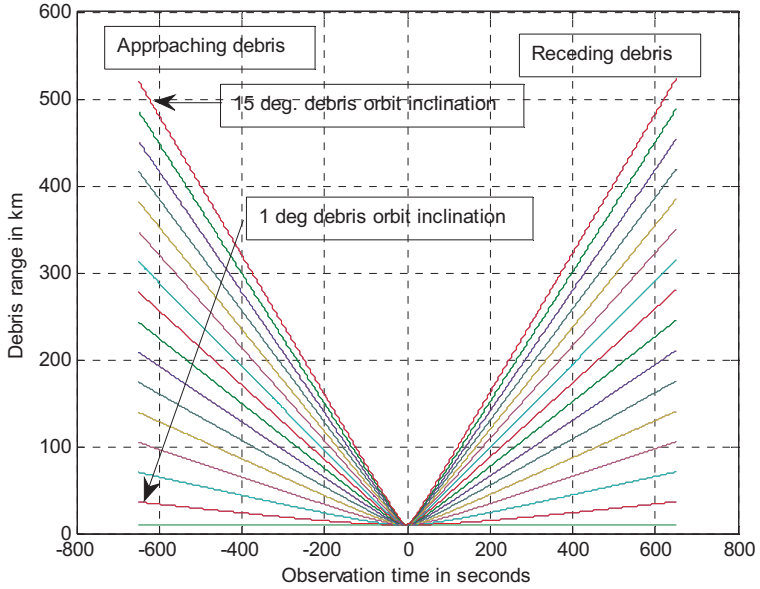

Figure A4: Debris range in km as a function of observation time

The maximum debris range in Figure A4 for 15º debris orbit inclination is 523.3 km and the maximum debris range for debris orbit inclination 1º is 36.38 km. Both maxima correspond to observation times ± 650.48 seconds.

5. The relationship between the radial speed of the debris and the observation time is shown in Figure A5.

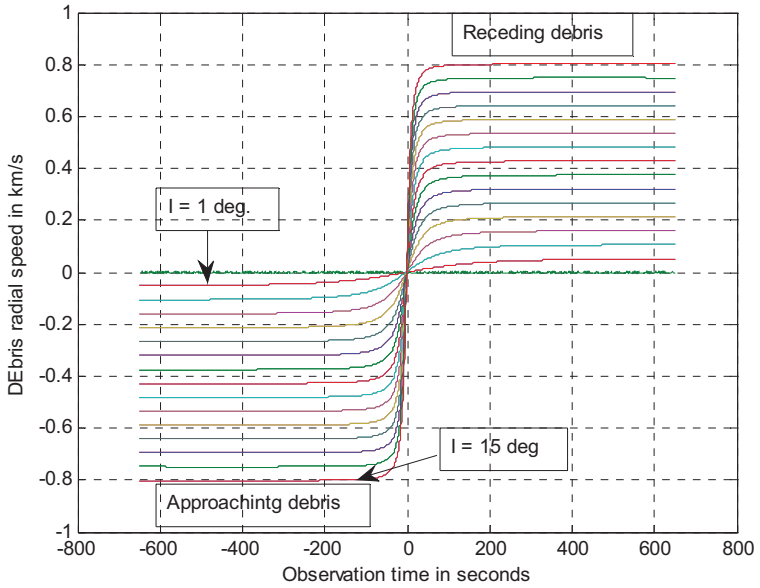

Figure A5: Debris radial speed in km/s as a function of radar range in km

At debris orbit inclination 15º the maximum radial speed of the debris is 802.9 m/s. At debris orbit inclination 1º the maximum radial speed is 51.5 m/s.

6. The relationship between the radial speed of the debris and its radar range is shown in Figure A6 for the observation time window.

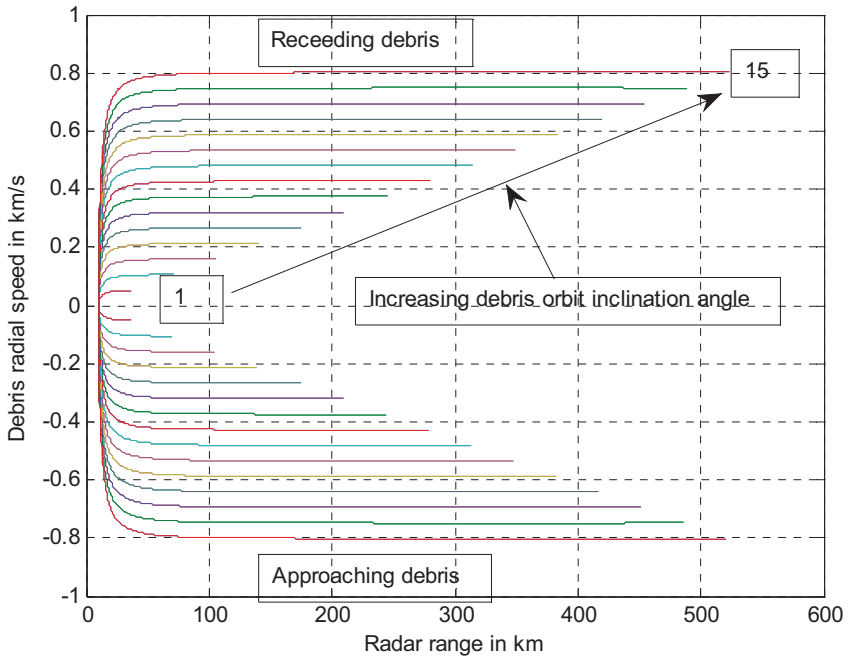

Figure A6: Debris radial speed as a function of radar range over the 1300 second observation interval

To summarize the results for debris orbits that do not drift with respect to the radar's host satellite:

1. The debris motion lies close to (within ± 1° of) the X,Z observation plane.
2. The relationship between radar range and observation time offers significant radar beam schedule opportunities for observations of debris at all common debris orbit plane inclination angles.
3. Debris radial speeds are a linear function of the debris orbit inclination angle for radar ranges greater than 50 km.

A.3.4 Radar observations for debris in drifting orbit planes

To examine the impact of the debris orbit drift rate on radar observations from a geostationary host satellite, evaluate the radar parameters in Section A.3.2 for selected debris orbit plane drift rates between 2°/day and 10°/day. At geostationary orbit altitude these correspond to drift velocities between 17.1 m/s at 2°/day and 85 m/s at 10°/day.

The debris angle from the Z axis shown in Figures A7(a) to A7(f) illustrates the effect of the debris orbit plane drift rate on the radar observation geometry.

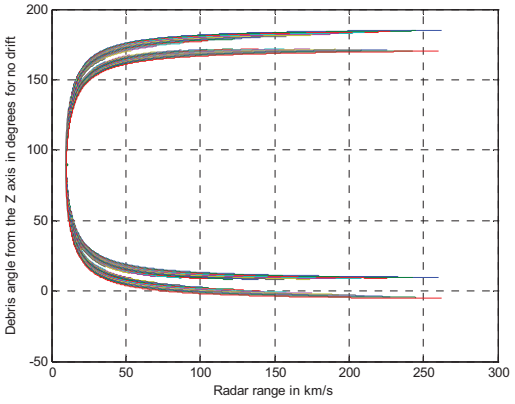

Figure A7 (a): Debris angle from the Z axis for no orbit plane drift

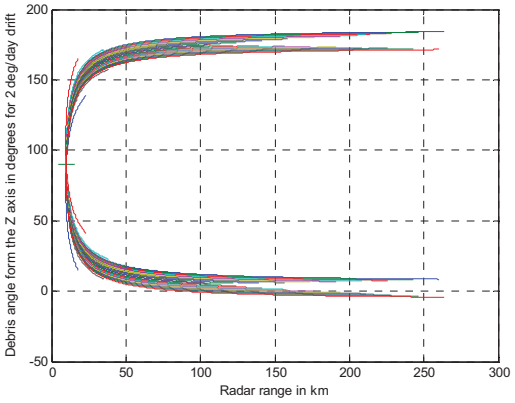

Figure A7 (b): Debris angle from the Z axis for 2 degrees/day orbit plane drift

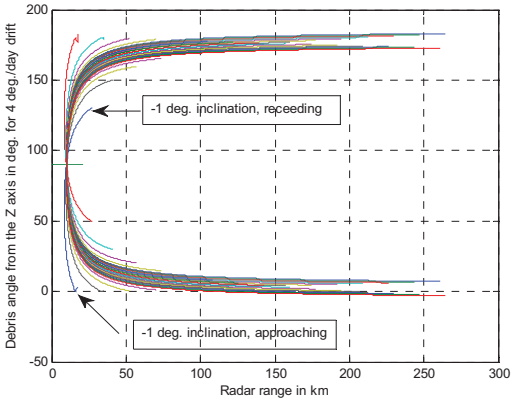

Figure A7 (c): debris angle from the Z axis for 4 degrees/day orbit drift

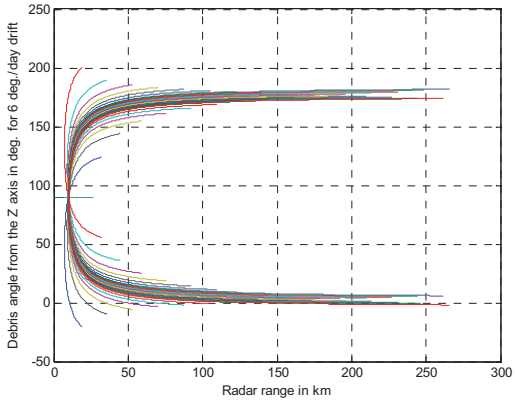

Figure A7 (d): Debris angle from the Z axis for 6 degree/day debris orbit drift

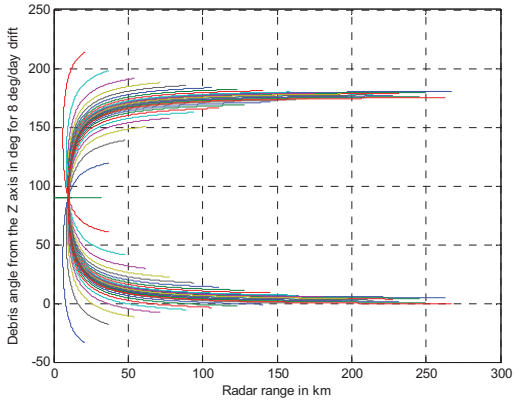

Figure A7 (e): Debris angle from the Z axis for 8 degree/day debris orbit drift

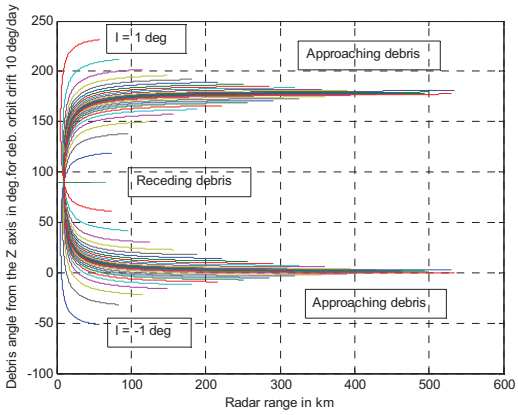

Figure A7 (f): Debris angle from the Z axis for 10 degrees/day debris orbit drift

As the drift rate of the debris orbit plane increases, the angle between the debris and the Z axis increases or decreases depending on the debris orbit inclination angle. The effects are strongest for small inclination angles and are negligible as the inclination angle approaches 15°. For orbit inclination angles ± 1° the debris orbit plane drift rate becomes measureable (depending on angle of arrival measurement accuracy) at drift rates between 2°/day and 4°/day). Depending on the radar angle of arrival measurement accuracy, debris orbit plane drift rates may be estimated for debris orbit inclination angles up to 5°.

Figures A8 (a) and A8 (b) show that the debris angle from the X axis is not strongly dependent on the drift rate of the debris orbit plane (The debris lies within 2.7° of the X axis at 10°/day drift rate.) and that the measureable debris motion lies close to the X, Z plane.

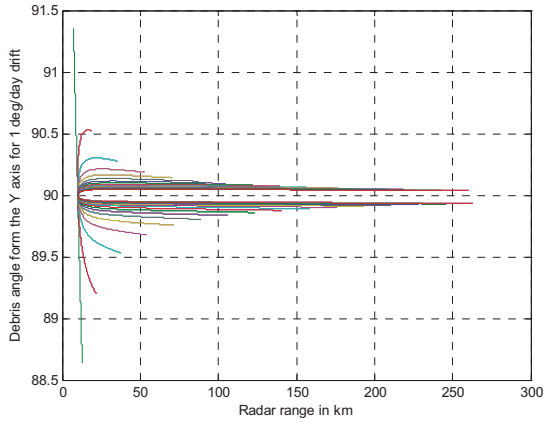

Figure A8 (a): Debris angle from the X axis for no debris orbit plane drift.

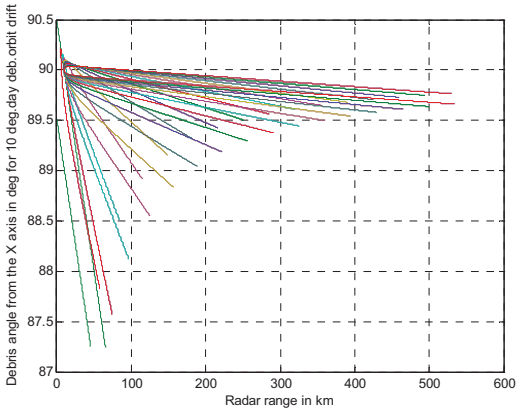

Figure A8 (b): Debris angle from the X axis for 10 °/day debris orbit plane drift.

A comparison of Figure A5 and Figure A9 shows that debris radial speed estimates have debris-orbit plane drift rate effects.

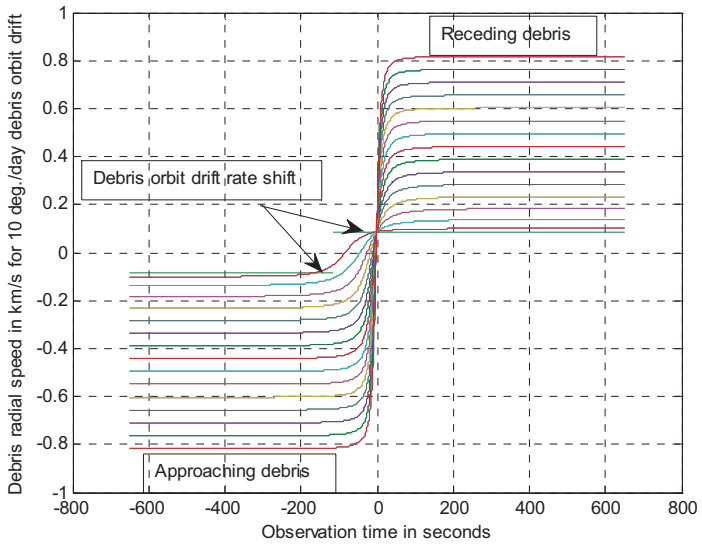

Figure A9: Debris radial speed over the observation time.

Depending on the sensitivity of the radar radial speed estimates, the radial velocity may provide a useful metric.

From Figures A7 (a to f), it is evident that radar observations of debris in the X-Z plane require debris approach angle measurements over ± 50^{o} from the Z axis when small debris orbit inclination angles must be observed at large debris orbit plane drift rates. Actively steered antenna beams may be required to provide reasonable trade-offs between the radar power and the antenna gain.

The Y axis (satellite velocity direction) component of the debris position is less than 2.7^{o} for debris orbit plane inclinations that are less than 1^{o} and so the Y component of the radar beam width can be small.

Since the observation time windows for approaching debris are long, radar power can be traded against bandwidth and integration gain to measure parameters of the debris orbits.

Figure A10 shows the debris observation time available for a radar whose maximum range is 250 km.

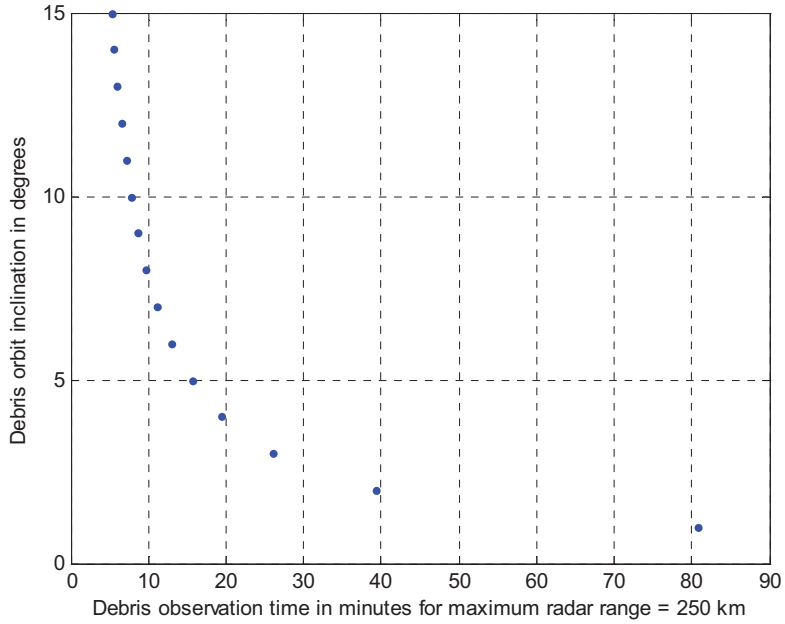

Figure A10: Debris observation time in minutes as a function of debris orbit inclination angle when the maximum range of the radar is 250 km.

A.4 Elliptical debris orbits in the geosynchronous orbit belt

Geostationary satellites that have active longitude and orbit plane inclination control operate within a defined orbit keeping box that lies in the local, equatorial X, Z plane and has an arc length that is determined by a trade-off between the required satellite position accuracy and the ground-based communication station properties. If the control range for an equatorial plane satellite corresponds to an elevation angle variation of 0.1° as seen by a ground station at N 45°, the allowed X, Z plane arc length for the satellite station-keeping box is 74 km. This corresponds to a satellite orbit plane inclination angle variation over the control range of ± 0.044°. For simple model calculations, any debris whose orbit inclination angle lies within ± 0.1° will be considered to be coplanar with the satellite to create a worst-case geometry that assumes that the debris orbit inclination is equal to the satellite orbit inclination.

A.4.1 Coplanar debris observation by a geostationary satellite

Debris objects that originate in the geostationary plane have an elliptical orbit semi major axis equal to the geostationary orbit radius. The debris orbit radius can be expressed as

(A-13) $$r_{Deb} = \frac{a(1-e^2)}{1+ecos(v)}$$

where: a, is the orbit semi-major axis; e, is the eccentricity of the debris orbit and, v, is the orbit central angle measured from perigee (v is the true anomaly of the orbit). When the debris orbit is coplanar with the satellite orbit, $r_{Deb} = r_S = a$, v = acos(-e) and the debris intersects the geostationary satellite orbit near true anomaly 90° and 270°. Expressing the debris orbit ellipse in terms of the ellipse radius from a focus and in terms of the true anomaly angle, the intersection of

coplanar elliptical orbits with circular orbits that have the same semi-major axis lengths occurs at the semi-minor axis of the ellipse.

Writing the equation of the ellipse in the equatorial plane we have

(A-14) $$\vec{R}_{Deb} = r_{Deb}\begin{bmatrix}\cos(\nu)\\ \sin(\nu)\\ 0\end{bmatrix} = \frac{a(1-e^2)}{1+ecos(\nu)}\begin{bmatrix}\cos(\nu)\\ \sin(\nu)\\ 0\end{bmatrix}$$

where: a = the semi-major axis length of the debris orbit,
e = the debris orbit eccentricity, and
ν = the debris true anomaly angle in the debris orbit.

Expressing the satellite orbit in the same form and noting that the angle, ν, is the longitude of the debris in the satellite orbit plane, we have

(A-15) $$\vec{R}_{Sat} = a\begin{bmatrix}\cos(\nu)\\ \sin(\nu)\\ 0\end{bmatrix}.$$

The radar range vector to the debris, as measured by a satellite mounted radar, is

(A-16) $$\vec{R} = \vec{R}_{Sat} - \vec{R}_{Deb}.$$

Since the debris is in an elliptical orbit, the debris velocity vector is not normal to the debris position vector but varies from the normal direction by the flight-path angle given by

(A-17) $$\phi = atan2\big(1 - ecos(\nu), esin(\nu)\big)$$

and the debris speed along its orbit is given by

(A-18) $$V_{Deb} = \frac{\sqrt{GMa(1-e^2)}}{r_{Deb}\cos(\phi)}$$

where: GM = 3.986005 x 10^5 km^3/s^2 is the gravitational constant times the mass of the earth.

Two other parameters are needed to examine the radar observation geometry for coplanar debris in an elliptical orbit, the separation of the debris orbit crossing from the satellite and the debris orbit drift.

Define the orbit crossing angle offset as was done in Section A3.1, δ = d/a where d is the crossing separation in km. The angle, δ, can be accounted for by rotating the debris coordinates system by δ.

Define the debris orbit drift angle from the debris orbit drift rates as was done in Section A.3.1 so that the drift angle at any time can be expressed in terms of the drift rate, γ, in degrees per second and can be extracted from published drift rates in degrees per day by the division of the geostationary orbit period in seconds per sidereal day. The debris drift rate can be positive or negative depending on the debris position in a librational cycle. For any time t from an arbitrary reference, the debris orbit drift angle is ε = γt.

Rotating the debris orbit argument of perigee by the angle δ+γt, equation A-14 becomes

(A-19) $$\vec{R}_{Deb} = \frac{a(1-e^2)}{1+ecos(\nu+\delta+\gamma t)}\begin{bmatrix}\cos(\nu+\delta+\gamma t)\\ \sin(\nu+\delta+\gamma t)\\ 0\end{bmatrix}$$

and the radar range vector to the debris in equation A-16 can be expressed as

(A-20) $$\vec{R} = a\begin{bmatrix}\cos(\nu)\\ \sin(\nu)\\ 0\end{bmatrix} - \frac{a(1-e^2)}{1+ecos(\nu+\delta+\gamma t)}\begin{bmatrix}\cos(\nu+\delta+\gamma t)\\ \sin(\nu+\delta+\gamma t)\\ 0\end{bmatrix}.$$

The radar range to the debris is

(A-21) $$r = \sqrt{\vec{R}\cdot\vec{R}}.$$

A.4.2 Modelling radar observations of coplanar debris in elliptical orbits

For model calculations define a local Cartesian coordinate system at the satellite where the X axis is represented by a unit vector in the radial direction

A-22) $$\hat{X} = \begin{bmatrix}\cos(\nu)\\ \sin(\nu)\\ 0\end{bmatrix},$$

the Y axis is represented by a unit vector in the satellite anti-velocity direction

(A-23) $$\hat{Y} = \begin{bmatrix}-\sin(\nu)\\ \cos(\nu)\\ 0\end{bmatrix},$$

and the Z axis is represented by a unit vector parallel to the earth's polar axis

(A-24) $$\hat{Z} = \begin{bmatrix}0\\ 0\\ 1\end{bmatrix}.$$

This coordinate system choice places the orbit ellipse perigee and apogee near the X axis.

Noting that ν is an independent variable, we can choose ν = ωt where ω is the satellite orbit (and earth rotation) rotational rate.

The debris velocity vector that is observed by the satellite radar is

(A-25)

$$\vec{V}_{Rad} = \frac{d\vec{R}}{dt} =$$

$$a\left(\omega\hat{Y} - (\omega+\gamma)\left(\frac{(1-e^2)\,\mathrm{esin}((\omega+\gamma)t+\delta)}{(1+ecos((\omega+\gamma)t+\delta)^2}\right)\hat{X} - \frac{(\omega+\gamma)(1-e^2)}{1+ecos((\omega+\gamma)t+\delta)}\begin{bmatrix}-\sin((\omega+\gamma)t+\delta)\\ \cos((\omega+\gamma)t+\delta)\\ 0\end{bmatrix}\hat{X}\right).$$

The radar observations of the debris velocity can be decomposed into components along the X and Y unit vectors to yield

(A-26) $$V_{XRad} = \vec{V}_{Rad}\cdot\hat{X} \text{ and } V_{YRad} = \vec{V}_{Rad}\cdot\hat{Y}$$

and a similar treatment can be given to the radar range vector to yield

(A-27) $$R_X = \vec{R}\cdot\hat{X} \text{ and } R_Y = \hat{R}\cdot\hat{Y}$$

so that the debris motions can be easily related to the satellite coordinate system.

The angle between the satellite position vector axis and the radar range vector of the debris is

(A-28) $$\theta = atan2(R_Y, R_X)$$

and the angle between the satellite position vector and the radar radial velocity vector to the debris is

(A-29) $$\vartheta = atan2(V_{YRad}, V_{XRad}).$$

The angle between the radar range vector and the debris velocity vector measured by the radar is

$$\psi = acos\left(\frac{\vec{R}\cdot\vec{V}_{Rad}}{r\sqrt{\vec{V}_{Rad}\cdot\vec{V}_{Rad}}}\right). \quad \text{(A-30)}$$

The relative positions of a satellite and debris when the debris is in a coplanar elliptical orbit are determined by the debris orbit ellipticity and the drift rate of the debris orbit. For the following calculations the satellite orbit is assumed to be circular and the debris orbit arguments of perigee are positioned so that the debris passes the satellite at a fixed offset between 1 and 10 km.

A.4.3 Radar observations of debris in non-drifting orbit planes

The impact of the offset distance on the angle between a radar range vector from the satellite to the debris and the X axis is shown in Figure A11 for a debris orbit eccentricity of 0.005. The debris orbit eccentricity will affect the shape of the curves but not their minimum radar range.

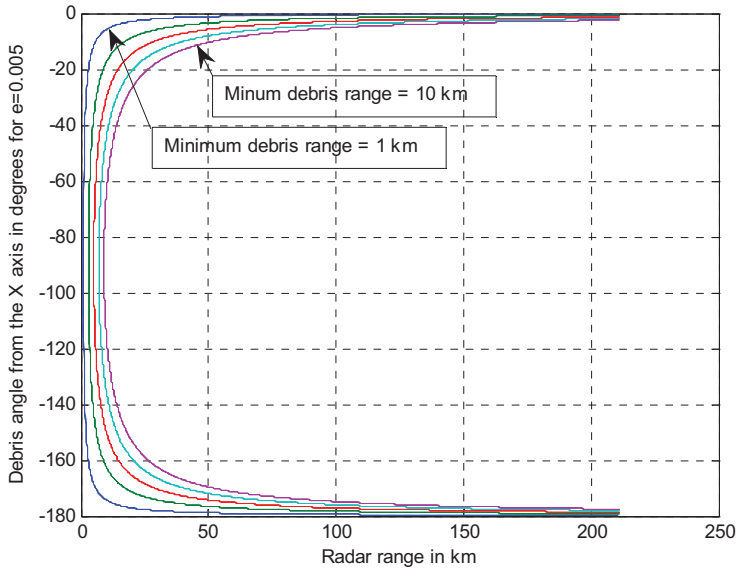

Figure A11: Debris position angle from the X axis as a function of the magnitude of the radar range vector for eccentricity 0.005 and no debris orbit drift

To look at the impact of debris orbit eccentricity on radar observations, the closest approach offset was set to 4 km and the debris orbit eccentricities were partitioned into two regimes covering nearly two orders of magnitude:

- eccentricity 0.0005 to 0.005 and
- eccentricity 0.005 to 0.03.

Most uncontrolled objects catalogued in [4] fall into this range.

For the eccentricity range 0.0005 to 0.005 the radar range for debris objects is less than 250 km at all times. Figure A12 illustrates the relationship between the radar range and the radar range rate over a day when the closest approach of the debris to the satellite is 4 km. The arrows around the eccentricity e = 0.005 contour show the debris path from debris orbit perigee to debris orbit

apogee and back to perigee. The convention used for this diagram has positive ranges for debris that is within the circular orbit of the satellite that carries the radar and has negative ranges for debris that is outside of the satellite orbit. Range changes most rapidly near the intersections of the satellite and debris orbits as expected.

Note: To simplify the display graphics to accommodate the signed range convention, the radar range scale shown in Figures A12 to A18, Figure A20, A 22, A25 and A26, is measured from the offset debris closest approach point instead of the from satellite.

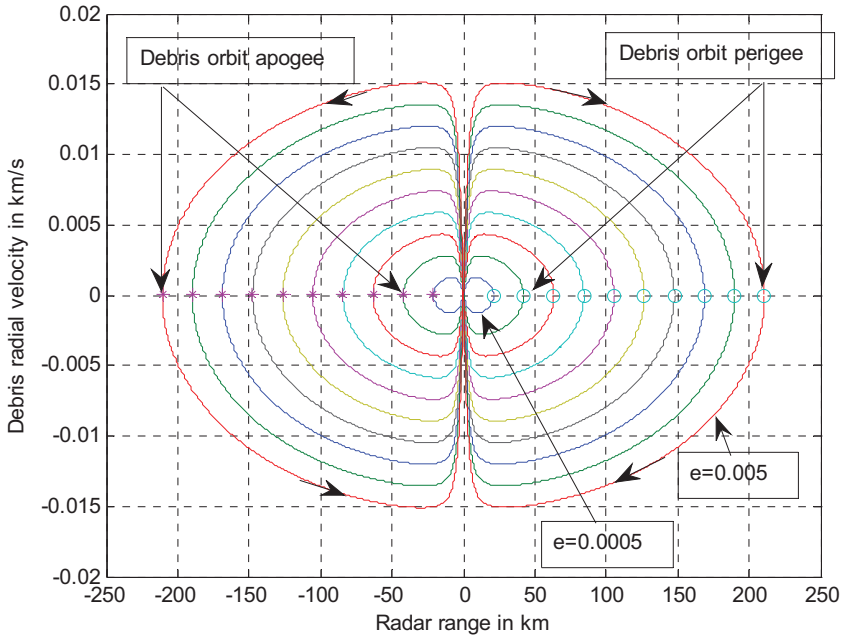

Figure A12: Debris range and range rate for debris orbit eccentricities 0.0005 to 0.005 for 4 km offset at the debris orbit crossing. The time period covered is one complete geostationary orbit.

Figure A13 shows the relationship between the radar range vector and the satellite local-coordinate X axis (the axis passing through the earth center) for the range/range rate relationship shown in Figure A10.

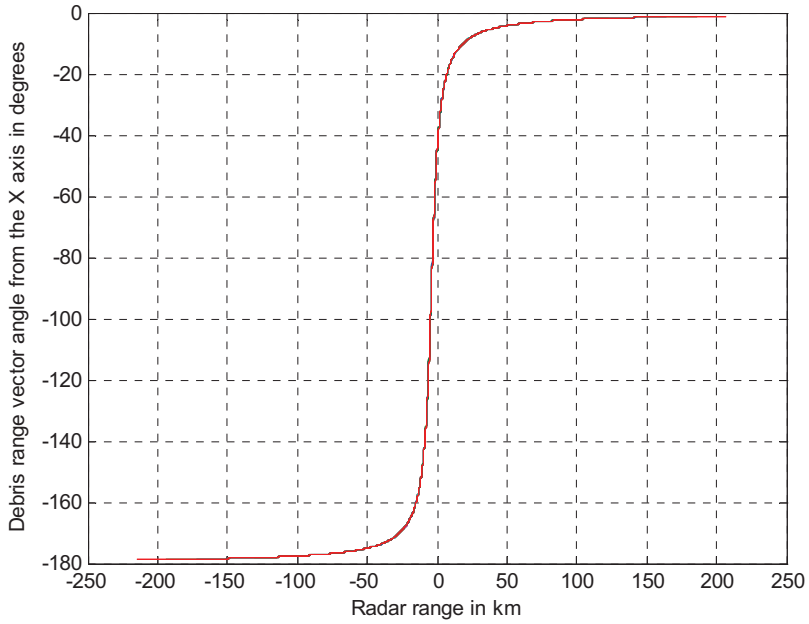

Figure A13: Debris range vector angle with the local X axis as a function of radar range for a debris closest approach of 4 km

Figures A14 and A15 show the same parameters for 10 km between debris orbit intersection with the satellite orbit and the satellite

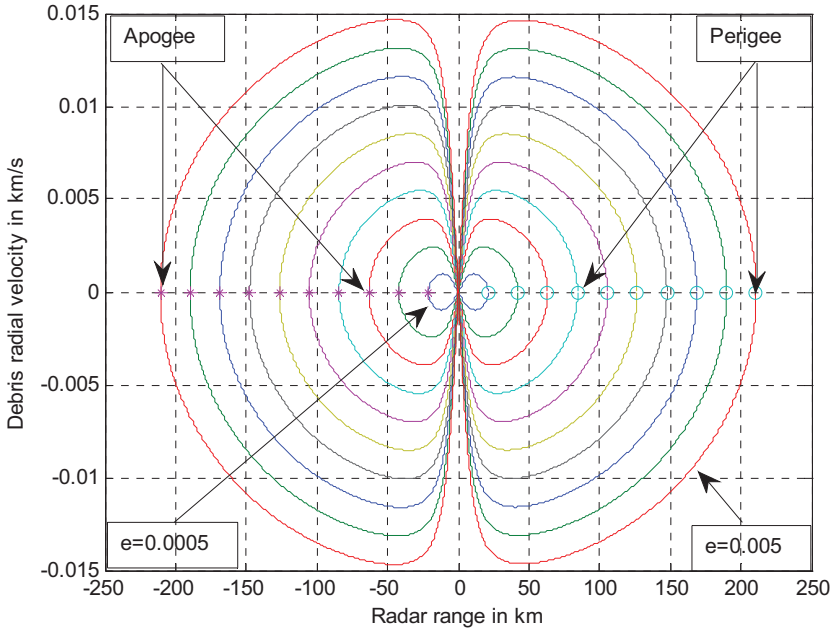

Figure A14: Debris range and range rate for debris orbit eccentricities 0.0005 to 0.005 for 10 km offset at the debris orbit crossing. The time period covered is one complete geostationary orbit.

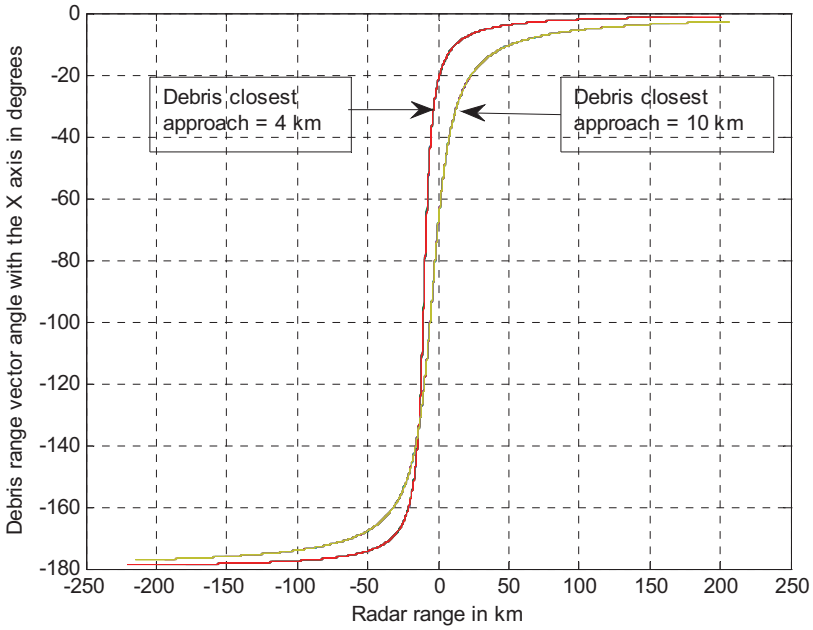

Figure A15: Debris range vector angle with the local X axis as a function of radar range for a debris closest approach of 4 km and 10 km

Figures A13 and A15 show that there is no dependence of the debris approach angle on the debris orbit eccentricity when the debris orbit does not drift.

Comparing figures A12 and A14 it is possible to extract the debris orbit eccentricity from measurements of the range, range rate. The debris orbit crossing proximity to the satellite can be estimated from the radar range and the angle between the radar range vector and the local X axis (the signal angle of arrival at the radar).

These form prediction tools for debris approaching the satellite and form debris orbit definition tools for debris orbit determination and catalogue maintenance when both approaching and receding debris measurements are made. A direct measurement of the debris separation from the satellite where the two orbits intersect shown in Figure A16 can be used to refine debris orbit data.

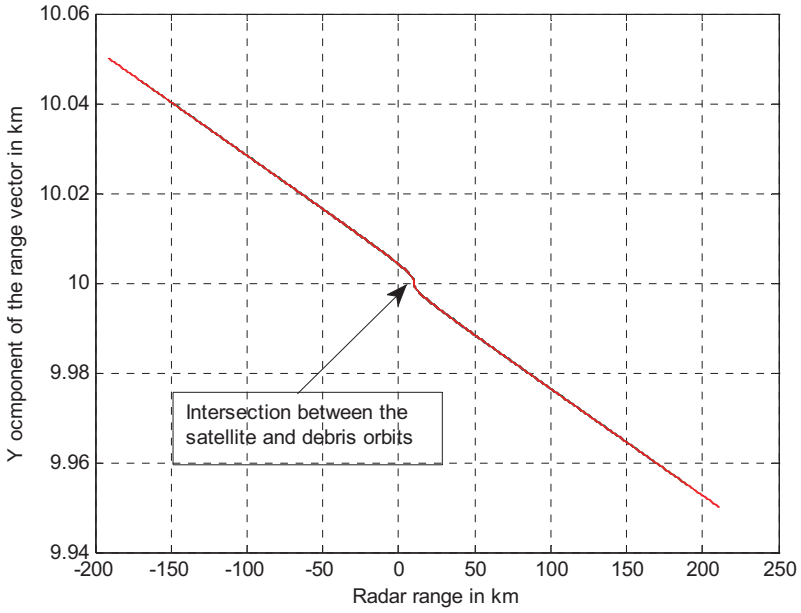

Figure A16: Y axis (satellite velocity vector) component of the debris position as an function of radar range for a debris closest approach of 10 km.

When debris orbit eccentricities are between 0.005 and 0.3 and when the intersection between the debris orbit and the satellite orbit is 4 km from the satellite, the relationship between the radar range and the measured radial speed of the debris (range rate) shown in Figure A11 (for eccentricities between 0,0005 and 0,005) takes the form shown in Figure A17. In Figure A17, the debris motion directions in the range-radial-velocity contours are the same as that shown in Figure A11 but the maximum radar range required to capture a full days worth of data increases from approximately 220 km to approximately 1300 km.

The maximum radial speed of the debris at e = 0.03 is 92 m/s as compared to 15 m/s for e = 0.005.

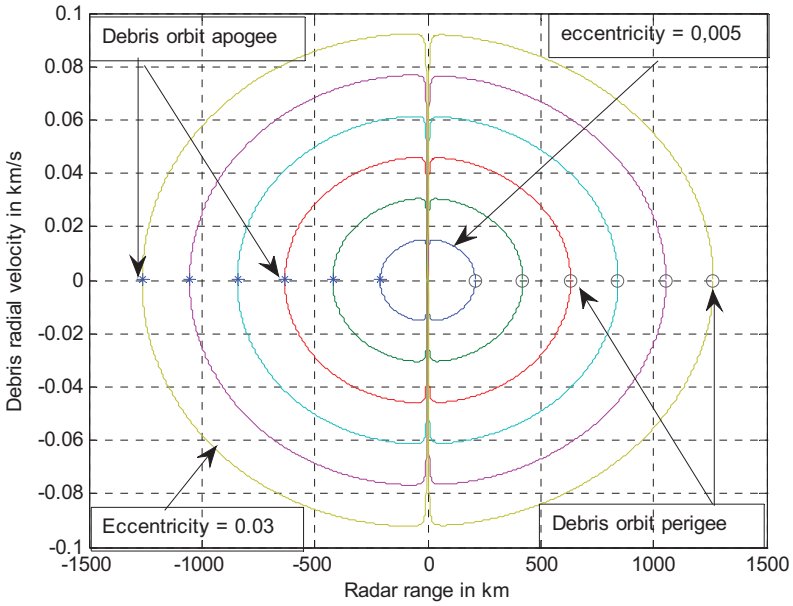

Figure A17: Debris range-velocity as a function of debris range for debris orbit eccentricities between 0.005 and 0.03 when the closest approach of the debris to the satellite is 4 km

When the maximum radar range is constrained to 250 km, the debris range/range-velocity relationship takes the form shown if Figure A18 for debris orbit eccentricities between 0.01 and 0.03 during the half orbit from perigee to apogee.

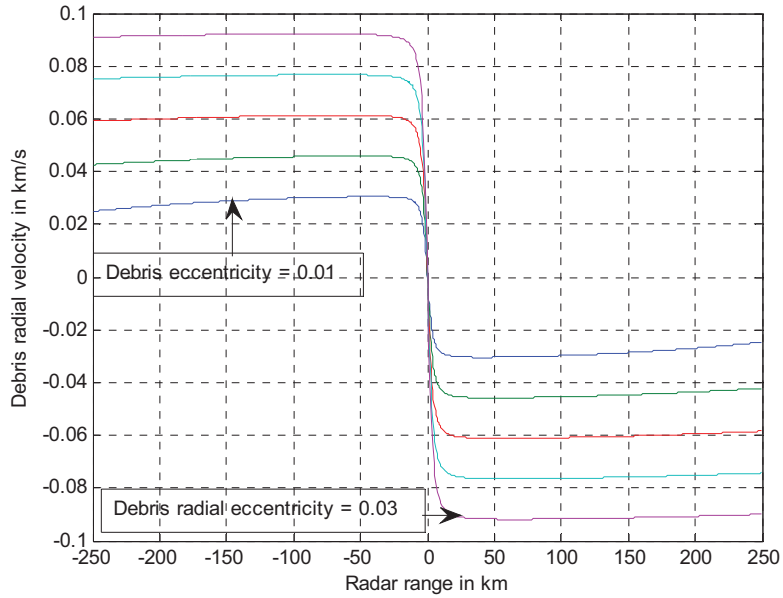

FigureA18: Debris range radial velocity relationship for e = 0.01 to e = 0.03, debris closest approach 4 km, and debris orbit segment from perigee to apogee.

Since the relationship between the range and range rate for the orbit segment from perigee to apogee is anti-symmetric with the relationship for the segment from apogee to perigee, both cases can be represented by the perigee to apogee transit.

The relationship between the radar observation time in hours and the debris orbit eccentricity is shown in Figure A19 for an orbit segment from perigee to apogee observed by a radar that has a maximum range of 250 km.

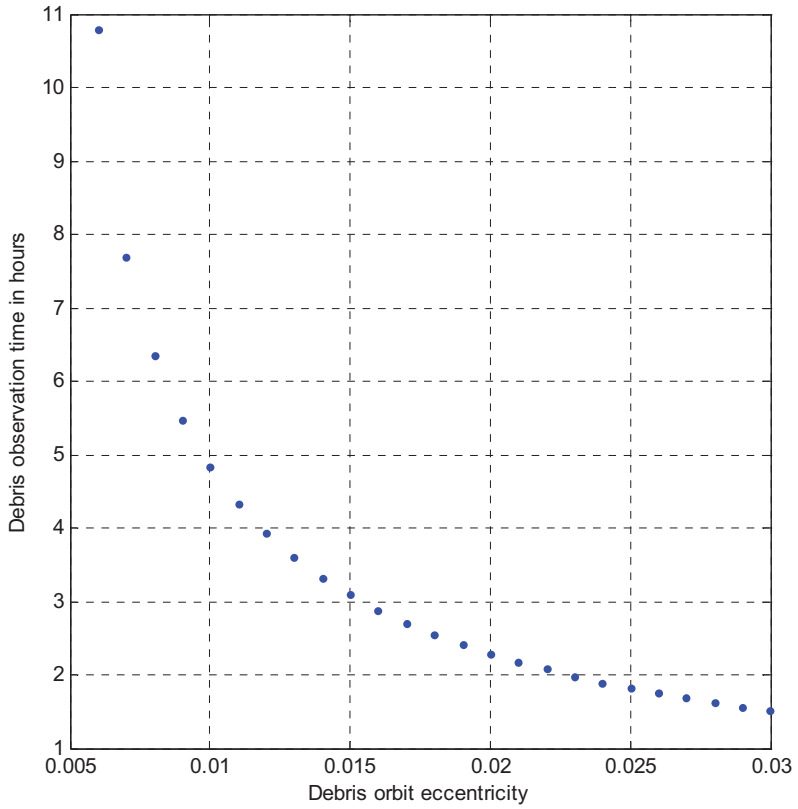

Figure A19: Debris observation time for debris transit from perigee to apogee or from apogee to perigee as a function of debris orbit eccentricity

Figure A19 shows the total time for the debris to approach the satellite and recede from it within a defined range interval of 250 km in each direction of debris motion. The approach observation time and the departure observation time are each one half of the times shown in Figure A19.

A.4.4 Radar observations of debris in drifting orbit planes

The model calculations in this section are based on debris that is in a coplanar orbit with the radar satellite, has an orbit eccentricity of 0.01 and has a closest approach distance to the satellite of 4 km. The debris orbits drift at rates between 1°/day and 10° day and between -1°/day and -10°/day.

Figure A20 shows the relationship between the radial velocity of the debris and its radar range for one full day. The arrows around the curve show the time sequence of the range and range-rate (radial velocity) observations as the debris moves from its orbit perigee to its orbit apogee.

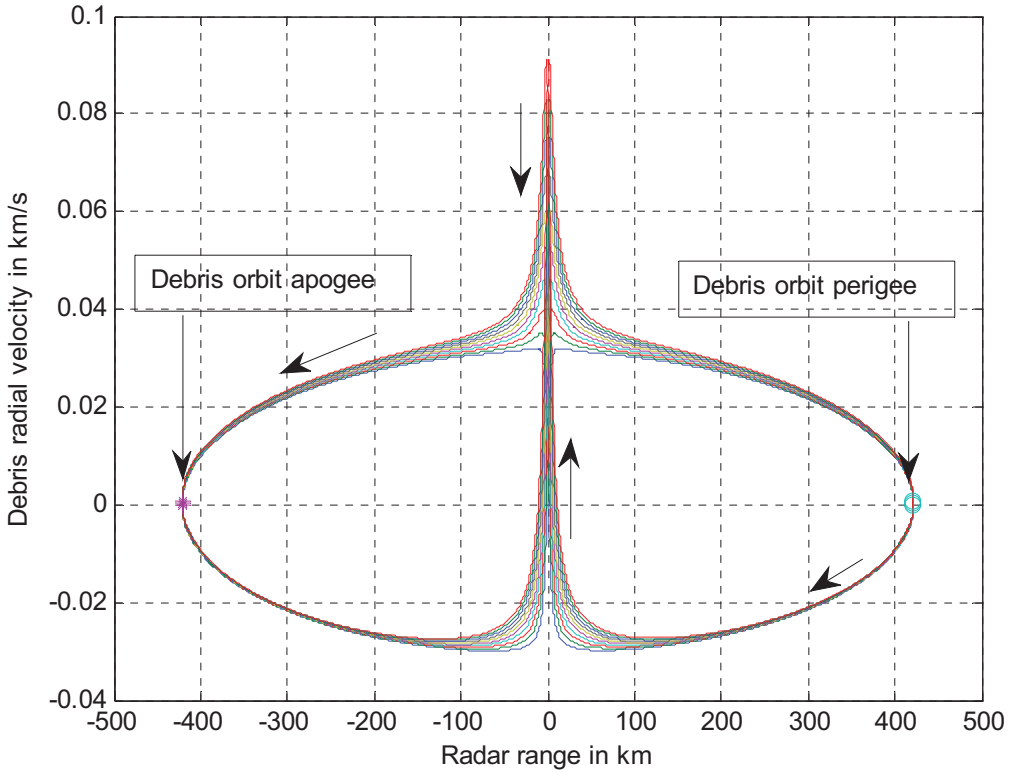

Figure A20: Radar range and range-rate for debris with orbit eccentricity 0.01 and drift rates between 1°/day and 10°/day

When the debris orbit drift rate is converted into a velocity component along the Y axis, a drift rate of 10°/day corresponds to a Y drift-velocity component of 0.085 km/s at the intersection between the debris orbit and the satellite orbit. The projection of the debris orbit drift onto the radar range vector accounts for the majority of the radial velocity spike seen as the debris passes the radar.

Figure A21 displays the debris radial velocity for these data as a function of time over the one sidereal day orbital period of the geostationary satellite.

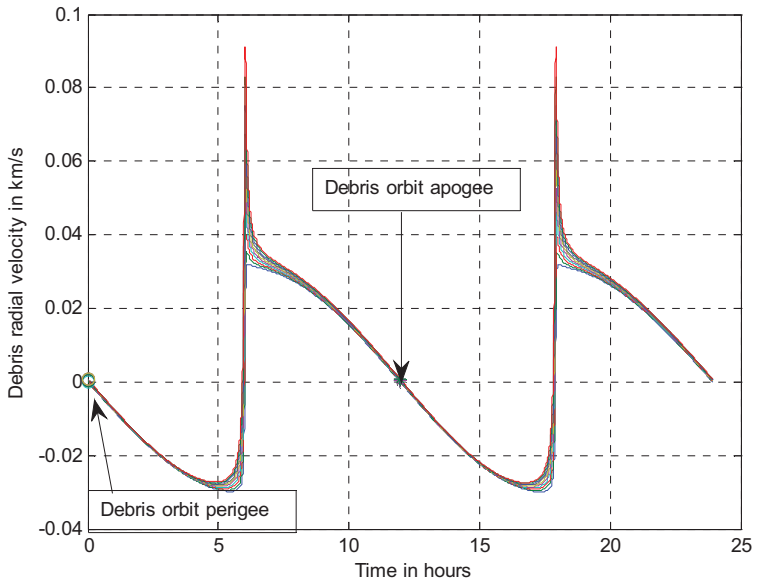

Figure A21: Debris radial velocity for debris that is coplanar with the radar platform, has an orbit eccentricity of 0.01 and has drift rates between 1°/day and 10°/day.

Figure A22 displays the 3°/day drift contour from Figure A20 for clarity. For this case, the debris orbit drift velocity results in a Y velocity of 0.025 km/s when the debris crosses the satellite orbit.

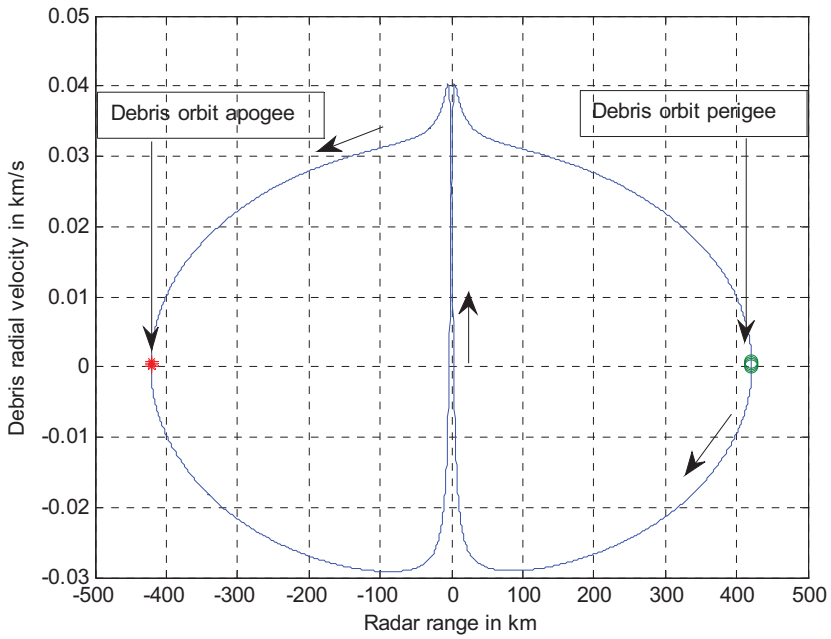

Figure A22: Radar range and range-rate for debris with orbit eccentricity 0.01 and drift rate 3°/day

When the signed radar range convention is used, the observation time windows for the data shown in Figure A22 are illustrated in Figure A23.

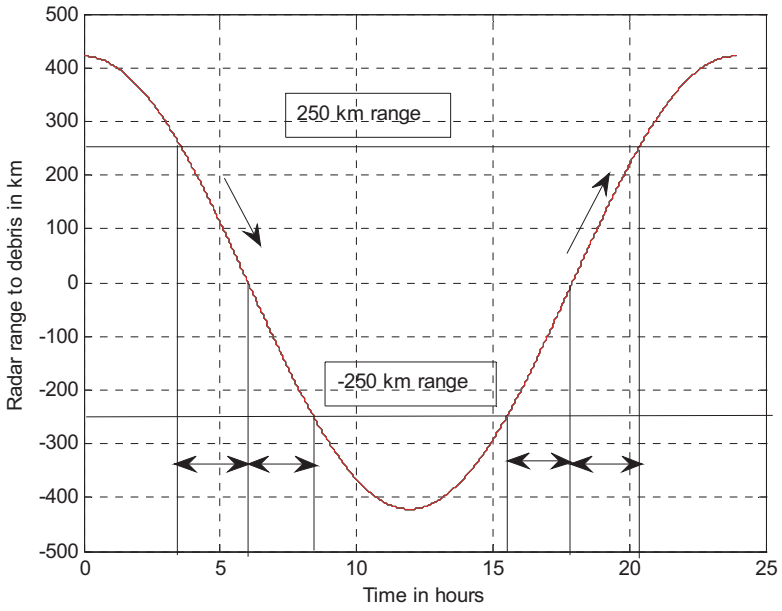

Figure A23: Signed radar range for coplanar debris with eccentricity 0.01 and debris orbit drift rate 3º. Positive ranges are within the orbit of the satellite that carries the radar.

The arrows along the range curve in Figure A23 show the debris progression around its orbit and the double-headed arrows show the time windows for debris approaching and receding from the radar. From Figure A23, the debris is visible to a bi-directional radar that has a ± 250 km observation range during two 4.9 hour time windows per day.

When the radar range is constrained to 250 km and the data set, whose range/radial velocity relationship, shown in Figure 20, is displayed using the magnitude of the radar range, Figure A24 shows that the debris orbit drift speed does not affect the distribution of radar observation angles in the X, Y plane.

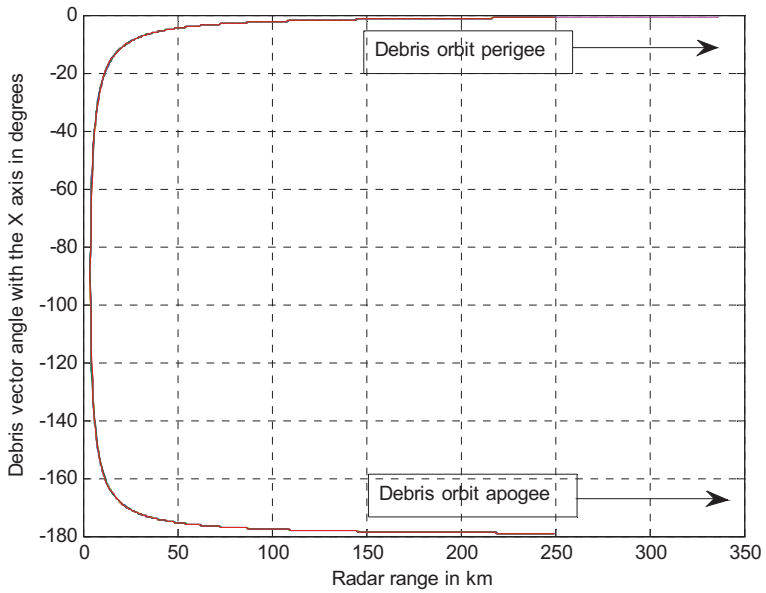

Figure A24: Debris range vector angle from the X axis as a function of radar range magnitude for drift orbit eccentricity and for debris orbit drift rates between -10 °/day and 10 °/day.

When the debris orbit plane drift rates are between -1°/day and -10°/day, Figure A20 transforms to Figure A25.

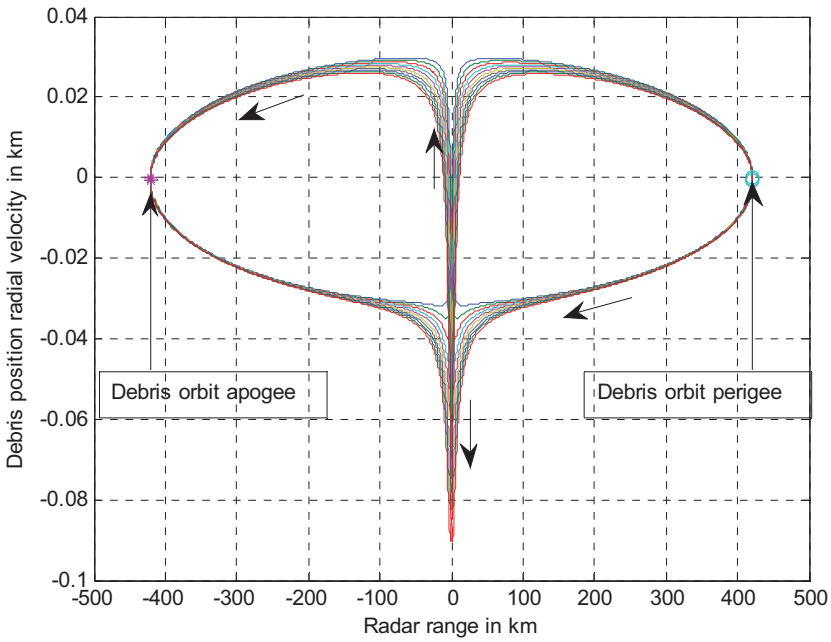

Figure A25: Radar range and range-rate for debris with orbit eccentricity 0.01 and drift rates between -1°/day and -10°/day

When the data in Figure A25 are constrained to 250 km range and only the debris orbit segment from perigee to apogee is displayed, we have the results shown in Figure A26.

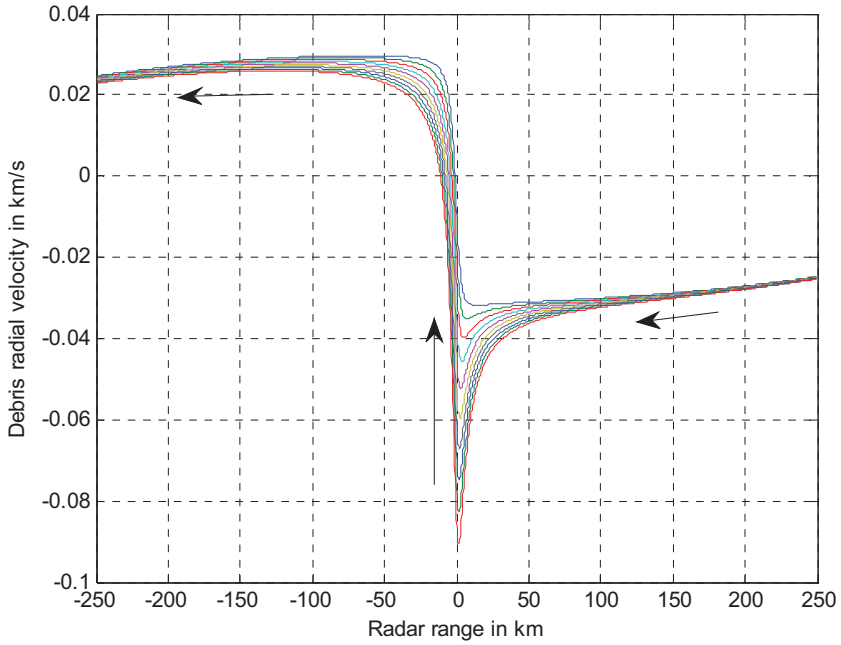

Figure A26: Radar range and range-rate for debris with orbit eccentricity 0.01 and drift rates between -1°/day and -10°/day for the debris orbit segment from perigee to apogee with the radar range constrained to 250 km.

Figure A24 shows that the debris lies within 5° of the X axis until the debris approaches within 50 km of the radar. At this point, the radar observation geometry is influenced by debris motion components along the Y axis as indicated by the rapid change in the angle between the radar range vector and the X axis. When the debris radial velocity is displayed as a function of the radar range vector angle from the X axis, as shown in Figure A27, the radial velocity (range rate) signatures show a strong dependence on the debris orbit drift rate.

These signatures are best observed by radar observations centered about the Y axis and require a radar that is designed to measure the approach angle of the debris.

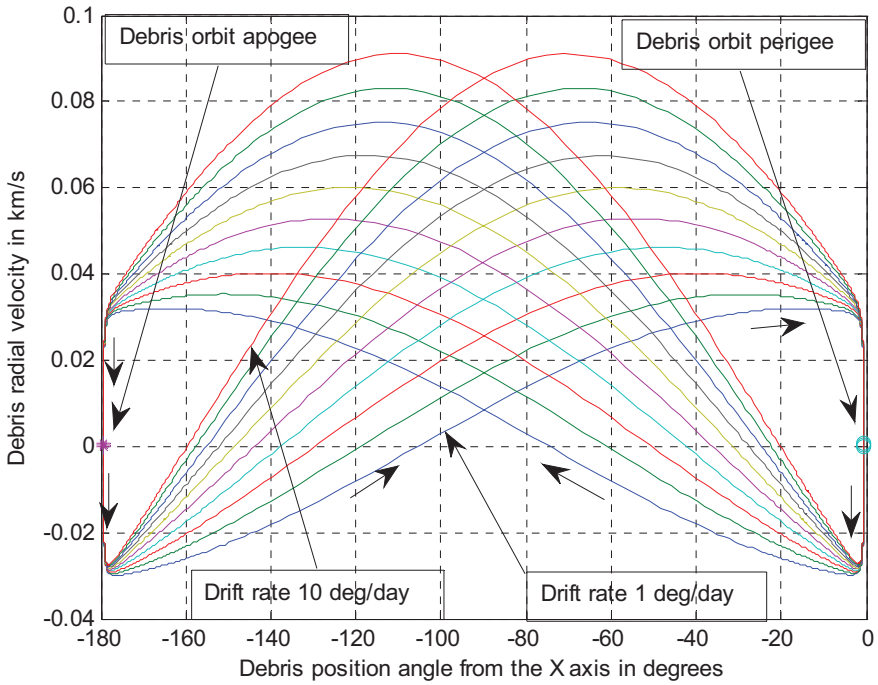

Figure A27: Debris radial velocity as a function of debris position angle from the X axis

The arrows along the 1°/day debris orbit drift rate contour of Figure A27 show the debris motion from debris orbit perigee to apogee and back. From Figure A24, all observations that contain significant drift rate data occur within 50 km of the radar antenna.

A.5 Model calculation summary

This Annex explores the problem of observing geosynchronous belt debris from a radar system that is mounted on a geostationary satellite. The model calculations that are used have been designed to identify key observational parameters of this radar type. The models examine the radar observation properties of the
debris field that may exist in the vicinity of the geostationary radar platform from the vantage point of the radar platform and extract range, range rate and observation angle requirements based on simple descriptions of the satellite and the debris orbits. The results obtained are applicable to a large range of real cases.

Model calculations are based on a local coordinate system that is attached to the satellite radar platform where the X axis is defined to be parallel to the outward projection of the satellite position vector, the Y axis is defined to be in the direction of the satellite velocity vector for a circular orbit and the Z axis is defined to be parallel to the satellite orbital momentum vector (the projection of the Z axis on the earth angular momentum vector {earth rotation axis} is positive north).

Orbit of the satellite that carries the radar is assumed to be perfectly circular and to be at the geostationary radius of 42164 km. Perfect station keeping is assumed but is not required for the results to be valid. The inclined debris orbit results will be valid for geostationary satellite orbit eccentricities up to 0.005, subject to the relationship between the arguments of perigee of the satellite and debris orbits. The general case of inclined, elliptical satellite orbits and inclined, elliptical debris orbits has not been studied here.

The modeled conditions in this document consider the cases where the debris passes within 10 km of the satellite. Two major conditions are examined:

1. The debris orbit eccentricity matches the satellite orbit eccentricity and the debris orbit is inclined with respect to the satellite orbit. This case is modeled in terms of the intersections of two, relatively inclined, circular orbits.
2. The debris orbit eccentricity differs from the satellite orbit eccentricity and the relative inclinations of the two orbits are smaller than 0.05^{o}. This is the coplanar orbit case.

Model calculations for both cases include the effects of the drift rate of the debris orbit plane.

Emphasis is placed on observations made by a radar that has a 250 km effective range for the smallest debris objects that can be reliably measured.

Results for the inclined orbit modeling show that:

1. Radar observations can be constrained to a spatial volume that is within 3^{o} of the X,Z plane for radar ranges that are greater than 50 km.
2. The angle between the radar range vector and the Y axis is only significant as the debris passes the satellite and depends on both the separation of the orbit crossing point and the radar and on the debris orbit drift rates.
3. Measurements of the radar range and range-rate (debris radial velocity) during the periods that the debris approaches and recedes from the radar can be used to estimate:
    a. the debris orbit inclination angle,
    b. the debris orbit drift rate, and
    c. the distance between the satellite and the point where the debris crosses the satellite orbit.

    The debris orbit drift rate estimation errors using this measurement approach are largest for small drift rates at all inclination angles.
4. Measurements of the radar range and the angle between the radar range vector and the Z axis can be used to estimate debris orbit drift rates at debris orbit inclination angles less than 4^{o} and can be used to measure the distance between the satellite and the debris orbit crossing point.
5. Available observation times for debris approaching from 250 km range vary from approximately 5 minutes for a debris orbit inclination of 15^{o} to approximately 83 minutes for a debris orbit inclination of 1^{o} when the debris orbit drift rate is 10^{o}/day. For low drift rates, there will be two observation opportunities within a day.

Results for the modeling of variable-eccentricity debris orbits that have small inclination angles ($<0.5^{o}$) with respect to the satellite orbit show that:

1. Radar range and range-rate observations provide a sensitive measure of the relative eccentricity of the debris orbits.
2. Range/range-rate measurements for ranges less than 50 km allow the distance between the satellite and the debris orbit crossing point to be measured.
3. Measurements of the radar range and the angle between the radar range vector and the X axis are not sensitive to the debris orbit eccentricity but allow estimates of the closest approach of the debris to the satellite (the debris orbit crossing point distance).
4. Measurements of debris radial velocity and the angle between the debris range vector and the Y axis while the debris passes the satellite allow direct measurement of the debris orbit drift rate.
5. Available observation times for approaching or receding debris vary from approximately 15 minutes for an orbit eccentricity of 0.03 to approximately 5.5 hours at an orbit eccentricity of 0.007. Depending on the radar's maximum range along the Y axis, debris orbit drift rates smaller than 0.3^{o}/day will permit two observations of the debris orbit during one day.

For all cases modeled, debris tracking during the measurement process is important and measurements made on both approaching and receding debris allow the debris orbits to be estimated with reasonable accuracy.

This page intentionally left blank.

List of symbols/abbreviations/acronyms/initialisms

CFB	Canadian Forces Base
CSA	Canadian Space Agency
DND	Department of National Defence
DRAO	Dominion Radio Astrophysical Observatory
DRDC	Defence Research & Development Canada
DRDKIM	Director Research and Development Knowledge and Information Management
ECEF	Earth Centered Earth Fixed
IADC	Inter-Agency Space Debris Coordination committee
LEO	Low Earth Orbit
LFM	Linear Frequency Modulation
MEO	Medium Earth Orbit
PRF	Pulse Repetition Frequency
R&D	Research & Development
RCP	Right Circular Polarization
RF	Radio Frequency
SSN	Space Surveillance Network
TR	Transmit-Receive
WGS 84	World Geodetic System 1984 (earth ellipsoid model)

This page intentionally left blank.

DOCUMENT CONTROL DATA

(Security classification of title, body of abstract and indexing annotation must be entered when the overall document is classified)

1. ORIGINATOR (The name and address of the organization preparing the document. Organizations for whom the document was prepared, e.g. Centre sponsoring a contractor's report, or tasking agency, are entered in section 8.)

Defence R&D Canada – Ottawa
3701 Carling Avenue
Ottawa, Ontario K1A 0Z4

2. SECURITY CLASSIFICATION (Overall security classification of the document including special warning terms if applicable.)

UNCLASSIFIED
(NON-CONTROLLED GOODS)
DMC A
REVIEW: GCEC JUNE 2010

3. TITLE (The complete document title as indicated on the title page. Its classification should be indicated by the appropriate abbreviation (S, C or U) in parentheses after the title.)

Radar systems for monitoring objects in geosynchronous orbit

4. AUTHORS (last name, followed by initials – ranks, titles, etc. not to be used)

Chuck Livingstone

5. DATE OF PUBLICATION (Month and year of publication of document.)	6a. NO. OF PAGES (Total containing information, including Annexes, Appendices, etc.)	6b. NO. OF REFS (Total cited in document.)
June 2013	96	36

7. DESCRIPTIVE NOTES (The category of the document, e.g. technical report, technical note or memorandum. If appropriate, enter the type of report, e.g. interim, progress, summary, annual or final. Give the inclusive dates when a specific reporting period is covered.)

Technical Report

8. SPONSORING ACTIVITY (The name of the department project office or laboratory sponsoring the research and development – include address.)

Defence R&D Canada – Ottawa
3701 Carling Avenue
Ottawa, Ontario K1A 0Z4

9a. PROJECT OR GRANT NO. (If appropriate, the applicable research and development project or grant number under which the document was written. Please specify whether project or grant.)	9b. CONTRACT NO. (If appropriate, the applicable number under which the document was written.)

10a. ORIGINATOR'S DOCUMENT NUMBER (The official document number by which the document is identified by the originating activity. This number must be unique to this document.)	10b. OTHER DOCUMENT NO(s). (Any other numbers which may be assigned this document either by the originator or by the sponsor.)
DRDC Ottawa TR 2013-009	

11. DOCUMENT AVAILABILITY (Any limitations on further dissemination of the document, other than those imposed by security classification.)

Unlimited

12. DOCUMENT ANNOUNCEMENT (Any limitation to the bibliographic announcement of this document. This will normally correspond to the Document Availability (11). However, where further distribution (beyond the audience specified in (11) is possible, a wider announcement audience may be selected.))

Unlimited

13. ABSTRACT (A brief and factual summary of the document. It may also appear elsewhere in the body of the document itself. It is highly desirable that the abstract of classified documents be unclassified. Each paragraph of the abstract shall begin with an indication of the security classification of the information in the paragraph (unless the document itself is unclassified) represented as (S), (C), (R), or (U). It is not necessary to include here abstracts in both official languages unless the text is bilingual.)

Current deep-space surveillance systems are incapable of detecting small (~30cm) debris objects in the geosynchronous orbit belt that contains active geostationary satellites. Because of battery and residual fuel explosions in derelict spacecraft and rocket bodies in this orbit regime, small debris is expected to exist and to pose a hazard to the increasing population of geostationary satellites. Possible ground and space based radar sensors have been examined as part of a larger exploration of alternatives for systems to perform deep-space object detection and orbit determination for small, geosynchronous debris objects in the context of Canadian contributions to the Space Surveillance Network following the demise of the Sapphire space surveillance satellite circa 2019.

A first-order investigations of possible ground-based radars, designed under the small target detection and tracking constraint, shows that cost roughly tracks capability as the complexity of possible solutions ranges from: a deep-space radar upgrade to a large radio telescope (ROM cost $5M to$10M), to a purpose-designed dish-antenna deep-space radar (ROM cost $100 M to $150 M), to an electronically-steered-array radar (ROM cost $1.5 B to $2.0 B). The cost figures are guesses that are based on the costs for systems with related complexity.

First-order investigations of possible space-based deep-space surveillance systems examine the concepts of using a secondary sensor payload on a geostationary satellite platform for local area debris monitoring; and developing a dedicated debris surveillance radar that would fly in a sub-geosynchronous orbit.

All investigations in this study were constrained to consider technologies that are available and are considered to be robust in 2012.

14. KEYWORDS, DESCRIPTORS or IDENTIFIERS (Technically meaningful terms or short phrases that characterize a document and could be helpful in cataloguing the document. They should be selected so that no security classification is required. Identifiers, such as equipment model designation, trade name, military project code name, geographic location may also be included. If possible keywords should be selected from a published thesaurus, e.g. Thesaurus of Engineering and Scientific Terms (TEST) and that thesaurus identified. If it is not possible to select indexing terms which are Unclassified, the classification of each should be indicated as with the title.)

deep-space radar;geosyschronous orbits;geostationary orbits;space debris;radar detection;debris motion

Defence R&D Canada

Canada's leader in Defence
and National Security
Science and Technology

R & D pour la défense Canada

Chef de file au Canada en matière
de science et de technologie pour
la défense et la sécurité nationale

DEFENCE DÉFENSE

www.drdc-rddc.gc.ca